UNCONVENTIONAL ROLES OF HUMAN N-MYRISTOYLTRANSFERASES

A Dissertation

Presented to the Faculty of the Graduate School

of Cornell University

In Partial Fulfillment of the Requirements for the Degree of

Doctor of Philosophy

by

Tatsiana Kosciuk

August 2020

UNCONVENTIONAL ROLES OF HUMAN N-MYRISTOYLTRANSFERASES

Tatsiana Kosciuk, Ph. D.

Cornell University 2020

N-myristoyltransferases (NMTs) are ubiquitous among eukaryotes and are widely known for adding a myristoyl, saturated 14-carbon chain, to the amino group of the N-terminal glycine on proteins. This modification in turn regulates essential protein properties such as membrane binding, stability, enzymatic activity, and interactions with other proteins. Decades of elegant studies have established the rules that govern this modification, such as the substrate sequence with the indispensable N-terminal glycine and co-translational mode of action. During my graduate work I discovered functions of NMT that do not conform to the known principles of this enzyme.

I began my work with discovering that the small GTPase ADP-ribosylation factor 6 (ARF6) is myristoylated on lysine 3 in addition to its common to the ARF family N-terminal glycine myristoylation. Excitingly, this finding offered an explanation to the puzzling properties of ARF6 compared to ARF1-5 such as its retention at the membrane during the GTPase cycle. We became curious in finding the enzyme that adds this modification, however there was no reported mammalian lysine fatty-acyl transferases. Because N-terminal myristoylation occurs at the amino group, just like lysine myristoylation, my advisor Prof. Hening Lin suggested to test NMT. With the experimental help and suggestions of several amazing scientists, I demonstrated that it was indeed true. I then found that SIRT2 removes this modification, which closed the fascinating myristoylation-demyristoylation cycle essential for ARF6

activation. My following work focused on establishing the role of this cycle in colon cancer progression and on discovering other unconventional substrates of NMT such as Dynamin 2.

BIOGRAPHICAL SKETCH

Tatsiana Kosciuk was born in Minsk, Belarus where she worked as a TV news reporter. After immigrating to the US, she received a bachelor's degree in biochemistry from the University of Southern Maine (USM). There, she was awarded the Charles J. Hoff scholarship, Outstanding Achievement Louis B. Woodward Scholarship and Outstanding Student of the Year awards. At USM she also worked as an organic chemistry tutor and an undergraduate researcher under the guidance of Prof. Au-Kau Ng with whom she developed a quantitative ELISA for measuring plasma osteopontin. During her undergraduate years, for two summers Tatsiana worked with Dr. Jeong Yoon at Maine Medical Center Research Institute on discovering the function of Leucine-Rich Repeat-Containing G Protein-Coupled Receptors in skeletal muscle and adipose tissue. Her first internship was funded by the Holden Agency scholarship and the second by the American Heart Association Undergraduate Research fellowship. After graduation she briefly worked on a collaborative project between the Frank Gertler and Robert Langer laboratories at MIT. At Cornell, she studied the enzymes that regulate lysine fatty acylation and their substrates under the guidance of Prof. Hening Lin, and received the SUNY Diversity and NSF GRFP fellowships.

Dedicated to my beloved husband Nick Kosciuk, mother and father in-law Agnes and Serge Kosciuk, and to the memory of my dearest aunt Valentina Davidovich

ACKNOWLEDGMENTS

The path to a Ph.D. is much more challenging than I could ever imagine, and so I am immensely grateful to the many people who helped me along the way by generously sharing their expertise, data, suggestions, encouragement, friendship and love. This made my graduate years a time of tremendous growth as a scientist and person. I first would like to express my deep gratitude to my advisor Prof. Hening Lin for the guidance and support of my work. It has been an honor to learn from his knowledge and successful career in science. I am immensely grateful to my committee members Prof. Richard Cerione, Prof. Benjamin Cosgrove and Prof. Jeffrey Pleiss for all the valuable scientific discussions and for the much-needed guidance on navigating the field of science beyond research. Much appreciation to Prof. Chris Fromme for the guidance on the crystallography work and to Dr. Steve Halaby and Dr. Ian Price for performing the crystallography studies. I am very thankful to Prof. Neil L. Kelleher, Dr. Caroline J. DeHart and Dr. Paul M. Thomas for the analysis of ARF6 by top-down mass spectrometry and for the guidance on preparing the sample; to Dr. Xiaoyu Zhang for the ARF6 G2A analysis by mass spectrometry and for always being available to help; to Dr. Chengliang Zhu for the synthesis of some important peptides; to Dr. Ming Yang for the synthesis of ALK12, ALK12-CoA, TM and for his kind, cheerful nature; to Dr. Shuai Zhang for the DNM2 construct and suggestions and help with protein purification and proteomics experiments; to Kayla N. Johnson and Garrison P. Komaniecki for experimental replication; to Xuan Lu, Dr. Ji Cao and Kayla N. Johnson for the wonderful collaboration on the mouse work. Many thanks to all the lab members past and present – it have been a pleasure and amazing opportunity to work with and learn from these talents; special thanks to Dr. Hui Jing for being a wonderful mentor during my rotation in the lab.

I am very grateful to Prof. Maurine Linder for her support, honesty and being an amazing role model as a successful female-scientist. I am most grateful to my dear husband Nick Kosciuk for his unconditional love and support that gave me strength all these years, and to my precious family and friends here in the US and back in Belarus who were always there to rejoice during moments of success and to help through hardship along the way.

My graduate work was supported by the National Science Foundation Graduate Research Fellowship Program and SUNY Diversity Fellowship awards, for which I am immensely thankful.

TABLE OF CONTENTS

LIST OF FIGURES

LIST OF TABLES

CHAPTER 1

NMT AS A GLYCINE AND LYSINE MYRISTOYLTRANSFERASE IN CANCER, IMMUNITY, AND INFECTIONS

This chapter is adapted from: Tatsiana Kosciuk and Hening Lin. *NMT as a glycine and lysine myristoyltransferase in cancer, immunity, and infections*. ACS Chem. Biol. 10, 1021 (2020)

ABSTRACT

Protein myristoylation, the addition of a 14-carbon saturated acyl group, is an abundant modification implicated in biological events as diverse as development, immunity, oncogenesis, and infections. N-myristoyltransferase (NMT) is the enzyme that catalyzes this modification. Many elegant studies have established the rules guiding the catalysis including substrate amino acid sequence requirement with the indispensable N-terminal glycine, and a co-translational mode of action. Recent advances in technology such as the development of fatty acid analogs, small molecule inhibitors, and new proteomic strategies, allowed a deeper insight into the NMT activity and function. Here we focus on discussing recent work demonstrating NMT as also a lysine myristoyltransferase, the enzyme's regulation by a previously unnoticed solvent channel, and mechanism of NMT regulation by protein-protein interactions. We also summarize recent findings of NMT's role in cancer, immunity and infections, and the advances in pharmacological targeting of myristoylation. Our analyses highlight opportunities for further understanding and discoveries.

Keywords

Myristoylation, N-myristoyltransferasem, NMT, lysine fatty acylation, solvent channel, membrane anchor, inhibior, cancer, parasite

INTRODUCTION

N-myristoyltransferase (NMT) is a ubiquitous eukaryotic enzyme that for decades has been known to have a single role – myristylation of the amino group of the N-terminal glycine on proteins. This function is of high specificity guided by several factors such as substrate sequence requirements, protein interactions, and expression levels. N-myristoylation is the addition of a 14-carbon chain to the alpha amine (Nα) of the N-terminal glycine on proteins, exposed after the initiator methionine is cleaved by methionine aminopeptidase during translation, or after caspase cleavage during proteolytic events such as apoptosis. This modification often regulates protein-membrane or protein partner binding and is thought to be irreversible although there is some evidence of an ATP-dependent demyristoylase in the cytoplasmic fraction of the brain synaptosomes.[1] Recent findings implicate N-myristoylation in protein stability, where free N-terminal glycine is recognized by E3 ubiquitin ligases leading to degradation of unmyristoylated proteins.[2] NMT is essential for the survival of many eukaryotic organisms such as *S. cerevisiae*[3] and pathogens *C. albicans, T. brucei*,[4] *C. neoformans*[5], and many viruses utilize host NMT for replication and infectivity,[6] which made the enzyme an attractive therapeutic target. Furthermore, NMT knockout causes embryonic lethality in mice and *Drosophila*, pointing to its role in develepment.[7, 8] Here we discuss the recent advances in understanding the NMT catalysis, especially its activity on lysine residues, and the enzyme's potential for therapeutic use in cancer, immunity and infectious diseases, including viral infections. We note the areas that warrant further investigation such as reevaluation of eukaryotic and viral proteomes for lysine substrates of NMT and provide a brief update on the progress in the development of NMT-selective small molecule inhibitors.

STRUCTURE AND REGULATION OF NMT CATALYSIS

Several studies have elucidated that the catalytic mechanism of NMT follows an ordered bi-bi reaction where myristoyl-CoA binds to the enzyme in a bent fashion resembling a "question mark", which causes a conformational change allowing the peptide substrate to bind (Figure 1.1A). The interaction of the thioester carbonyl with the backbone amides of the enzyme (Phe 247 and Leu 248 in human NMT1) forms an oxy-anion hole activating the carbonyl for the nucleophilic attack by the Gly2 amine of the peptide substrate.[9, 10] This reaction was thought to occur only with the N-terminal glycine, not any other amino acids because the absence of a side chain allows free rotation of the N-terminal amine necessary for the nucleophilic attack on the carbonyl carbon of the thioester bond of myristoyl-CoA.[11] Later we will discuss recent studies that elegantly demonstrated the activity of NMT on lysine. Recently, a detailed reaction mechanism revealed that the C-terminus carboxylate of Gln496 acts as an indirect catalytic base initiating the water-mediated deprotonation of the N-terminus amino group. The carboxylate is located at the end of a 22 Å long previously unnoticed solvent channel that is thought to be important for the deprotonation.[10] After catalysis, CoA is released followed by the myristoylated product.[12] In addition to the N-terminal Gly, the peptide substrate specificity is dictated by other residues near the N-terminus. Although not an absolute requirement, NMT often prefers substrates with the sequence GXXXSK.[13-16] Ser 6 interacts with a small hydrophilic pocket explaining the enzyme's preference for this position.[13, 14, 16] Lys 7 of the peptide substrate allows a tight binding and occupies a distinct negatively charged pocket with three aspartate residues that stabilize the substrate binding via a salt bridge between the Asp carboxylates and the epsilon amino group (Nε) of the lysine.[14, 16] The sequence recognition is rather mosaic suggesting that NMT can accommodate various substrates and that other factors such as interacting partners might regulate substrate specificity in cells.[15] For instance, the known NMT substrate ARF1 has the N-terminal sequence GNIFAN, which does not conform

to the NMT preference. This example emphasizes the need to keep an open mind while examining potential NMT substrates. Furthermore, there are variations in sequence preference across species,[14, 16, 17] suggesting the need for species-specific predictive tools of N-terminal myristoylation, which can be of use for developing NMT-targeted therapies.

The exceptional preference of NMT for myristoyl-CoA remains puzzling given that in cells myristic acid comprises less than 1% of total fatty acids compared to about 20 % for palmitic acid.[18] Structural work suggests that the length of the NMT hydrophobic pocket is best suited for a myristoyl chain,[9] which partially explains this selectivity. Yet under some conditions, NMT can efficiently utilize other acyl-CoAs. For instance, the introduction of a triple bond at C6 of the acyl chain of palmitoyl-CoA results in a strong enhancement of the activity of *S. cerevisiae* Nmt, which is thought to result from inducing a bend in palmitoyl-CoA where it would naturally occur in myristoyl-CoA bound to NMT.[19] It was also shown that on the peptide GARASVLS-NH_2 derived from the HIV Gag protein the myristoyl-peptide formation was progressively inhibited as the acyl-CoA chain shortened with nearly no myristoylation upon shortening to 7 carbons.[20] Whether these trends of acyl-CoA utilization efficiency depend on the peptide substrate in vitro and in cells is unclear. Yet some reports suggest a similar binding affinity for myristoyl-CoA and palmitoyl-CoA[21, 22] and explain that NMT is "protected" from other acyl-CoAs by the acyl-CoA binding protein ACBD6.[22-24] The ACBD6 binding to NMT via its ankyrin-repeat motif (ANK) allosterically activates the enzyme for myristoyl-CoA acceptance independently from the acyl-CoA binding domain of ACBD6. The ANK domain alone is able to stimulate NMT and it produces the same effect when attached via the linker domain to ACBD1 protein, which otherwise does not regulate NMT.[24] At the same time, myristoyl-CoA bound to ACBD6 can be transferred to NMT. When NMT is introduced to myristoyl-CoA bound ACBD6, the formation of myristoyl-peptide is observed suggesting that ACBD6 hands myristoyl-CoA over to NMT; and this process is potentiated by ACBD6

phosphorylation at Ser106 and Ser108.[23] Of note is that ACBD6 binds to NMT2 about 10-fold better than to NMT1 potentially acting as a regulator of the differences between the two NMTs.[22] While it is clear that ACBD6 acts as an activator of NMT, the underlying mechanism warrants clarification on whether and how it guards the acyl-CoA specificity or whether it allosterically promotes peptide substrate binding. NMT does not seem to efficiently utilize acyl-CoAs with shorter chains such as the far more abundant acetyl-CoA, likely because the binding affinities of these short-chain acyl-CoA are too low.

There is also evidence for substrate-specific regulation of NMT activity. The cellular senescence-inhibited gene (CSIG) was shown to enhance the interaction between NMT1 and the serine/threonine protein phosphatase PPM1A promoting PPM1A myristoylation, which enhances its phosphatase activity on SMAD2 to inhibit TFG-β signaling.[25] Other interactions might regulate NMT localization. While NMT is thought to be largely cytosolic, its interactions with calnexin[26] and ribosomes[27] are thought to keep some of the enzyme at the endoplasmic reticulum.

In vitro, a truncation of 28 amino acids from the N-terminus of NMT1 catalytic domain resulted in a ~3 fold increase in the enzyme activity suggesting that additional post-translational modifications can further modulate the enzyme function.[28] During apoptosis, proteolytic cleavage regulates NMT localization. Both human NMT1 and NMT2 are cleaved in a time-dependent manner upon induction of apoptosis with Staurosporine and anti-Fas antibody in Hela and Jurkat T cells.[29, 30] NMT1 is cleaved by Caspases-3 and -8 at Asp81, while NMT2 is cleaved at Asp 25 by caspase-3. This leads to the re-localization of NMT1 from the membrane to the cytosol, while the opposite is observed for NMT2.[30] The truncated NMTs appear to remain the same activity level, but are thought to recognize substrates that can act either in a pro-survival or pro-apoptosis manner. At the same time proteolysis generates new substrates of NMT.[29] For

example, a pro-apoptotic protein BID is cleaved by caspase 8, which exposes an N-terminal glycine on a 15 kDa fragment that gets myristoylated by NMT.[31] This targets the cleaved BID to the outer mitochondrial membrane to promote cytochrome c release and subsequent cell death. The discovery of this sophisticated molecular switch regulating apoptosis opened an avenue for understanding the mechanism of posttranslational myristoylation by NMT.

Human NMT1 and NMT2 are 77% identical at the amino acid sequence with the greatest divergence at their N-termini. In basal conditions they appear to have largely overlapping substrates, so their differential processing during proteolytic stress might result in more divergent substrate profiles, yet this warrants more investigation. Interestingly, NMT2 knockdown in SKOV-3 cells induced apoptosis to a greater extent than NMT1 knockdown hinting that the two human NMT enzymes might have different functions in regulating cell survival.[32] The catalytic domains of NMT1 and NMT2 are nearly identical and the most divergence comes from the N-terminus. There is no structure reported for the N-terminus of NMT1 or NMT2, which hinders the understanding of this region. The two NMTs have nonoverlapping roles as NMT2 is typically unable to compensate for NMT1 depletion. Further investigation into the potential regulation of this region by metabolite binding, protein or nucleic acid interactions and post-translational modification might shed light on the need for the two NMT enzymes in higher eukaryotes.

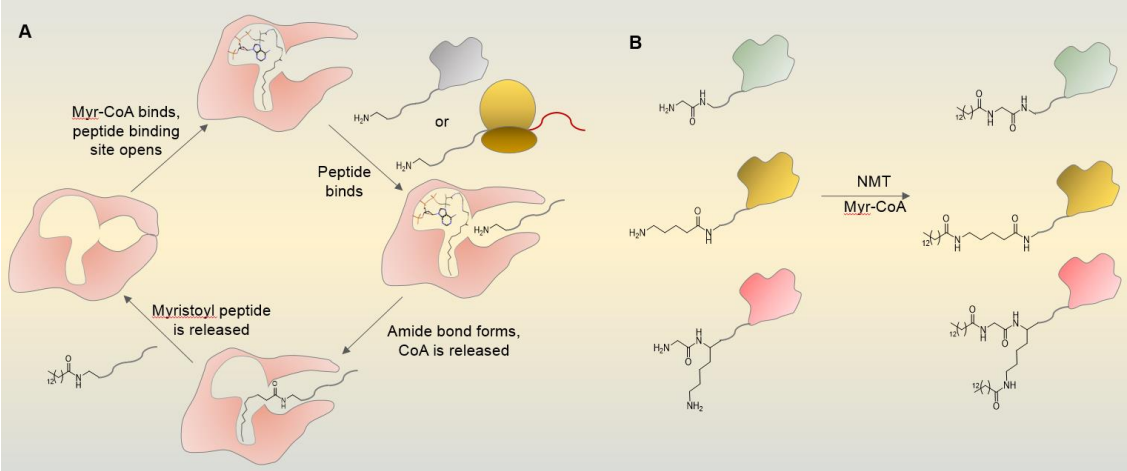

Figure 1.1 Mechanism of NMT-catalyzed myristoylation. Mechanism of NMT-catalyzed myristoylation. (A) Myristoyl-CoA binds to NMT in a question mark-like fashion. This causes a conformational change that opens the peptide-binding site. Peptide substrate of a folded protein or nascent peptide with a sterically unhindered N-terminal amino group binds to NMT allowing amide bond formation between the amino group and the myristoyl group and release of CoA. The modified peptide exits the active site and the enzyme is ready for the next catalytic cycle. (B) NMT can myristoylate the amino groups of N-terminal glycine, lysine, or both.

NMT IS THE FIRST MAMMALIAN LYSINE FATTY ACYL TRANSFERASE

It was recently established that human NMT1 and NMT2 also act as mammalian lysine fatty acyl transferases. While lysine fatty acylation has been known to occur on mammalian proteins for nearly two decades[33], the enzymes catalyzing such lysine modifications remained unknown. The amino group of the N-terminal glycine and that of the lysine side chain are chemically similar displaying similar lengths and steric properties where both are free to rotate, hinting that both could react in the active site of NMT. The modification of a Lys3 residue would be similar to the modification of a Gly2 (Figure 1.2). In vitro and in cells NMT can myristoylate lysine residues positioned near the N-terminus with decreased catalytic ability as the lysine moves away from the N-terminus.[34] The overall catalytic mechanism appears similar to that of the N-terminal glycine, yet the structural data suggest that the solvent channel may not facilitate the reaction on lysine as the C-terminus catalytic base interacts directly with the Nε in contrast to the indirect interaction through a water molecule with the Nα of the N-terminal glycine.[10] The first cellular lysine myristoylation substrate is the small GTPase ADP-

ribosylation factor (ARF6), which has a Lys3 following the N-terminal Gly2. After the reaction at the N-terminus, the Gly-myristoyl might move into the solvent channel positioning Lys3 into the catalytic center. These studies expand the repertoire of the NMT substrates: it can act on glycine, lysine, or both when located at the N-terminus (Figure 1.1B).

Interestingly, unlike other GNAT family enzymes, NMT contains two GNAT domains thought to result from gene duplication[35] with the solvent channel in the second domain. This channel is lined with hydrophobic residues and is of a similar length to the canonical myristoyl pocket allowing speculation that while the second domain lost its catalytic function, it might have retained its ability to hold a myristoyl group, which can explain the di-myristoylation ability of NMT. The second pocket, therefore, may serve as both the facilitator of the deprotonation event during Gly myristylation and the binding pocket for the Gly-myristoyl moiety during di-myristoylation. While the NMT sequence preference for lysine myristoylation is similar to that of glycine, in vitro and cellular studies suggest that the reaction on lysine might be regulated by the 3D structure of the substrate protein. Interestingly, in cells, NMT2 appears a better di-myristoyltransferase than NMT1, which again suggests an additional level of cellular regulation of this function.

Unlike glycine myristoylation, lysine myristoylation is reversible. SIRT2 is the eraser of ARF6 lysine myristoylation which is important for its localization and activation. Interestingly, it appears that SIRT2 prefers the GDP-bound form of ARF6 as the substrate, while NMT preferentially acts on ARF6-GTP. This substrate specificity allows the lysine myristoylation-demyristoylation cycle to connect to and drive the GTPase cycle (Figure 1.3). The newly identified reversible lysine myristoylation-demyristoylation cycle opens an avenue

for future studies to further characterize the new function of NMT, identify additional substrates, and understand its other functional consequences.

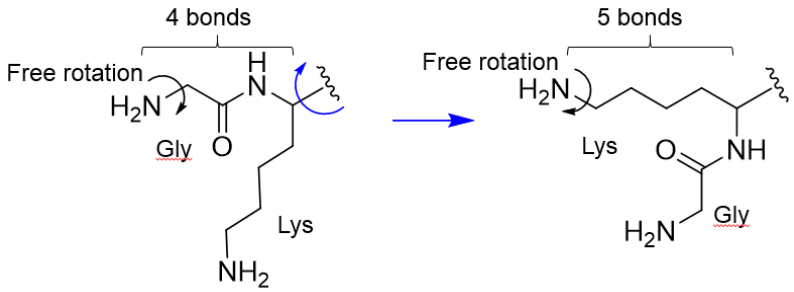

Figure 1.1 Similarities between the N-terminal glycine and lysine. In both cases, the amino groups are free to rotate and are a similar distance away from the Cα of lysine.

FUNCTIONAL EFFECTS OF N-MYRISTOYLATION

N-myristoylation most often serves as a protein membrane targeting signals such as that in the ARF, Src, and G protein families. The hydrophobic myristoyl chain can insert into the lipid bilayer anchoring proteins to membranes where they get activated and perform their roles. The G2A mutants of N-terminally myristoylated proteins are typically inactive. To date, no erasers of N-terminal glycine myristoylation have been identified, but the membrane-binding cycle is known to be regulated by other switch mechanisms. Ca^{+}-dependent myristoyl switches have been described for several proteins: among them are hippocalcin,[36] recoverin[37], and visin-like protein 3.[38] The ARF proteins, like ARF1, use nucleotide binding to turn the myristoyl switch on and off. In the GDP bound state, the N-terminal helix along with its myristoyl chain is sequestered into a hydrophobic pocket, but the exchange to GTP facilitated by GEFs causes a conformation change that extrudes the myristoylated N-terminal helix allowing its insertion into membranes. Upon GTP hydrolysis accelerated by GTPase activating proteins (GAPs), the myristoyl moiety is again sequestered releasing the ARF protein from the membrane (Figure 1.3).[39, 40] A myristoyl binding site was recently identified in the SH3 domain of c-Src. In the presence of lipid membranes, the myristoyl group is released and inserted into the lipid layer

allowing c-Src activation and transforming ability.[41] How c-Src switches between membrane-bound and cytosolic forms is an area of active research. In contrast to c-Src, the elegant study by Hantschel et al. demonstrated that the N-terminal myristoylation of another tyrosine kinase c-Abl does not regulate its membrane binding and is inhibitory to the enzyme's kinase activity.[42] The G2A mutation abrogates myristoylation leading to a dramatic increase in phosphotyrosine levels and kinase activity of c-Abl. Surprisingly, the mutation does not affect c-Abl localization as demonstrated by subcellular fractionation and macroscopy studies. This is a rare case of a myristoylation control of an enzyme activity that is independent of membrane binding.

A second membrane targeting signal such as a basic patch or palmitoylation of a nearby cysteine is often necessary for an efficient plasma membrane binding. Such mechanisms are utilized by the Src and G proteins where cysteine palmitoylation is catalyzed by one of the 23 human DHHC enzymes.[43, 44] The lysine myristoylation on ARF6 discussed above also represents a second membrane targeting signal that is regulated by the enzyme SIRT2. ARFs 1-5 reside in the Golgi and regulate the ER-Golgi transport while ARF6 is found at the plasma membrane and endosomes and, unlike other ARFs tends to remain membrane-bound during its GTPase cycle (Figure 1.3).[45] The second acylation on lysine allows efficient membrane anchoring of ARF6 and membrane retention even when it is inactive.[34] Further studies are needed to understand how widespread this mode of regulation is in the mammalian proteome.

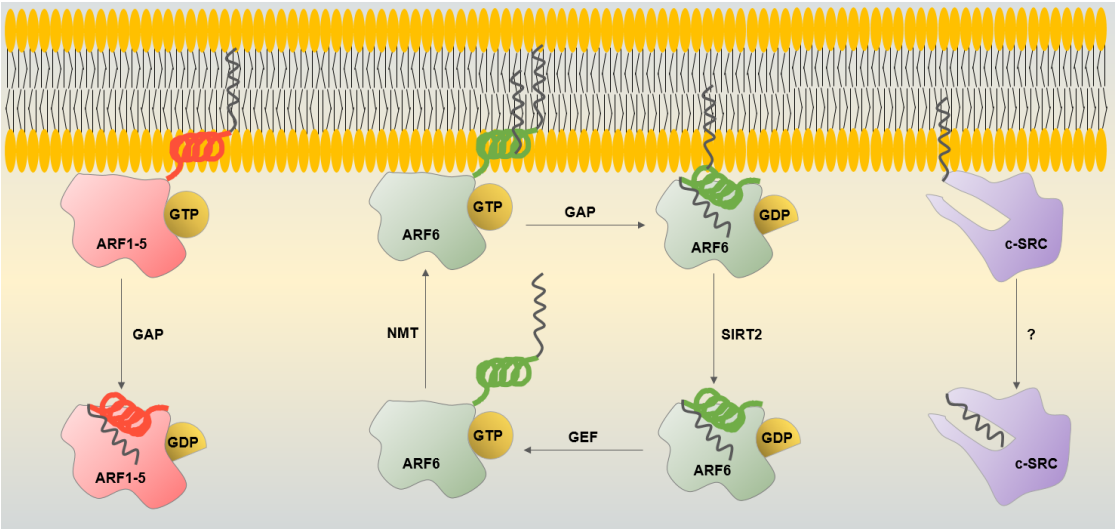

Figure 1.2 Myristoyl switches of ARF GTPases and c-Src. ARF1-5 are membrane-bound in the GTP-bound state via their amphipathic helix with one myristoyl group. The GTP hydrolysis facilitated by GAP causes a conformational change that sequesters the myristoylated helix releasing ARF1-5 from membranes. ARF6 has an additional myristoyl chain on lysine 3 that helps to retain ARF6-GDP on the plasma membrane and endomembranes. SIRT2 removes lysine myristoylation allowing ARF6-GDP to be activated by GEF. NMT myristoylates lysine 3 of ARF6-GTP, promoting its plasma membrane localization and completing the cycle. c-Src contains a hydrophobic pocket in its SH3 domain, that sequesters the myristoyl chain, but what causes the switch is unclear.

N-MYRISTOYLATION PROMOTES CANCER PROGRESSION

Targeting human NMT has recently emerged as a therapeutic strategy to treat cancer. Colon, gallbladder, and brain tumors have been shown to have elevated levels of NMT suggesting the reliance of cancer cells on protein myristoylation.[46-48] The elevation of NMT2 in osteosarcoma might be contributing to the chemoresistance of this disease.[49] Similarly, a down-regulation of miR-181c that among other genes targets NMT2 is found in imatinib-resistant chronic myeloid leukemia.[50] This suggests that NMT2 levels can be used as a predictor of response to chemotherapeutics. Interestingly, an NMT inhibitor PCLX-001, which is also called DDD86481[51] (Figure 1.4), is effective against NMT2 deficient blood cancers and is being advanced to clinical trials.[52] The fact that it works well in NMT2-deficient blood cancers could be related to the chemoresistance effect of NMT2. Alternatively, it could be that lower levels of NMT2 make the cells more easily to be inhibited by PCLX-001.

There could be multiple mechanisms for the anticancer effects of NMT inhibition. In breast cancer, including triple-negative breast cancer, the knockdown of NMT1 suppresses tumor initiation, proliferation, and invasion by promoting oxidative and ER stress, which in turn activates autophagy via the JNK pathway.[53] Quantitative proteomics revealed that the ER stress followed by cell cycle arrest and apoptosis was also induced in breast and colon cancer cell models upon small molecule-mediated NMT inhibition.[54] The inhibition of the cell cycle was also observed in prostate cancer upon NMT knockdown or inhibition with a myristoyl-CoA analog B13. This cell cycle arrest led to the suppression of malignant growth and invasion, which occurred via the inhibition of Src myristoylation and subsequent downregulation of its oncogenic signaling.[55] In MCF7 estrogen receptor-positive breast cancer cells, mTOR inhibition with rapamycin leads to NMT1 upregulation.[56] NMT1 promotes lung cancer cell viability by supporting mitophagy. This occurs via the AMPKβ myristoylation that is required for the AMPK recruitment to the mitochondria where it physically associates with ATG16 and ATG5-12 and recruits VPS34 and ATG16 during mitochondrial damage. NMT1 mediated targeting to mitochondria is sufficient to initiate mitophagy and to promote cancer cell survival.[57] Thus, NMT plays an important role in multiple cancers. However, given the NMT regulation of different substrate proteins in both normal cells and cancer cells, anti-cancer targeting of NMT would benefit from selective inhibition of NMT in cancer cells over normal cells.

NMT IN THE IMMUNE RESPONSE

It is becoming more evident that NMT acts as a guardian of the immune response by regulating myelopoiesis, lymphopoiesis, innate immune response, and the immunological synapse.[58] NMT1 is essential to monocytic differentiation during which the NMT activity is modulated by the expression levels of the enzyme and its inhibitor protein HSC70. NMT1 deficient mouse embryonic fibroblasts are strongly impaired in differentiating into macrophages.[59] N-myristoylation also appears essential for thymocyte development and

function. In a mouse model with a lineage-specific T cell deficiency in NMT1 and NMT2, T cell development and activation are severely impaired suggesting that N-myristoylation positively regulates immune response. Unlike the NMT1 thymocyte mutant mice, the NMT2 mutants demonstrate a largely wild type phenotype, but the double mutation strongly enhances the inhibition of T cell development and reduction in T cell numbers in the thymus, blood, lymph nodes, and spleen. The NMT deficiency leads to increased apoptosis during all stages of T cell development, decreased Erk phosphorylation, and mislocalization of myristoylated proteins.[60] Interestingly, in rheumatoid arthritis (RA) NMT appears to play an anti-inflammatory role. T cells from RA patients have low NMT1 levels which suppress the myristoylation-dependent AMPK lysosomal translocation and activation. This leads to hyperactivation of mTORC1 signaling in RA T cells promoting their differentiation into pro-inflammatory Th1 and Th17 cells aggravating RA. In a humanized mouse model where synovitis was induced by transferring human peripheral blood mononuclear cells and ingrafting human synovial tissue, NMT1 overexpression had a strong anti-inflammatory effect.[61] The inefficient mitophagy due to impaired AMPK function[57] may reconcile this observation in RA with the necessity for NMT activity during T cell development.[60] Mitochondrial dysfunction is the hallmark of RA and is thought to promote inflammation,[62, 63] which might be aggravated by the impaired clearance of damaged mitochondria as a result of suppressed AMPK myristoylation in RA.[64]

T cell maturation depends on the Notch1 signaling pathway.[65, 66] This might occur through the myristoylated Neutralized like-1 E3 ubiquitin ligase that facilitates the turnover and trafficking of Jagged, the Notch receptor ligand.[67, 68] In developed T cells, myristoylation of LCK governs an intricate trafficking mechanism of the kinase and is necessary for the LCK localization to the T cell immune synapse, the interface between the target cell and the T cell. The myristoyl group anchors LCK to membranes and acts as a signal for UNC119A binding that allows LCK extraction from the membranes and delivery to the synapse where it is released

with the help of ARL3 and ARL13B.[69] LCK phosphorylates immunoreceptor tyrosine-based activation motifs (ITAMs) that regulate signaling cascades essential for T cell activation. Myristoylated Fyn and c-Src orchestrate centrosome and actin-dependent movements during immune synapse. [58, 70] These reports point to a multifaceted and context-dependent role of NMT in the immune response which warrants further work to aid informed therapeutic interventions.

PARASITIC NMT AS A THERAPEUTIC TARGET IN MALARIA AND SLEEPING SICKNESS

Eukaryotic parasites have their own single NMT, which is being explored as a potential therapeutic target in infectious diseases like malaria and sleeping sickness. Malaria is caused by the infections with the species of the genus *Plasmodium* such as *Plasmodium falciparum* and leads to nearly a million deaths worldwide annually. The low vaccination efficacy and development of resistance to available therapies call for new therapeutic strategies. In 2014, over 30 NMT substrates were identified in *P. falciparum* using chemical proteomics. These proteins are involved in a range of functions such as protein trafficking, migration, development, and signaling pathways, suggesting that NMT is necessary for the parasite viability. This study identified a promising small molecule displaying selectivity towards PfNMT over hNMT and the ability to inhibit parasite viability and invasion of red blood cells. Excitingly, this agent caused a strong reduction in the rodent malaria parasite *P. berghei* in mice without acute toxicity to the animals.[71] A more recent high throughput screening identified 23 chemical classes of inhibitors that were selected for *Plasmodium* NMT over the human NMT enzymes, but further lead optimization is needed for in vivo testing.[72] To address a potential resistance of the parasite to NMT inhibition, another study identified the PfNMT G386E mutant that conferred resistance to the NMT inhibitor IMP-1002. DDD85646 could overcome this resistance suggesting that a combinatorial approach might be of use when targeting NMT in this disease.[73]

Sleeping sickness is another deadly infection caused by the *Trypanosoma brucei* parasites. Similar to *P. falciparum*, *T. brucei* has its own single NMT with more than 60

predicted substrates, some of which have been experimentally validated, and is being explored as a target against sleeping sickness. Administration of the NMT inhibitor DDD86546 cures trypanosomiasis in mice potentially through disruption of the endocytic pathway by inhibiting TbARF1 myristoylation.[74] A recent chemical proteomics study in the clinically relevant bloodstream form of the parasite identified 53 high confidence and 10 medium confidence NMT substrate hits, many of which overlapped with the predicted group. Among these substrates were phosphatases, ARF GTPases, calpain-like proteins, and several uncharacterized proteins.[75] *T. brucei* infection proceeds in two stages where it dwells in the bloodstream during the first stage and infects the nervous system in the second stage. This indicates the need for drugs able to cross the blood-brain barrier and a few promising leads were recently found.[76, 77] While it is clear that NMT is a promising therapeutic target in malaria and sleeping sickness, the understanding of the underlying mechanisms is lacking. Further identification of specific NMT-regulated substrates and pathways essential to parasite viability might facilitate the pathogen-specific therapeutic intervention.

VIRAL UTILIZATION OF THE HOST NMT

NMT has been widely explored as a therapeutic target for viral infections because many viruses use host NMT for increased pathogenesis (Table 1). Some of the known myristoylated viral proteins are the VP4 of poliovirus, hepatitis B virus pre-S1 protein and Gag and Nef of simian and human immunodeficiency viruses (SIV and HIV).[78] Myristoylation of Nef and Gag are essential to HIV-1 replication and virulence. Nef myristoylation induces endocytosis of CD4 on the surface of T cells, which prevents superinfections detrimental to cell survival,[79] and interestingly it is preferentially myristoylated by NMT2.[80] Myristoylation of Gag is necessary for its membrane association followed by the assembly and budding of new viral particles.[81] NMT1 enhances the replication of human immunodeficiency virus type-1 by increasing the expression of viral RNA.[82, 83]

Most picornaviruses such as poliovirus and coxsackievirus utilize host NMT for capsid protein myristoylation. The capsid protein VP0 is cleaved to VP2 and VP4 and shares the same myristoylated N-terminus with VP4. Genetic knockout of NMT1 or NMT2 in HAP1 cells demonstrated that only NMT1 is necessary for viral replication. Pharmacological inhibition of NMT with DDD85646 led to a strong reduction of myristoylation of VP0 and suppression of particle infectivity. Surprisingly, electron microscopy studies revealed that these particles were identical to the control particles and did not display a defect in cell attachment suggesting that lack of myristoylation might cause a defect in the transfer of viral RNA into the host cell.[84] However, the myristoylation of VP0 of rhinoviruses, the cause for respiratory diseases such as common cold, is necessary for the assembly of the viral capsid to support viral replication.[85] Interestingly, parechoviruses and kobuviruses that do not undergo VP0 cleavage are not affected by NMT inhibition suggesting that VP0 processing confers reliance on NMT.[84]

Dengue virus, the cause of dangerous dengue fever, appears to rely on NMT as well. NMT is upregulated during the infection of dendritic cells and it interacts with the viral envelope protein, while NMT gene silencing significantly suppresses dengue virus replication.[86] Thus far myristoylation of the Dengue viral proteins has only been predicted but lacks experimental proof, which is also true for many other viruses.[6] Coronaviruses such as those that caused SARS and COVID-19 pandemics are thought to lack myristoylation because they do not contain the preferred NMT recognition sequence, however, this has no experimental evidence.[78] Given the recent finding of the NMT activity towards lysine and the fluidity of NMT substrate recognition preference, it might be of use to reevaluate viral proteins for potential lysine substrate sites of NMT. For instance, the N-terminal sequence of SARS-CoV nsp4 protein is KIVSTCFK, and nsp4 of SARS-CoV2 and some bat viruses contain similar motifs with the N-terminal lysine, which raises curiosity in whether they are modified by NMT.

Viral protein myristoylation might be important in generating an immune response. X-ray crystallography analyses revealed that MHC class I proteins Mamu-B*05104 and Mamu-B*098 contain a large hydrophobic pocket that can bind a myristoylated glycine of the peptides C14-Gly-Gly-Ala-Ile and C14-Gly-Gly-Ala-Ile-Ser, respectively, which are derived from the viral Nef protein. Gly2 and Ala3 or Ile4 are exposed for the recognition by the cytotoxic T lymphocytes to initiate their activation.[87] While myristoylation of viral proteins has been known for decades, its inhibition as a therapeutic strategy is still at the stage of exploration. Given the importance of NMT to the function of normal cells, its inhibition might be toxic, therefore small molecule inhibitors with increased specificity for viral protein myristylation are needed. This could be aided by the identification of regulatory proteins of NMT. For instance, it is tempting to speculate that targeting ACBD6-NMT2 interaction could preferentially inhibit myristoylation of Nef, a better substrate of NMT2 than NMT1, given the preference of ACBD6 for NMT2 over NMT1.

Table 1.1 Myristoylated viral proteins. The table was adapted from Maurer-Stroh and Frank Eisenhaber, Trends in Microbiology, 2004.[6]

Protein	Virus	Function	N-terminal sequence	Ref.
Nef	Lentiviruses (HIV, SIV)	Membrane targeting to downregulate immune cell surface molecules	GGKWSKSSI	88
Gag	Retroviruses, Poxviruses (HIV)	Binds plasma membrane to initiate viral particle assembly		
❖ P17matrix protein	Lentiviruses (HIV, SIV, FIV)		GARASVLSG	89
❖ P15 matrix protein	Gammaretroviruses (e.g. murine and feline leukemia viruses, rat and avian sarcoma virus, avian spleen necrosis virus, baboon and porcine endogenous retroviruses, reticuloendotheliosis virus), human endogenous retrovirus S71, Poxviridae (Fowl pox)		GQTITTPLS	90
❖ P10 matrix protein	Betaretroviruses (mouse mammary tumor virus, Mason-Pfizer monkey virus, simian retrovirus 2, ovine pulmonary adenocarcinoma virus), wooly monkey sarcoma virus, human endogenous retrovirus K, hamster intracisternal A-particle and python endogenous retrovirus		GVSGSKGQK	91

❖ P19 protein of nucleocapsid inner layer	Deltaretroviruses (human/simian T-cell lymphotropic virus, bovine leukemia virus)		GQIFSRSAS	92
VP4 coat protein	Picornaviridae [rhino-, cardio-, aphtho-, entero- (echo-, coxsackie-, polio-) viruses]	Virion assembly	GAQVSTQKS	93
Large surface antigen	Hepadnaviridae (hepatitis B virus)	Essential for viral infectivity but not assembly	GQNLSTSNP	94
L1R envelope protein	Poxviridae [Chordopoxvirinae (e.g. variola, vaccinia)and Enteropoxvirinae], Asfiviridae, Iridoviridae (lymphocysti-, rana-, iridovirus), Ascoviridae (Ascovirus)	Membrane targeting and virion assembly	GAAASIQTT	95, 96
v-src	Rous sarcoma virus	Membrane binding necessary for oncogenic transformation	GSSKSKPKD	97, 98
A16L late protein	Poxviridae [Chordopoxvirinae (e.g. variola, vaccinia) and Enteropoxvirinae]	Protein associates with viral, not cellular, structures	GAAVTLNRI	99, 100
VP2 coat protein	Polyomaviruses	Viral assembly and infectivity	GAALALLGD	101, 102
G9R	Poxviridae [Chordopoxvirinae (e.g. variola, vaccinia)]	Protein associates with viral, not cellular, structures	GGGVSVELP	99
UL11	Alphaherpesvirinae (simplex-, varicello-, Marek's disease-like and infectious laryngotracheitis-like viruses)	Association with lipid rafts	GLSFSGARP	103, 104
UL99, U71, BBLF1	Betaherpesvirinae (roseolo-, cytomegalo-, muromegalovirus), Gammaherpesvirinae (e.g. lymphocryptovirus), Alphaherpesvirinae	Association with ERGIC necessary for virion assembly	GAELCKRIC GAKCCKPVS GALWSLCRR	105
Major outer capsid protein µ1	Ortho- and aquareoviruses	Cleavage of µ1 to µ1C	GNASSIVQT	106
E7R	Orthopoxviruses	Soluble protein	GTAATIQTP	99
Polyprotein pp220	Asfivirus	Potential membrane-anchor regulating core assembly	GNRGSSTSS	107, 108
Membrane fusion protein p15	Orthoreovirus	Required for membrane fusion activity	GQRHSIVQP	109, 110

PHARMACOLOGICAL TARGETING OF NMT

Because of the mentioned earlier roles of NMT in cancer and parasitic and viral infections, inhibition of N-myristoylation has been explored as an attractive therapeutic strategy against these diseases. 2-hydroxymyristic acid, D-NMAPPD (B13), or Tris-DBA palladium,

IMP-366 (DDD85646), PCLX-001(DDD86481) and IMP-1088 are most commonly used pan-N-myristoylation inhibitors (Figure 1.4). The high structural similarity between NMT1 and NMT2 poses a challenge for the design of NMT1/NMT2-selective inhibitors and there have been no reports of such selective small molecules so far. A recent comparison of the potency and selectivity of the widely used NMT inhibitors revealed that 2-hydroxymyristic acid, D-NMAPPD, and Tris-DBA palladium are poor inhibitors of NMT. D-NMAPPD and Tris-DBA palladium cause off-target mediated cell cytotoxicity. In the same study IMP-366 (DDD85646) and IMP-1088 appeared as highly specific and potent inhibitors of NMT1 and NMT2 with nanomolar IC_{50} values.[111]

Small molecule NMT inhibition has shown therapeutic potential in viral and parasitic infections and cancer. 2-Hydroxymyristic acid was shown to suppress replication of enterovirus 71, [112] while the recently discovered IMP-1088 had a therapeutic potential against rhinovirus by inhibiting capsid protein myristoylation.[85] DDD85646 is the most widely used NMT inhibitor that can suppress picornavirus replication via the host NMT inhibition,[84] as well as malaria and sleeping sickness parasites by inhibiting their NMTs.[73-75] In addition, DDD85646 suppressed breast and colon cancer cell growth by inducing ER stress and consequent cell cycle arrest and apoptosis.[54] PCLX-001 (DDD864) is being advanced to clinical trials for treating hematologic cancers by Pacylex, which represents the most promising NMT inhibitor in cancer treatment. An anticancer effect was also achieved with D-NMAPPD, a myristoyl-CoA analog that has been reported to suppress prostate cancer progression by inhibiting Src myristoylation,[55] and Tris-DBA palladium that was effective against melanoma.[113] Further understanding of the differences in structure and regulation between human and pathogenic NMTs and between

human NMT1 and NMT2 could aid the development of small molecules with increased selectivity and decreased toxicity.

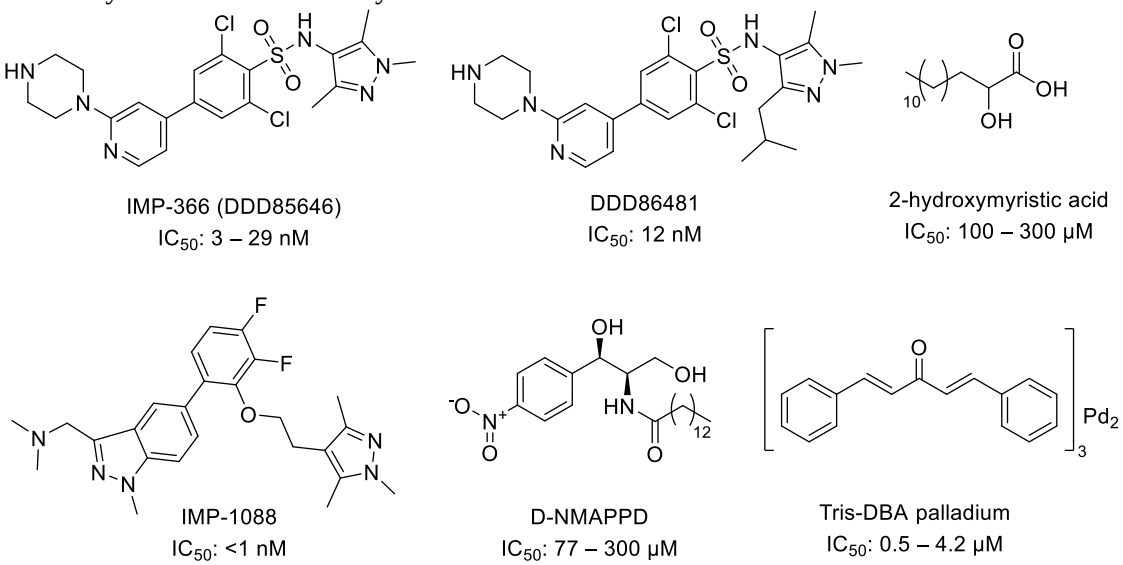

Figure 1.4 Structures and IC50 of small molecule NMT inhibitors.

CONCLUSIONS AND OUTSTANDING QUESTIONS

In recent years much has been learned about the catalytic mechanism and physiological functions of NMT. This knowledge opened several exciting and important research avenues. Given the nearly identical catalytic domains of the two human NMT enzymes, the necessity for both remains elusive and is likely hidden in the divergence of their N-termini that could potentially differ in protein, metabolite, or nucleic acid binding and posttranslational modifications. This area remains underexplored perhaps in part due to the unstructured nature of these regions. Furthermore, additional work is needed to identify NMT regulators and to understand the NMT selectivity for myristoyl-CoA and its mechanism of activation by ACBD6.

NMT has recently emerged as the first mammalian lysine myristoyltransferase with so far a single protein substrate, ARF6. Interestingly, in cells, NMT2 appears as a more potent lysine transferase than NMT1 due to an unknown level of regulation. It is of interest to further characterize the differences in the two activities of NMT, identify new lysine substrates while including viral proteins in evaluation, and determine the physiological implications of the lysine

modification. Exploring conditions of proteolysis could aid the identification of new substrates followed by finding lysine myristoylation erasers such as sirtuins or HDACs. In cancer, there is a need for more mechanistic understandings of how NMT controls the oxidative and ER stress and whether NMT regulates cancer stemness. The role of NMT in immunity appears context-dependent, which is important to consider in evaluating NMT as a modulatory node for inflammation. Having this knowledge could aid in the development of highly selective NMT inhibitors with therapeutic potential.

ACKNOWLEDGMENTS

The work was supported by the NSF Graduate Research Fellowship Program and SUNY Diversity fellowship as well as NIH/NIDDK grant R01DK107868.

REFERENCES

1. Manenti, S., Sorokine, O., Van Dorsselaer, A. & Taniguchi, H. Demyristoylation of the major substrate of protein kinase C (MARCKS) by the cytoplasmic fraction of brain synaptosomes. *J Biol Chem* **269**, 8309-8313 (1994).
2. Timms, R.T. *et al.* A glycine-specific N-degron pathway mediates the quality control of protein N-myristoylation. *Science* **365**, eaaw4912 (2019).
3. Duronio, R.J., Towler, D.A., Heuckeroth, R.O. & Gordon, J.I. Disruption of the yeast N-myristoyl transferase gene causes recessive lethality. *Science* **243**, 796-800 (1989).
4. Weinberg, R.A. *et al.* Genetic studies reveal that myristoylCoA:protein N-myristoyltransferase is an essential enzyme in Candida albicans. *Mol Microbiol* **16**, 241-250 (1995).
5. Lodge, J.K., Jackson-Machelski, E., Toffaletti, D.L., Perfect, J.R. & Gordon, J.I. Targeted gene replacement demonstrates that myristoyl-CoA: protein N-myristoyltransferase is essential for viability of Cryptococcus neoformans. *Proc Natl Acad Sci U S A* **91**, 12008-12012 (1994).
6. Maurer-Stroh, S. & Eisenhaber, F. Myristoylation of viral and bacterial proteins. *Trends Microbiol* **12**, 178-185 (2004).
7. Yang, S.H. *et al.* N-myristoyltransferase 1 is essential in early mouse development. *J Biol Chem* **280**, 18990-18995 (2005).
8. Ntwasa, M., Aapies, S., Schiffmann, D.A. & Gay, N.J. Drosophila embryos lacking N-myristoyltransferase have multiple developmental defects. *Exp Cell Res* **262**, 134-144 (2001).
9. Bhatnagar, R.S. *et al.* Structure of N-myristoyltransferase with bound myristoylCoA and peptide substrate analogs. *Nat Struct Biol* **5**, 1091-1097 (1998).
10. Dian, C. *et al.* High-resolution snapshots of human N-myristoyltransferase in action illuminate a mechanism promoting N-terminal Lys and Gly myristoylation. *Nat Commun* **11**, 1132 (2020).

11. Towler, D. & Glaser, L. Protein fatty acid acylation: enzymatic synthesis of an N-myristoylglycyl peptide. *Proc Natl Acad Sci U S A* **83**, 2812-2816 (1986).
12. Farazi, T.A., Waksman, G. & Gordon, J.I. Structures of Saccharomyces cerevisiae N-myristoyltransferase with bound myristoylCoA and peptide provide insights about substrate recognition and catalysis. *Biochemistry* **40**, 6335-6343 (2001).
13. Jiang, H. *et al.* Protein Lipidation: Occurrence, Mechanisms, Biological Functions, and Enabling Technologies. *Chemical reviews* **118**, 919-988 (2018).
14. Castrec, B. *et al.* Structural and genomic decoding of human and plant myristoylomes reveals a definitive recognition pattern. *Nat Chem Biol* **14**, 671-679 (2018).
15. Towler, D.A. *et al.* Purification and characterization of yeast myristoyl CoA:protein N-myristoyltransferase. *Proc Natl Acad Sci U S A* **84**, 2708-2712 (1987).
16. Towler, D.A. *et al.* Myristoyl CoA:protein N-myristoyltransferase activities from rat liver and yeast possess overlapping yet distinct peptide substrate specificities. *J Biol Chem* **263**, 1784-1790 (1988).
17. Traverso, J.A., Giglione, C. & Meinnel, T. High-throughput profiling of N-myristoylation substrate specificity across species including pathogens. *Proteomics* **13**, 25-36 (2013).
18. Rioux, V. & Legrand, P. Saturated fatty acids: simple molecular structures with complex cellular functions. *Curr Opin Clin Nutr Metab Care* **10**, 752-758 (2007).
19. Rudnick, D.A. *et al.* Analogs of palmitoyl-CoA that are substrates for myristoyl-CoA:protein N-myristoyltransferase. *Proc Natl Acad Sci U S A* **89**, 10507-10511 (1992).
20. Kishore, N.S. *et al.* Comparison of the acyl chain specificities of human myristoyl-CoA synthetase and human myristoyl-CoA:protein N-myristoyltransferase. *J Biol Chem* **268**, 4889-4902 (1993).
21. Bhatnagar, R.S., Jackson-Machelski, E., McWherter, C.A. & Gordon, J.I. Isothermal titration calorimetric studies of Saccharomyces cerevisiae myristoyl-CoA:protein N-myristoyltransferase. Determinants of binding energy and catalytic discrimination among acyl-CoA and peptide ligands. *J Biol Chem* **269**, 11045-11053 (1994).
22. Soupene, E. *et al.* Association of NMT2 with the acyl-CoA carrier ACBD6 protects the N-myristoyltransferase reaction from palmitoyl-CoA. *J Lipid Res* **57**, 288-298 (2016).
23. Soupene, E. & Kuypers, F.A. ACBD6 protein controls acyl chain availability and specificity of the N-myristoylation modification of proteins. *J Lipid Res* **60**, 624-635 (2019).
24. Soupene, E., Schatz, U.A., Rudnik-Schoneborn, S. & Kuypers, F.A. Requirement of the acyl-CoA carrier ACBD6 in myristoylation of proteins: Activation by ligand binding and protein interaction. *PLoS One* **15**, e0229718 (2020).
25. Zhu, F. *et al.* The Cellular Senescence-Inhibited Gene Is Essential for PPM1A Myristoylation To Modulate Transforming Growth Factor beta Signaling. *Mol Cell Biol* **38**, e00414-00418 (2018).
26. Dudek, E. *et al.* N-Myristoyltransferase 1 interacts with calnexin at the endoplasmic reticulum. *Biochem Biophys Res Commun* **468**, 889-893 (2015).
27. Glover, C.J., Hartman, K.D. & Felsted, R.L. Human N-myristoyltransferase amino-terminal domain involved in targeting the enzyme to the ribosomal subcellular fraction. *J Biol Chem* **272**, 28680-28689 (1997).
28. Kumar, S. & Sharma, R.K. N-terminal region of the catalytic domain of human N-myristoyltransferase 1 acts as an inhibitory module. *PLoS One* **10**, e0127661 (2015).
29. Thinon, E. *et al.* Global profiling of co- and post-translationally N-myristoylated proteomes in human cells. *Nat Commun* **5**, 4919 (2014).

30. Perinpanayagam, M.A. *et al.* Regulation of co- and post-translational myristoylation of proteins during apoptosis: interplay of N-myristoyltransferases and caspases. *FASEB J* **27**, 811-821 (2013).
31. Zha, J., Weiler, S., Oh, K.J., Wei, M.C. & Korsmeyer, S.J. Posttranslational N-myristoylation of BID as a molecular switch for targeting mitochondria and apoptosis. *Science* **290**, 1761-1765 (2000).
32. Ducker, C.E., Upson, J.J., French, K.J. & Smith, C.D. Two N-myristoyltransferase isozymes play unique roles in protein myristoylation, proliferation, and apoptosis. *Mol Cancer Res* **3**, 463-476 (2005).
33. Stevenson, F.T., Bursten, S.L., Locksley, R.M. & Lovett, D.H. Myristyl acylation of the tumor necrosis factor alpha precursor on specific lysine residues. *J Exp Med* **176**, 1053-1062 (1992).
34. Kosciuk, T. *et al.* NMT1 and NMT2 are lysine myristoyltransferases regulating the ARF6 GTPase cycle. *Nat Commun* **11**, 1067 (2020).
35. Weston, S.A. *et al.* Crystal structure of the anti-fungal target N-myristoyl transferase. *Nat Struct Biol* **5**, 213-221 (1998).
36. O'Callaghan, D.W., Tepikin, A.V. & Burgoyne, R.D. Dynamics and calcium sensitivity of the Ca2+/myristoyl switch protein hippocalcin in living cells. *J Cell Biol* **163**, 715-721 (2003).
37. Ames, J.B. *et al.* Molecular mechanics of calcium-myristoyl switches. *Nature* **389**, 198-202 (1997).
38. Li, C., Lim, S., Braunewell, K.H. & Ames, J.B. Structure and Calcium Binding Properties of a Neuronal Calcium-Myristoyl Switch Protein, Visinin-Like Protein 3. *PLoS One* **11**, e0165921 (2016).
39. Randazzo, P.A. *et al.* The myristoylated amino terminus of ADP-ribosylation factor 1 is a phospholipid- and GTP-sensitive switch. *The Journal of biological chemistry* **270**, 14809-14815 (1995).
40. Kahn, R.A. *et al.* The amino terminus of ADP-ribosylation factor (ARF) is a critical determinant of ARF activities and is a potent and specific inhibitor of protein transport. *J Biol Chem* **267**, 13039-13046 (1992).
41. Le Roux, A.L. *et al.* A Myristoyl-Binding Site in the SH3 Domain Modulates c-Src Membrane Anchoring. *iScience* **12**, 194-203 (2019).
42. Hantschel, O. *et al.* A myristoyl/phosphotyrosine switch regulates c-Abl. *Cell* **112**, 845-857 (2003).
43. Wedegaertner, P.B., Wilson, P.T. & Bourne, H.R. Lipid modifications of trimeric G proteins. *J Biol Chem* **270**, 503-506 (1995).
44. Koegl, M., Zlatkine, P., Ley, S.C., Courtneidge, S.A. & Magee, A.I. Palmitoylation of multiple Src-family kinases at a homologous N-terminal motif. *Biochem J* **303 (Pt 3)**, 749-753 (1994).
45. Peters, P.J. *et al.* Overexpression of wild-type and mutant ARF1 and ARF6: distinct perturbations of nonoverlapping membrane compartments. *J Cell Biol* **128**, 1003-1017 (1995).
46. Raju, R.V., Moyana, T.N. & Sharma, R.K. N-Myristoyltransferase overexpression in human colorectal adenocarcinomas. *Exp Cell Res* **235**, 145-154 (1997).
47. Rajala, R.V., Radhi, J.M., Kakkar, R., Datla, R.S. & Sharma, R.K. Increased expression of N-myristoyltransferase in gallbladder carcinomas. *Cancer* **88**, 1992-1999 (2000).
48. Lu, Y. *et al.* Expression of N-myristoyltransferase in human brain tumors. *Neurochem Res* **30**, 9-13 (2005).

49. Walters, D.K. *et al.* Identification of potential chemoresistance genes in osteosarcoma. *Anticancer Res* **28**, 673-679 (2008).
50. Mosakhani, N., Mustjoki, S. & Knuutila, S. Down-regulation of miR-181c in imatinib-resistant chronic myeloid leukemia. *Mol Cytogenet* **6**, 27 (2013).
51. Fang, W. *et al.* N-myristoyltransferase is a cell wall target in Aspergillus fumigatus. *ACS Chem Biol* **10**, 1425-1434 (2015).
52. Berthiaume, L.G. & Beauchamp, E., Vol. US 20180208990A1. (ed. P.P. Inc.) 1-23 (US; 2018).
53. Deng, L. *et al.* NMT1 inhibition modulates breast cancer progression through stress-triggered JNK pathway. *Cell Death Dis* **9**, 1143 (2018).
54. Thinon, E., Morales-Sanfrutos, J., Mann, D.J. & Tate, E.W. N-Myristoyltransferase Inhibition Induces ER-Stress, Cell Cycle Arrest, and Apoptosis in Cancer Cells. *ACS Chem Biol* **11**, 2165-2176 (2016).
55. Kim, S. *et al.* Blocking Myristoylation of Src Inhibits Its Kinase Activity and Suppresses Prostate Cancer Progression. *Cancer Res* **77**, 6950-6962 (2017).
56. Jacquier, M. *et al.* Investigation of Novel Regulation of N-myristoyltransferase by Mammalian Target of Rapamycin in Breast Cancer Cells. *Sci Rep* **8**, 12969 (2018).
57. Liang, J. *et al.* Myristoylation confers noncanonical AMPK functions in autophagy selectivity and mitochondrial surveillance. *Nat Commun* **6**, 7926 (2015).
58. Udenwobele, D.I. *et al.* Myristoylation: An Important Protein Modification in the Immune Response. *Front Immunol* **8**, 751 (2017).
59. Shrivastav, A. *et al.* Requirement of N-myristoyltransferase 1 in the development of monocytic lineage. *J Immunol* **180**, 1019-1028 (2008).
60. Rampoldi, F. *et al.* Immunosuppression and Aberrant T Cell Development in the Absence of N-Myristoylation. *J Immunol* **195**, 4228-4243 (2015).
61. Wen, Z. *et al.* N-myristoyltransferase deficiency impairs activation of kinase AMPK and promotes synovial tissue inflammation. *Nat Immunol* **20**, 313-325 (2019).
62. Valcarcel-Ares, M.N. *et al.* Mitochondrial dysfunction promotes and aggravates the inflammatory response in normal human synoviocytes. *Rheumatology (Oxford)* **53**, 1332-1343 (2014).
63. Falconer, J. *et al.* Review: Synovial Cell Metabolism and Chronic Inflammation in Rheumatoid Arthritis. *Arthritis Rheumatol* **70**, 984-999 (2018).
64. Krysko, D.V. *et al.* Emerging role of damage-associated molecular patterns derived from mitochondria in inflammation. *Trends Immunol* **32**, 157-164 (2011).
65. Deftos, M.L., Huang, E., Ojala, E.W., Forbush, K.A. & Bevan, M.J. Notch1 signaling promotes the maturation of CD4 and CD8 SP thymocytes. *Immunity* **13**, 73-84 (2000).
66. MacDonald, H.R., Wilson, A. & Radtke, F. Notch1 and T-cell development: insights from conditional knockout mice. *Trends Immunol* **22**, 155-160 (2001).
67. Koutelou, E. *et al.* Neuralized-like 1 (Neurl1) targeted to the plasma membrane by N-myristoylation regulates the Notch ligand Jagged1. *J Biol Chem* **283**, 3846-3853 (2008).
68. Lee, H.J. *et al.* Fe65 negatively regulates Jagged1 signaling by decreasing Jagged1 protein stability through the E3 ligase Neuralized-like 1. *Biochim Biophys Acta* **1853**, 2918-2928 (2015).
69. Stephen, L.A. *et al.* The Ciliary Machinery Is Repurposed for T Cell Immune Synapse Trafficking of LCK. *Dev Cell* **47**, 122-132 e124 (2018).
70. Martin-Cofreces, N.B. *et al.* Role of Fyn in the rearrangement of tubulin cytoskeleton induced through TCR. *J Immunol* **176**, 4201-4207 (2006).
71. Chan, X.W. *et al.* Chemical and genetic validation of thiamine utilization as an antimalarial drug target. *Nat Commun* **4**, 2060 (2013).

72. Harupa, A. *et al.* Identification of Selective Inhibitors of Plasmodium N-Myristoyltransferase by High-Throughput Screening. *J Med Chem* **63**, 591-600 (2020).
73. Schlott, A.C. *et al.* Structure-Guided Identification of Resistance Breaking Antimalarial NMyristoyltransferase Inhibitors. *Cell Chem Biol* **26**, 991-1000 e1007 (2019).
74. Frearson, J.A. *et al.* N-myristoyltransferase inhibitors as new leads to treat sleeping sickness. *Nature* **464**, 728-732 (2010).
75. Wright, M.H., Paape, D., Price, H.P., Smith, D.F. & Tate, E.W. Global Profiling and Inhibition of Protein Lipidation in Vector and Host Stages of the Sleeping Sickness Parasite Trypanosoma brucei. *ACS Infect Dis* **2**, 427-441 (2016).
76. Harrison, J.R. *et al.* A Molecular Hybridization Approach for the Design of Potent, Highly Selective, and Brain-Penetrant N-Myristoyltransferase Inhibitors. *J Med Chem* **61**, 8374-8389 (2018).
77. Bayliss, T. *et al.* Design and Synthesis of Brain Penetrant Trypanocidal N-Myristoyltransferase Inhibitors. *J Med Chem* **60**, 9790-9806 (2017).
78. Schoeman, D. & Fielding, B.C. Coronavirus envelope protein: current knowledge. *Virol J* **16**, 69 (2019).
79. Aiken, C., Konner, J., Landau, N.R., Lenburg, M.E. & Trono, D. Nef induces CD4 endocytosis: requirement for a critical dileucine motif in the membrane-proximal CD4 cytoplasmic domain. *Cell* **76**, 853-864 (1994).
80. Seaton, K.E. & Smith, C.D. N-Myristoyltransferase isozymes exhibit differential specificity for human immunodeficiency virus type 1 Gag and Nef. *J Gen Virol* **89**, 288-296 (2008).
81. Bryant, M. & Ratner, L. Myristoylation-dependent replication and assembly of human immunodeficiency virus 1. *Proc Natl Acad Sci U S A* **87**, 523-527 (1990).
82. Ohta, H., Takamune, N., Kishimoto, N., Shoji, S. & Misumi, S. N-Myristoyltransferase 1 enhances human immunodeficiency virus replication through regulation of viral RNA expression level. *Biochem Biophys Res Commun* **463**, 988-993 (2015).
83. Bhargavan, B. & Kanmogne, G.D. Epigenetics, N-myrystoyltransferase-1 and casein kinase-2-alpha modulates the increased replication of HIV-1 CRF02_AG, compared to subtype-B viruses. *Sci Rep* **9**, 10689 (2019).
84. Corbic Ramljak, I. *et al.* Cellular N-myristoyltransferases play a crucial picornavirus genus-specific role in viral assembly, virion maturation, and infectivity. *PLoS Pathog* **14**, e1007203 (2018).
85. Mousnier, A. *et al.* Fragment-derived inhibitors of human N-myristoyltransferase block capsid assembly and replication of the common cold virus. *Nat Chem* **10**, 599-606 (2018).
86. Suwanmanee, S. *et al.* Inhibition of N-myristoyltransferase1 affects dengue virus replication. *Microbiologyopen* **8**, e00831 (2019).
87. Yamamoto, Y. *et al.* Identification and Structure of an MHC Class I-Encoded Protein with the Potential to Present N-Myristoylated 4-mer Peptides to T Cells. *J Immunol* **202**, 3349-3358 (2019).
88. Yu, G. & Felsted, R.L. Effect of myristoylation on p27 nef subcellular distribution and suppression of HIV-LTR transcription. *Virology* **187**, 46-55 (1992).
89. Ono, A. & Freed, E.O. Binding of human immunodeficiency virus type 1 Gag to membrane: role of the matrix amino terminus. *J Virol* **73**, 4136-4144 (1999).

90. Rein, A., McClure, M.R., Rice, N.R., Luftig, R.B. & Schultz, A.M. Myristylation site in Pr65gag is essential for virus particle formation by Moloney murine leukemia virus. *Proc Natl Acad Sci U S A* **83**, 7246-7250 (1986).
91. Hizi, A. *et al.* Analysis of gag proteins from mouse mammary tumor virus. *J Virol* **63**, 2543-2549 (1989).
92. Shoji, S. *et al.* Antibodies to an NH2-terminal myristoyl glycine moiety can detect NH2-terminal myristoylated proteins in the retrovirus-infected cells. *Biochem Biophys Res Commun* **162**, 724-732 (1989).
93. Moscufo, N., Simons, J. & Chow, M. Myristoylation is important at multiple stages in poliovirus assembly. *J Virol* **65**, 2372-2380 (1991).
94. Gripon, P., Le Seyec, J., Rumin, S. & Guguen-Guillouzo, C. Myristylation of the hepatitis B virus large surface protein is essential for viral infectivity. *Virology* **213**, 292-299 (1995).
95. Ravanello, M.P., Franke, C.A. & Hruby, D.E. An NH2-terminal peptide from the vaccinia virus L1R protein directs the myristylation and virion envelope localization of a heterologous fusion protein. *J Biol Chem* **268**, 7585-7593 (1993).
96. Ravanello, M.P. & Hruby, D.E. Conditional lethal expression of the vaccinia virus L1R myristylated protein reveals a role in virion assembly. *J Virol* **68**, 6401-6410 (1994).
97. Garber, E.A., Cross, F.R. & Hanafusa, H. Processing of p60v-src to its myristylated membrane-bound form. *Mol Cell Biol* **5**, 2781-2788 (1985).
98. Kamps, M.P., Buss, J.E. & Sefton, B.M. Rous sarcoma virus transforming protein lacking myristic acid phosphorylates known polypeptide substrates without inducing transformation. *Cell* **45**, 105-112 (1986).
99. Martin, K.H., Grosenbach, D.W., Franke, C.A. & Hruby, D.E. Identification and analysis of three myristylated vaccinia virus late proteins. *J Virol* **71**, 5218-5226 (1997).
100. Ojeda, S., Senkevich, T.G. & Moss, B. Entry of vaccinia virus and cell-cell fusion require a highly conserved cysteine-rich membrane protein encoded by the A16L gene. *J Virol* **80**, 51-61 (2006).
101. Streuli, C.H. & Griffin, B.E. Myristic acid is coupled to a structural protein of polyoma virus and SV40. *Nature* **326**, 619-622 (1987).
102. Krauzewicz, N. *et al.* Myristylated polyomavirus VP2: role in the life cycle of the virus. *J Virol* **64**, 4414-4420 (1990).
103. MacLean, C.A., Dolan, A., Jamieson, F.E. & McGeoch, D.J. The myristylated virion proteins of herpes simplex virus type 1: investigation of their role in the virus life cycle. *J Gen Virol* **73 (Pt 3)**, 539-547 (1992).
104. Koshizuka, T., Kawaguchi, Y., Nozawa, N., Mori, I. & Nishiyama, Y. Herpes simplex virus protein UL11 but not UL51 is associated with lipid rafts. *Virus Genes* **35**, 571-575 (2007).
105. Sanchez, V., Sztul, E. & Britt, W.J. Human cytomegalovirus pp28 (UL99) localizes to a cytoplasmic compartment which overlaps the endoplasmic reticulum-golgi-intermediate compartment. *J Virol* **74**, 3842-3851 (2000).
106. Tillotson, L. & Shatkin, A.J. Reovirus polypeptide sigma 3 and N-terminal myristoylation of polypeptide mu 1 are required for site-specific cleavage to mu 1C in transfected cells. *J Virol* **66**, 2180-2186 (1992).
107. Simon-Mateo, C., Andres, G. & Vinuela, E. Polyprotein processing in African swine fever virus: a novel gene expression strategy for a DNA virus. *EMBO J* **12**, 2977-2987 (1993).

108. Andres, G., Garcia-Escudero, R., Salas, M.L. & Rodriguez, J.M. Repression of African swine fever virus polyprotein pp220-encoding gene leads to the assembly of icosahedral core-less particles. *J Virol* **76**, 2654-2666 (2002).
109. Dawe, S. & Duncan, R. The S4 genome segment of baboon reovirus is bicistronic and encodes a novel fusion-associated small transmembrane protein. *J Virol* **76**, 2131-2140 (2002).
110. Top, D., Read, J.A., Dawe, S.J., Syvitski, R.T. & Duncan, R. Cell-cell membrane fusion induced by p15 fusion-associated small transmembrane (FAST) protein requires a novel fusion peptide motif containing a myristoylated polyproline type II helix. *J Biol Chem* **287**, 3403-3414 (2012).
111. Kallemeijn, W.W. *et al.* Validation and Invalidation of Chemical Probes for the Human N-myristoyltransferases. *Cell Chem Biol* **26**, 892-900 e894 (2019).
112. Tan, Y.W., Hong, W.J. & Chu, J.J. Inhibition of enterovirus VP4 myristoylation is a potential antiviral strategy for hand, foot and mouth disease. *Antiviral Res* **133**, 191-195 (2016).
113. Bhandarkar, S.S. *et al.* Tris (dibenzylideneacetone) dipalladium, a N-myristoyltransferase-1 inhibitor, is effective against melanoma growth in vitro and in vivo. *Clin Cancer Res* **14**, 5743-5748 (2008).

CHAPTER 2

NMT1 AND NMT2 ARE LYSINE MYRISTOYLTRANSFERASES REGULATING THE ARF6 GTPASE CYCLE

This chapter is adapted from: Tatsiana Kosciuk, Ian R. Price, Xiaoyu Zhang, Chengliang Zhu, Kayla N. Johnson, Shuai Zhang, Steve L. Halaby, Garrison P. Komaniecki, Min Yang, Caroline J. DeHart, Paul M. Thomas, Neil L. Kelleher, J. Christopher Fromme & Hening Lin. *NMT1 and NMT2 are lysine myristoyltransferases regulating the ARF6 GTPase cycle*. Nat Commun 11, 1067 (2020)

ABSTRACT

Lysine fatty acylation in mammalian cells was discovered nearly three decades ago, yet the enzymes catalyzing it remain unknown. Unexpectedly, we find that human N-terminal glycine myristoyltransferases (NMT) 1 and 2 can efficiently myristoylate specific lysine residues. They modify ADP-ribosylation factor 6 (ARF6) on lysine 3 allowing it to remain on membranes during the GTPase cycle. We demonstrate that the NAD^+-dependent deacylase SIRT2 removes the myristoyl group, and our evidence suggests that NMT prefers the GTP-bound while SIRT2 prefers the GDP-bound ARF6. This allows the lysine myrisotylation-demyristoylation cycle to couple to and promote the GTPase cycle of ARF6. Our study provides an explanation for the puzzling dissimilarity of ARF6 to other ARFs and suggests the existence of other substrates regulated by this previously unknown function of NMT. Furthermore, we identified a NMT/SIRT2-ARF6 regulatory axis, which may offer new ways to treat human diseases.

INTRODUCTION

Lysine fatty acylation was recently identified on several Ras small GTPases and was found to regulate their cellular localization and activity.[1-3] Members of the sirtuin family

of NAD^+-dependent deacylases are known erasers of lysine fatty acylation in mammalian cells.[1-5] Although several bacterial toxins have been reported to catalyze lysine fatty acylation,[6, 7] such enzymes in mammals have not been found despite the long-known occurrence of lysine fatty acylation in uninfected cells.[8, 9]

N-terminal glycine myristoylation is catalyzed by the N-terminal myristoyltransferases (NMT) after the initiator methionine is removed by methionine aminopeptidase.[10] There are two human NMT enzymes and they have been explored as therapeutic targets for malaria,[11] sleeping sickness,[12-14] common cold,[15] and cancer.[16-18] N-terminal glycine myristoylation is required for the reversible membrane association of ARF (ADP-ribosylation factor) proteins.[19, 20] ARFs are small GTPases that cycle between the active GTP-bound and the inactive GDP-bound states. The GTP hydrolysis is facilitated by GTPase-activating proteins (GAPs) followed by guanine nucleotide exchange factor (GEF)-mediated exchange of GDP to GTP. In the GTP-bound state the amphipathic N-terminal helix with the myristoyl group is inserted into membranes and ARFs bind their effectors to regulate essential trafficking and signaling pathways. Due to the conformational change caused by GTP hydrolysis, the myristoylated amphipathic helix is sequestered in a hydrophobic pocket allowing ARFs dissociating from membranes and effectors leading to attenuation of signaling.[21] ARF1-5 reside at the Golgi and regulate the Golgi-ER traffic. ARF6 however, localizes to the plasma membrane and the endocytic system and, unlike other ARFs, tends to remain membrane-bound even in the inactive state.[21, 22] This has been a puzzle as ARF6 has a high structural similarity to ARF1 and follows the same nucleotide-dependent dynamics of the amphipathic helix.[23, 24] Unexpectedly, we found that human NMT1 and NMT2

can catalyze lysine myristoylation of ARF6 providing an explanation for its unusual membrane association.

RESULTS

NMT1 and NMT2 act on lysine residues in vitro

NMTs have a strong preference for the peptide sequence GXXXS[20, 25] It has been shown that the selectivity for glycine is due to the ability of the α-amine of the N-terminal glycine to rotate and attack the carbonyl carbon of myristoyl-CoA in the active site of NMT without the steric hindrance that would be experienced by other residues.[26] We reasoned that the α-amine of lysine could sterically mimic the ε-amine of the N-terminal glycine and therefore might react in the active site of NMT (Figure 2.1A). Given this, we thought that, if the lysine reaction is possible, the NMT substrate sequence requirements for lysine and N-terminal glycine modifications would also be similar. Therefore, we predicted that the preferred sequence for lysine myristoylation would be XKXXS or KXXS. The N-terminus of ARF6, the known substrate of NMT, fits this motif with a lysine residue (K3) following the N-terminal glycine (Figure 2.1B). Thus, we hypothesized that ARF6 could be an NMT lysine myristoylation substrate.

We first tested this possibility *in vitro* using purified recombinant NMT and synthetic peptides derived from the N-terminus of ARF6. To block the NMT activity towards the N-terminal glycine (G2), we deleted G2 leaving lysine at the N-terminus, or changed G2 to alanine (G2A), or acetylated the amino group of G2 (Ac-G). Excitingly, both NMT1 and NMT2 were able to modify all these peptides (Figure 2.1C). With the KVLSIF peptide, the reaction still occurred when the α-amino group of K was acetylated, but no reaction occurred when switching K to R (Figure 2.1C,

Supplementary Figure 2.1A, B and F), confirming that the lysine side chain, but not the N-terminal α-amino group or other residues, was modified. The modification of the lysine on the peptides was further confirmed by tandem mass spectrometry (Supplementary Figure 2.2). Kinetics comparison revealed that the modification of the G2A peptide proceeded with an overall efficiency of about half to a third of that for K3R (Supplementary Figure 2.1C), suggesting that K3 lysine myristoylation could occur rather efficiently.

Next, we tested whether the ARF6 N-terminal peptide with available N-terminal glycine could be modified on lysine 3. We used synthetic peptide standards myristoylated on lysine or glycine to determine the identity of the formed species using HPLC. Due to the high peptide hydrophobicity we were unable to obtain the doubly myristoylated peptide standard. Under the reaction conditions used mostly glycine myristoylation occurred and the lysine myristoylation product peak was very small (Figure 2.1D), suggesting that under these conditions, glycine myristoylation was more efficient on peptide substrates.

NMT is thought to predominantly act cotranslationally, however there is mounting evidence for its posttranslational activity.[27] We therefore asked whether the substrate three dimensional structure could affect lysine myristoylation. We expressed and affinity-purified Flag-tagged ARF6 and its G2A, K3R and G2A/K3R mutants from cells treated with a dual NMT1/NMT2 inhibitor DDD85646. We then incubated the purified proteins with recombinant NMT1 or NMT2 in the presence of Alk12-CoA, an alkyne-tagged myristoyl-CoA analog. An azide-containing fluorescent dye was conjugated to the alkyne tag via click chemistry and the labeling was analyzed by in-gel fluorescence.

Consistent with the synthetic peptide results, both NMTs could modify ARF6 WT, G2A, and K3R mutants, but not G2A/K3R, supporting that NMT can myristoylate K3 of ARF6 *in vitro* (Figure 1E and Supplementary Figure 2.1D). Interestingly, the reaction on the ARF6 WT produced a laddering fluorescence and immunoblot band patterns, suggesting that there were several populations of myristoylated ARF6 proteins, likely due to myristoylation on glycine or lysine (1-myr), or both (2-myr). Later we provided more evidence that one of the 1-myr bands is indeed lysine myristoylated ARF6. We therefore concluded that the three dimensional structure of the substrate might influence the NMT lysine myristoylation activity.

To further understand the new activity of NMT, we obtained X-ray crystal structures of NMT in complex with lysine peptide substrates. Co-crystallization of NMT2 with a KVLSKIF peptide and myristoyl-CoA resulted in a 1.93 Å structure capturing the myristoyl lysine peptide product, clearly showing that the lysine ε-amine, but not the α-amine, was modified (Supplementary Figure 2.6A). Furthermore, the simulated-annealing omit map unambiguously demonstrates the covalent bond between the lysine and myristoyl, concomitant with the loss of electron density connecting the myristoyl group and CoA (Figure 2.1F). The comparison of our NMT2 structure with previously-determined structures of NMT1 bound to myristoylated peptide products[25] revealed that lysine binds analogously to the glycine substrate, with the amide bond directly overlapping between the structures (Figure 2.1H).

Interestingly, there was little electron density for the adenosine-3'-phosphate of the CoA bound to NMT2, suggesting that it was either very flexible or hydrolyzed at the 5' phosphate. Including or omitting this moiety made little difference in the R-free

value, so it was removed from the final model (Supplementary Figure 2.6A, 2.1F and Supplementary Table 2.1). Similarly, the region from Arg115 to His135, involved in binding to the adenosine, was also flexible and thus not modeled, unlike in previous NMT structures.

We then determined a 2.5 Å crystal structure of NMT1 with an Ac-KVLSKIF peptide, in which the N-terminus (α-amine) is acetylated and thus cannot be myristoylated. Analogous to the higher-resolution NMT2 structure with KVLSKIF peptide, we still observed continuous electron density between the lysine and the myristoyl, with a loss of electron density connecting the CoA sulfur to the myristoyl (Figure 2.1G and Supplementary Figure 2.6B). The carbonyl of the acetyl N-terminus forms a hydrogen bond with Tyr296, similarly to the acetyl in PDB structure 5O9T[25]. This structure confirms that the lysine residue, not the N-terminus, is modified.

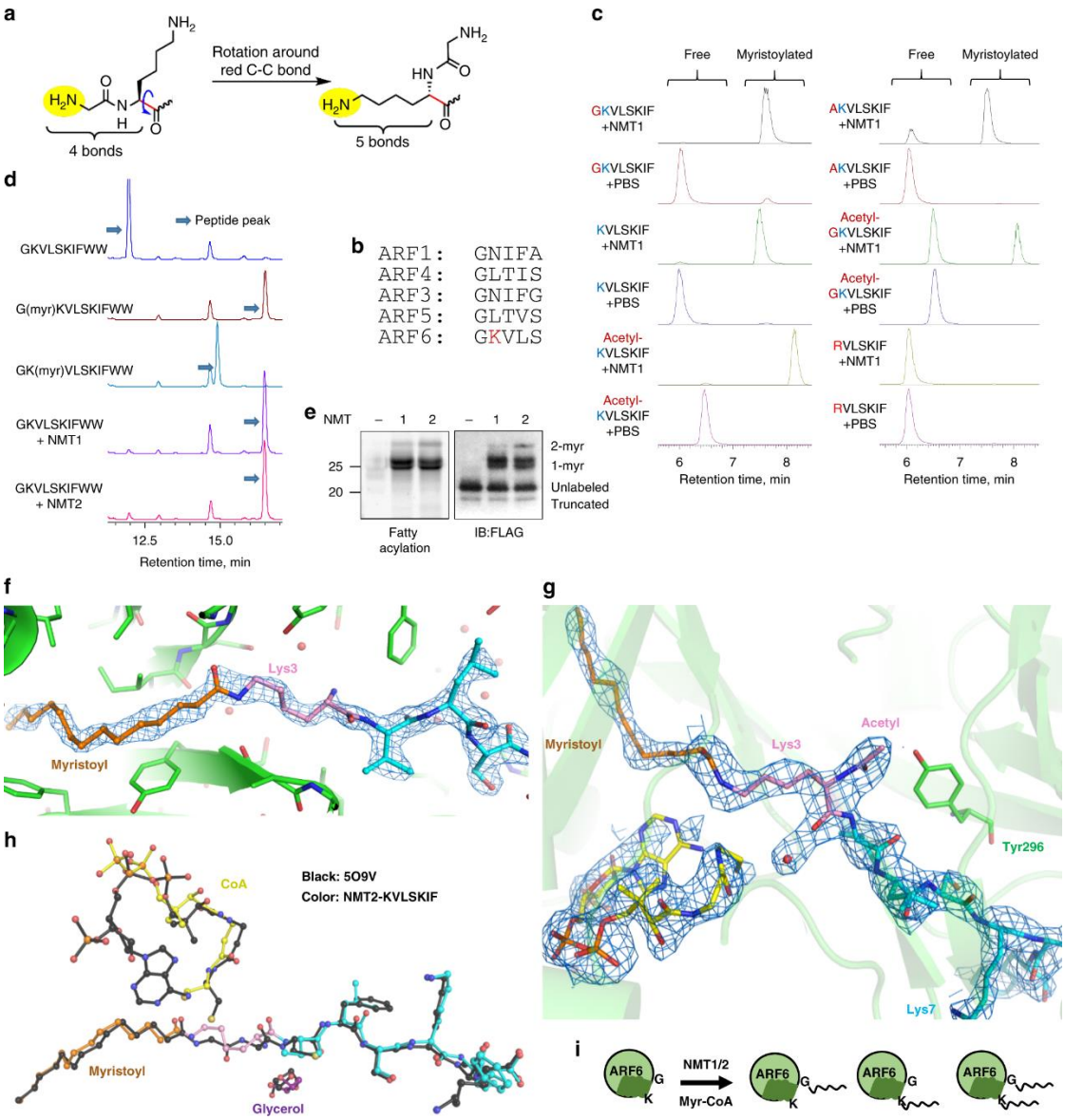

Figure 2.1 NMT1 and NMT2 have lysine transferase activity and can modify ARF6 on K3. **a** Lysine steric properties resemble those of N-terminal glycine. **b** The alignment of the N-terminal sequences of human ARFs reveals a unique lysine residue in ARF6. **c** Monitoring NMT1 in vitro reactions on different ARF6 peptides using LC-MS. Total ion chromatograms searched for the substrate and product ions are shown. **d** HPLC separation of NMT reaction on ARF6 WT N-terminal peptide reveals mostly glycine myristoylated product. **e** NMT reaction with ARF6 WT protein and Alk12-CoA generates several modified species. Shown are in-gel fluorescence and FLAG western blot after TAMRA azide conjugation via click chemistry. **f** Simulated annealing omit 2FO–FC map (at 1.2 σ) surrounding the myristoyl-KVLSKIF product in NMT2. Peptide: cyan, Lys3: pink, myristoyl: orange. **g** Myristoyl–peptide and CoA products bound to chain A in the NMT1 myristoyl-AcKVLSKIF structure. The 1.0 σ 2FO–FC electron density map around the ligands is shown (blue mesh). **h** Comparison with PDB structure 509V (black), NMT1 containing myristoyl-glycine peptide product. **i** Model showing that NMT1 and NMT2 enzymes can modify G2, K3 of ARF6, or both.

NMT catalyzes ARF6 lysine myristoylation in cells

To test whether lysine myristoylation by NMT can occur in live cells, we treated HEK293T cells transiently expressing ARF6 G2A that could only be myristoylated on lysine with Alk12 or Alk14, two clickable myristic acid analogs, with or without the NMT inhibitor, and the fatty acylation levels were analyzed as outlined in Figure 2.2A. Since NMT prefers myristoyl-CoA over palmitoyl-CoA, we speculated that Alk12 labeling would be more efficient than Alk14,[28] and would be abolished by the pharmacological NMT inhibition, if NMT was the transferase. We indeed observed the predicted effect (Figure 2.2B), supporting that NMT can myristoylate ARF6 G2A in cells. We further confirmed that myristoylation occurred on K3 of ARF6 G2A protein isolated from HEK 293T cells by mass spectrometry (Supplementary Figure 2.3).

To examine whether NMT knockdown (KD) could decrease lysine myristoylation of ARF6, we expressed ARF6 G2A in NMT1 or NMT2 knocked down (KD) HEK293T cells (Supplementary Figure 2.15). Only NMT1 KD decreased the myristoylation levels of ARF6 G2A, which could be rescued by the overexpression of HA-NMT1 or HA-NMT2 (Figure 2.2C). Therefore, both NMT enzymes can act on K3 of ARF6, but NMT1 is likely the major endogenous myristoyltransferase in HEK293T cells under our experimental conditions. Together these data suggest that NMT1 and NMT2 can myristoylate both G2 and K3 of ARF6.

Given that in vitro reaction with ARF6 and NMT produced di-myristoylated ARF6 (Figure 2.1E and Supplementary Figure 2.1D), we asked whether di-myristoylated ARF6 could also be produced in cells. To test that we expressed ARF6 WT, G2A, K3R, and G2A/K3R mutants in HEK 293T cells along with NMT1 or NMT2

and checked the Alk12 labeling. All variants except G2A/K3R produced fluorescent signal that was increased by NMT expression. However, for WT ARF6 and only for WT ARF6, NMT1 and NMT2 expression produced a higher molecular weight band (Figure 2.2D) similar to that in the in vitro labeling of purified proteins (Figure 2.1E and Supplementary Figure 2.1D), suggesting that ARF6 could have both mono- and di-myristoylation in cells. Interestingly, the doubly myristoylated band produced by NMT2 overexpression (OE) in cells was more pronounced compared to that from in vitro acylation (compare Figure 2.2D to Figure 2.1E), which suggests that other factors such as cellular localization or binding partners might regulate ARF6 di-myristoylation by NMT. In addition, NMT2 overexpression produced more doubly myrisotylated ARF6 than NMT1 overexpression (Figure 2.2D), but in vitro there was little difference between the two enzymes (Figure 2.1E and Supplementary Figure 2.1D), suggesting an additional level of regulation of this activity in cells. Since NMT2 produced more lysine myristoylated product than NMT1, we used NMT2 to further study ARF6 lysine myristoylation and to confirm di-myristoylation on G2 and K3 by top-down mass spectrometry (Figure 2.2E and Supplementary Figure 2.4). Based on the quantification of the total ion chromatogram peaks, the doubly myristoylated species is relatively abundant, about one third of the modified pool (Figure 2.2E). Top-down MS analysis also revealed a truncated ARF6 (Figure 2.2E) generated from an alternative start site, which explains the presence of the lowest unlabeled FLAG immunoblot band as those in Figure 2.1E and 2.2C.

Our X-ray crystal structures suggest a potential mechanism for di-myristoylation. We observed that the acetyl of the N-terminus of lysine myristoylated

peptide points into a hydrophobic region formed by the rings of the three tyrosine residues (Supplementary Figure 2.6B). Following that region, we found a long hydrophobic pocket (~23 Å) that emerges from the active site of NMT1 and NMT2 (Figure 2.2F, Supplementary Figure 2.6C). In both enzymes this pocket is surrounded by two phenylalanines, four leucines, one valine, one alanine, one methionine, one asparagine, six tyrosines, and one isoleucine. From the Lys3 C_{α}, the pocket is approximately the same length as the myristoyl-lysine pocket. In our structure it is occupied by glycerol and 9 waters, but it could potentially fit a myristoylated glycine (as modeled in Figure 2.2G), while orienting Lys3 for a second myristoylation reaction. This pocket is present in other NMT structures such as 5O9V but was previously unnoticed. While similar pockets in other GNAT family of enzymes are hypothesized to be water channels that function in deprotonation of the nucleophile[29], we speculate that in NMT it might also facilitate the second myristoylation event. Furthermore, NMT uniquely contains two GNAT domains thought to result from gene duplication[30], the hydrophobic pocket that we found is located in that domain, and so it is tempting to propose that the second domain, while lost its catalytic activity, is retained to hold a myristoyl moiety.

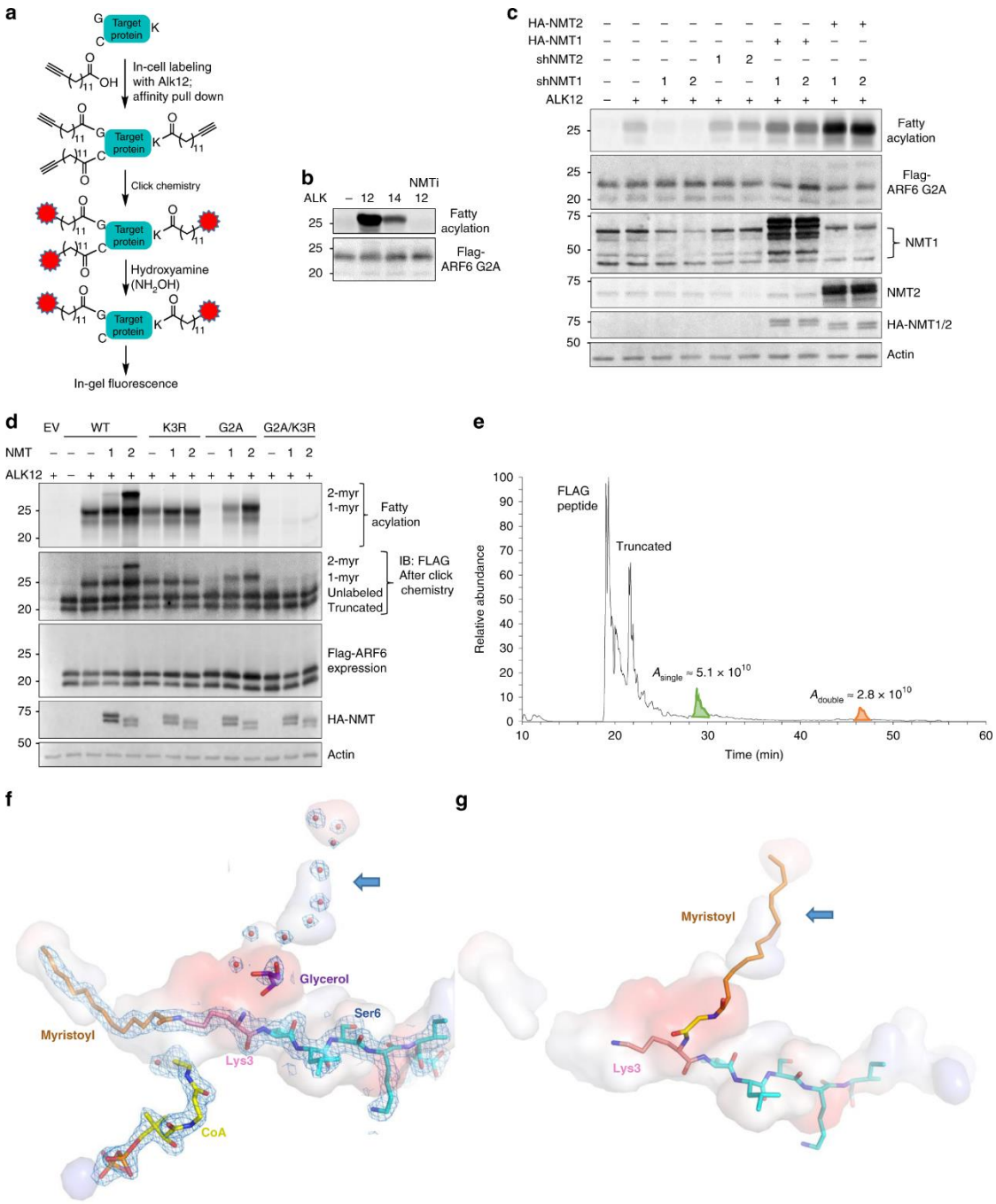

Figure 2.2 Biochemical and structural evidence for the NMT activity on lysine. **a** In-cell Alkyne probe labeling scheme. **b** Alk12 labeling is more efficient than Alk14 labeling and NMT inhibition abolishes labeling. **c** NMT1 but not NMT2 knockdown inhibits lysine myristoylation in HEK293T cells. **d** NMT1 and NMT2 overexpression produce singly and doubly myristoylated ARF6 based on Alk12 labeling. **e** Total ion chromatogram from a top–down mass spectrometric analysis that reveals di-myristoylated ARF6 isolated from HEK293T cells with NMT2 overexpression. Confirmatory MS/MS data are found in Supplementary Figure 2.4. **f** Interior pockets (shown as surface) around the NMT2 active site, showing possible channel for second myristoyl (blue arrow) currently occupied by waters (red dots) and glycerol

(purple). The surface is colored by the electrostatic properties of the surrounding residues: blue (positive), red (negative), and gray (hydrophobic). The 1.3 σ 2FO–FC electron density map is shown as a mesh. **g** Model of myristoyl-glycine docked in the second pocket, with lysine ready for a second myristoylation reaction.

NMT might have other lysine myristoylation substrates

We then explored NMT sequence requirement for lysine myristoylation. We first inserted one glycine or alanine, or two alanine residues between A2 and K3 of the ARF6 G2A mutant and performed Alk12 labeling in HEK293T cells overexpressing NMT2 or with NMT inhibition. While the insertion of one G was tolerated, the insertion of an alanine or two and three glycine residues significantly decreased myristoylation by NMT. A mutant containing two additional alanine residues (Figure 2.3A, lanes 6, 10, 14) could not be stably expressed (Figure 2.3A). Reactions on ARF6 N-terminal peptides with similar sequence changes led to the same conclusion (Figure 2.3B). This suggests that NMTs may regulate other substrates with lysine at position 3 or 4. Interestingly, we also identified a peptide with A2 acetylated and K3 myristoylated which, based on the MS/MS quantification, was about 4 times more abundant than the K3 myristoylated peptide without the acetylation (Supplementary Figure 2.5). This suggests that NMT can accommodate substrates with other N-terminal acylations *in vivo*.

We then varied amino acids within the ARF6 N-terminus on synthetic peptides and tested whether they remain NMT1 and NMT2 substrates. This revealed a strong preference for S6 and K7, which has been reported for N-terminal glycine myristoylation, and a lack of tolerance for charged residues at position 5 (Figure 2.3C). This is supported by our NMT2 structure where, the S6 side chain of the substrate is

specified by His296 side chain and the Gly472 backbone nitrogen, the K7 side chain is specified by a pocket of aspartates (183, 185, and 471), and residue 5 experiences favorable hydrophobic interactions with nearby phenylalanine residues 188, 190, and 311 as well as Leu416. Main chain contacts between NMT and peptide substrate residue 7-9 are also conserved (Figure 2.3E). Interestingly, when the sequence was changed to mimic the ARF1 sequence, but with lysine in position 3 (sequence AKIFANLFWW), the reaction did not occur on a peptide in vitro (Figure 2.3C) or on the protein in cells (Figure 2.3D). Only when S6 and K7 were introduced (sequence AKIFSKLFWW), did the reaction happen in vitro (Figure 2.3C, last entry). These observations suggest strong similarities in NMT N-terminal glycine and lysine substrate recognition mechanisms with more restrictions for lysine myristoylation.

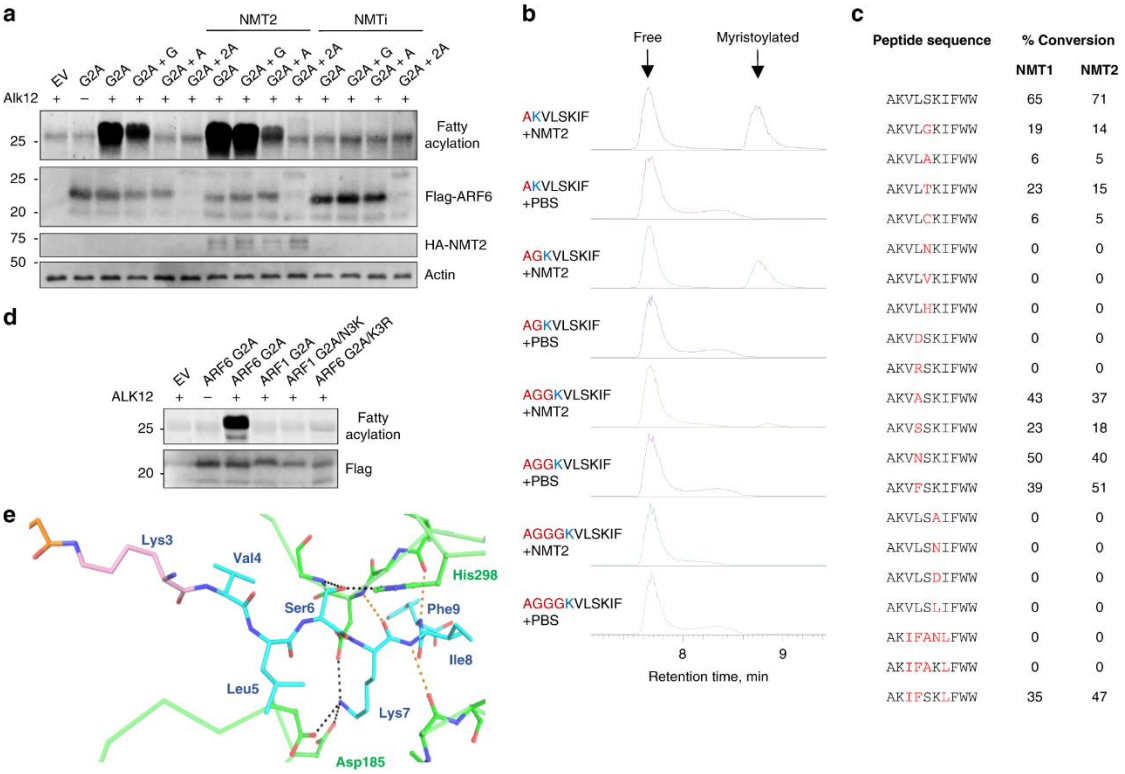

Figure 2.3 Sequence requirement for NMT lysine myristoylation. **a** Cellular Alk12 labeling results with the indicated mutants showing that NMT can accommodate other positions of K at the N-terminus in cells. The mutant containing two additional alanine residues at the N-terminus could not be stably expressed. **b** NMT can accommodate other N-terminal positions of K in vitro on synthetic peptides. Ion

chromatograms searched for the substrate and product ions are shown. **c** Amino acid sequence preference for NMT lysine myristoylation on ARF6 G2A-derived peptides. Red letters represent changed residues. The sequence IFANL is the ARF1-derived sequence. The product was detected by LC-MS and the percentage of conversion was calculated from the substrate and product peak areas on HPLC UV traces. **d** Alk12 labeling of the indicated mutants transiently overexpressed in HEK293T cells showing that, unlike ARF6 G2A, ARF1 G2A/N3K is not myristoylated. **e** Peptide recognition for Lys3 myristoylation appears similar to that for Gly2 myristoylation. NMT2 residues are shown in green. Hydrogen bonding to Ser6 by His298 and Gly472 backbone nitrogen and to Lys7 side chain by a cluster of aspartates 183, 185, and 471 are shown as black dotted lines. Further hydrogen bonding to the backbone of the peptide (orange dotted lines) is also the same as in previous structures.

SIRT2 removes ARF6 K3 myristoylation

In order to further study the biological significance of ARF6 K3 myristoylation, we sought to identify the eraser of this modification. This is important as NMT manipulation will affect both glycine and lysine myristoylation and thus make it difficult to analyze the contribution of lysine myristoylation. Lysine fatty acylation is reversible and several sirtuins were identified as lysine defatty-acylases[1, 2, 4, 5]. Given that SIRT2 is the only primarily cytosolic sirtuin, we asked whether SIRT2 could be the eraser of ARF6 lysine myristoylation. SIRT2 overexpression removed ARF6 lysine myristoylation in cells overexpressing NMT2 (Figure 2.4A). To confirm the direct deacylation by SIRT2, we purified ARF6 WT and G2A from cells overexpressing NMT2 and treated with Alk12, and then treated the purified ARF6 proteins with recombinant SIRT2 in the presence of NAD^+. This treatment strongly decreased lysine myristoylation (Figure 2.4B). We then asked whether other known demyristoylases can remove ARF6 lysine modification in HEK 293T cells. We performed Alk12 labeling of ARF6 G2A in SIRT1, SIRT3, SIRT6, SIRT7 and HDAC11 stable KD 293T cells using SIRT2 KD and TM, nicotinamide (NAM) or SAHA treatments as controls. Only SIRT2 KD, TM and NAM increased ARF6 G2A labeling suggesting that SIRT2 is the major eraser of ARF6 lysine myristoylation in HEK293T cells (Supplementary Figure 2.14).

To further confirm that lysine myristoylation of ARF6 is not an artifact of NMT overexpression, we used a previously reported sensitive ^{32}P-NAD^{+} assay to detect ARF6 myristoylation without overexpressing NMT.[31] We isolated ARF6 WT and K3R mutants from SIRT2 knockdown (KD) HEK 293T cells and treated them with recombinant SIRT2 in the presence of ^{32}P-NAD^{+} (Figure 2.4C). Myristoyl-H3K9 peptide, a known in vitro substrate of SIRT2, was used as a positive control. Separation of the reaction products by thin layer chromatography (TLC) revealed a myristoyl ADP-ribose product (MyADPR) in the reaction containing ARF6 WT, but not K3R mutant (Figure 2.4D). Furthermore, SIRT2 in the presence of NAD^{+} could remove K3 myristoylation but not G2 myristoylation from synthetic peptides (Supplementary Figure 2.8A and B). This strongly supports that ARF6 WT is myristoylated on K3 by endogenous NMT. We also used the ^{32}P-NAD^{+} assay to confirm that SIRT2 inhibition with a SIRT2-specific inhibitor TM[32] in cells (Fig 2.4E), and NMT overexpression or in vitro NMT treatment (Supplementary Figure 2.7A, B) can increase ARF6 K3 myristoylation. In addition, knockdown and inhibition of SIRT2 with TM increased the levels of ARF6 G2A lysine myristoylation, and this effect was rescued by SIRT2 overexpression (Figure 2.4F). Finally, co-immunoprecipitation studies suggested that ARF6 and SIRT2 interact (Supplementary Figure 2.8C). These data demonstrate that SIRT2 is the eraser of ARF6 K3 myristoylation.

With this knowledge we sought to confirm that one of the two single myristoylation bands generated by the NMT on ARF6 WT in vitro (Figure 2.1E) is lysine myristoylated ARF6. To achieve that, we reconstituted the NMT reaction on ARF6 WT and mutants with Alk12-CoA and followed with a SIRT2 reaction. SIRT2

removed the double acylation and the top half of single acylation bands from ARF6 WT and most of the modification from ARF6 G2A leaving the K3R and G2A/K3R mutants unaffected (Figure 2.4G). This confirms that NMT myristoylation on K3 of ARF6 protein may not require N-terminus sequestration and can occur to an extent similar to glycine myristoylation.

Next, we tested whether endogenous ARF6 is myristoylated on K3. Since we were unable to efficiently isolate endogenous ARF6 with commercial antibodies, we labeled ARF6 with Alk12 in cells with depleted or inhibited SIRT2. We then removed cysteine labeling in lysates with hydroxylamine, conjugated biotin azide followed by streptavidin pull down. Western blot analysis revealed a signal increase with SIRT2 KD or sirtuin inhibitor nicotinamide (NAM) (Figure 2.4H), suggesting a higher abundance of lysine modified species. Together these data suggest that endogenous ARF6 contains lysine myristoylation and SIRT2 is its physiological eraser (Figure 2.4I).

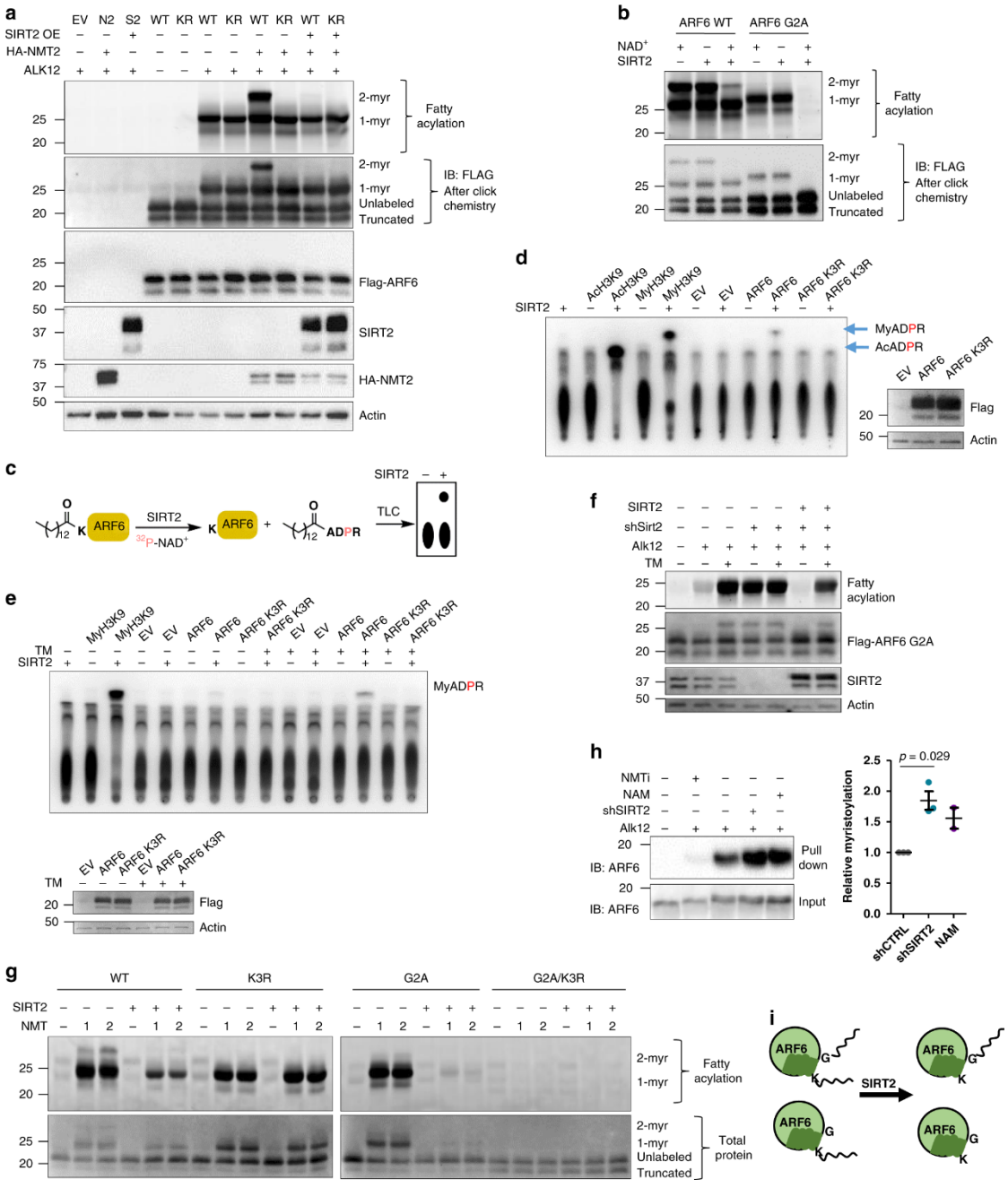

Figure 2.4 SIRT2 removes ARF6 K3 myristoylation. **a** Alk12 labeling results on overexpressed ARF6 WT or K3R mutant (KR) showing that SIRT2 demyristoylates ARF6 in HEK293T cells as indicated by the disappearance of the dimyristoylated species with SIRT2 OE. **b** SIRT2 demyristoylates ARF6 and ARF6 G2A in vitro. ARF6 WT and G2A were isolated from Alk12 treated cells with NMT2 overexpression and were treated with recombinant SIRT2 followed by TAMRA azide conjugation and in-gel fluorescence. **c** ^{32}P-NAD$^+$ assay scheme. **d** SIRT2 demyristoylates ARF6 K3 purified from cells with endogenous NMT in vitro (detected using the ^{32}P-NAD$^+$ assay). **e** SIRT2 inhibition with TM in cells increases lysine fatty acylation of ARF6 (detected using the ^{32}P-NAD$^+$ assay on ARF6 isolated from HEK293T cells treated with TM). **f** Alk12 labeling in HEK293T cells transiently overexpressing ARF6

G2A showing that SIRT2 KD or inhibition increase but SIRT2 OE removes the labeling. **g** SIRT2 removes double and single lysine myristoylation produced by in vitro acylation with NMT1/2. The indicated ARF6 proteins were isolated from cells with NMT inhibition and were first modified by NMT with Alk12-CoA in vitro and then reacted with SIRT2 in vitro. **h** Endogenous ARF6 has lysine myristoylation in HEK293T cells. Fifteen-hour treatment with 10 mM nicotinamide or 2 μM DDD85646 was used. Endogenous myristoylated proteins were labeled with Alk12 followed by conjugation to biotin azide via click chemistry and streptavidin pull down. The pull-down products were analyzed by western blot for ARF6. Data points represent biological replicates analyzed by unpaired two-tailed *t* test. Error bars represent SEM. **i** Model showing that SIRT2 can remove ARF6 K3 myristoylation.

NMT prefers ARF6-GTP while SIRT2 prefers ARF6-GDP

Because ARF6 cycles between GTP and GDP bound states, we reasoned that lysine myristoylation might need to be removed at a specific point to support the GTPase cycle. We therefore examined the ability of SIRT2 to act on active Q67L and inactive T27N mutants of ARF6 isolated from SIRT2 KD cells via ^{32}P-NAD^{+} assay. More My-ADPR was formed in the reaction with the T27N mutants suggesting that SIRT2 might have a preference for the GDP bound or nucleotide free ARF6 (Figure 2.5A). However, this could also indicate that ARF6 T27N contains more lysine myristoylation. To address that, we examined the abundance of lysine myristoylation by measuring the relative ratio of double to single myristoylation fluorescent bands of ARF6 Q67L and T27N. In control cells overexpressing NMT2, T27N had much less di-myristoylation compared to that of Q67L (Figure 2.5B and Supplementary Figure 2.12). T27N dimyristoylation strongly increased in SIRT2 KD cells yet was less abundant than that on Q67L. Unlike Q67L dimyristoylation, T27N dimyrisotylation was completely removed with SIRT2 OE (Figure 2.5B). Since the abundance of lysine myristoylation on T27N was not higher than that on Q67L (Figure 2.5B), but more My-ADPR was formed during SIRT2 in vitro reaction with T27N (Figure 2.5A), the data suggest that SIRT2 prefers the inactive GDP-bound ARF6.

We next asked whether the addition of this modification is also GTPase cycle dependent. In vitro using purified proteins, the reactions of NMT with the active ARF6 Q67L mutant produced more doubly myristoylated ARF6 (Figure 2.5C). In cells, co-IP experiments showed that NMT2 preferentially binds to Q67L (Figure 2.5D) over T27N and NMT2 co-localizes with ARF6 Q67L better than with ARF6 T27N (Figure 2.5E). Together these results suggest that NMT prefers the GTP-bound ARF6. Even without NMT overexpression, we were able to detect about 3% of dimyristoylated ARF6 Q67L (Supplementary Figure 2.16). We anticipate that endogenous ARF6-GTP may have a higher relative dimyristoylation due to a higher enzyme/substrate ratio, however we could not estimate this value due to technical limitations. Overall, our data support that lysine myristoylation is added and removed at distinct points of the ARF6 GTPase cycle (Figure 2.5F). Furthermore, Figure 2.1 suggests that on a synthetic ARF6 peptide lysine myristoylaiton by NMT is relatively inefficient compared to that on ARF6 protein in vitro or in cells (Figure 2.2D, 2E, 4G). The preference of NMT for ARF6-GTP could potentially explain these observations.

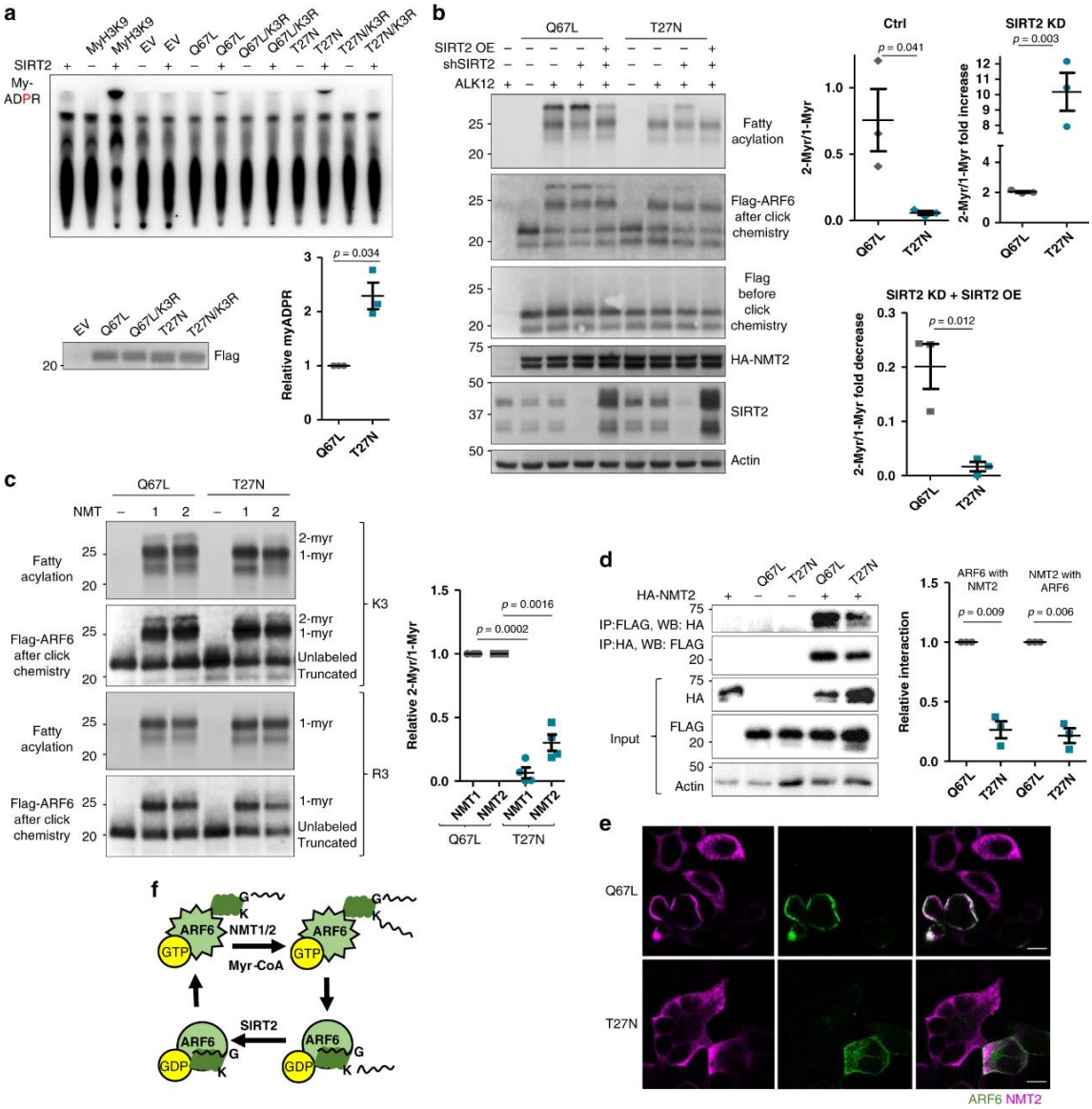

Figure 2.5 Lysine myristoylation cycle is coupled to the catalytic cycle of ARF6. **a** SIRT2 removes more lysine myristoylation from ARF6 T27N than from ARF6 Q67L in vitro. ARF6 proteins were purified from cells with endogenous NMT and SIRT2 KD and subjected to the ^{32}P-NAD^{+} assay with recombinant SIRT2. $n = 3$. **b** In-cell Alk12 labeling of ARF6 Q67L and T27N mutants during NMT2 OE showing more lysine acylation of ARF6 Q67L. $n = 3$. **c** In vitro NMT reaction on ARF6 Q67L and T27N showing more double acylation on ARF6 Q67L (ARF6-GTP). $n = 4$. **d** NMT2 preferentially binds ARF6-GTP. Flag-tagged ARF6 mutants and HA-NMT2 were overexpressed in HEK293T cells and subjected to the indicated pull downs. $n = 3$. **e** NMT2 is redistributed to the sites of ARF6 Q67L, but not ARF6 T27N. Confocal images of immunofluorescence in cells overexpressing FLAG-ARF6 mutants and HA-NMT2. Scale bars: 10 µm. **f** Model showing that NMT acts on active, but SIRT2 on inactive ARF6. For all experiments, error bars represent SEM and *n* represents biological replicates analyzed by unpaired two-tailed *t* test.

K3 myristoylation regulates ARF6 localization

The ARF GTPase cycle is regulated by a glycine myristoyl switch where upon GTP binding the myristoylated amphipathic N-terminal helix unfolds and inserts into the membrane bilayer. Two fatty acyl chains are often required for membrane binding of a number of proteins such as those in the Src and G alpha families.[33, 34] We asked whether ARF6 requires a second fatty acyl group for efficient membrane binding. To this end we first compared the localization of ARF6 WT and K3R in cells with NMT2 overexpression by immunofluorescence. ARF6 WT localized more to the cell periphery compared to ARF6 K3R (Figure 2.6A). We then compared the abundance of ARF6 WT and K3R in the membrane and cytosolic fractions in HEK293T cells with NMT2 OE. The K3R mutation decreased the abundance of ARF6 in the membrane fraction but increased its levels in the cytosol, and the doubly acylated ARF6 was mostly found in the membrane fraction suggesting that K3 myristoylation targets ARF6 to membranes (Figure 2.6B and Supplementary Figure 2.13A).

ARFs 1-5 are cytosolic when GDP bound, however ARF6 largely remains on the membrane when inactivated,[24, 35, 36] which has been a longstanding puzzle. We therefore hypothesized that lysine myristoylation contributes to the membrane association of inactive ARF6. It has been shown that the GTPase-activating protein (GAP)-catalyzed GTP hydrolysis of ARF6 is necessary for its transport to the endocytic recycling compartment via the endocytic pathway, while the GDP to GTP exchange catalyzed by guanine nucleotide exchange factors (GEFs) is necessary for its recycling to the plasma membrane.[37] Subcellular fractionation of ARF6 WT, Q67L and T27N in SIRT2 KD and NMT2 overexpression cells revealed that the Lys3 myristoylated ARF6

proteins were present in the membrane fraction more than the corresponding K3R mutants that cannot be myrisotylated (Figure 2.6C and Supplementary Figure 2.13B). Furthermore, in cells without NMT overexpression ARF6 T27N K3R was less abundant on the membrane than ARF6 T27N supporting that endogenous NMT and SIRT2 regulate the membrane binding cycle through K3 myristoylation of inactive ARF6 (Supplementary Figure 2.13C).

We then examined the localization of Q67L and T27N to the plasma membrane and the endocytic recycling compartment (ERC) located at the perinuclear region, where they are known to reside, by microscopy.[37, 38] We used TfR, a marker for plasma membrane and ERC,[39, 40] to examine the colocalization of ARF6 mutants. Q67L did not localize to ERC, but was found at the plasma membrane and plasma membrane folds under it and blocked TfR trafficking as was observed by others (Figure 2.6D).[37, 41, 42] Changing K3 to R3 in the Q67L mutant had very little effect on its colocalization with TfR, indicating that N-terminal glycine myristoylation might be sufficient for the correct cellular localization of GTP-bound ARF6. The T27N mutant is localized to the plasma membrane as well as the early endosomes and perinuclear ERC, as indicated by its colocalizaiton with TfR.[37, 38] However, the T27N K3R mutant, unlike T27N, was mostly cytosolic with little localization to ERC, suggesting that lysine myristoylation is necessary for its trafficking to this compartment. Consistent with this, SIRT2 KD increased, while NMT inhibition or NMT1 KD (but not NMT2 KD) decreased, ARF6 T27N colocalization with TfR (Supplementary Figure 2.10 and 2.11). Interestingly, we observed SIRT2 colocalization with TfR in HEK293T cells under basal conditions (Figure 2.6E), which suggests that SIRT2 might act on ARF6 at ERC or early

endosomes where TfR is known to be present.[43] Since inactive ARF6 localizes to ERC, this further supports that SIRT2 regulates inactive ARF6. NMT2 appeared largely cytosolic or on endomembranes (Figure 2.6A) suggesting that it might act on ARF6 before it is trafficked to the plasma membrane.

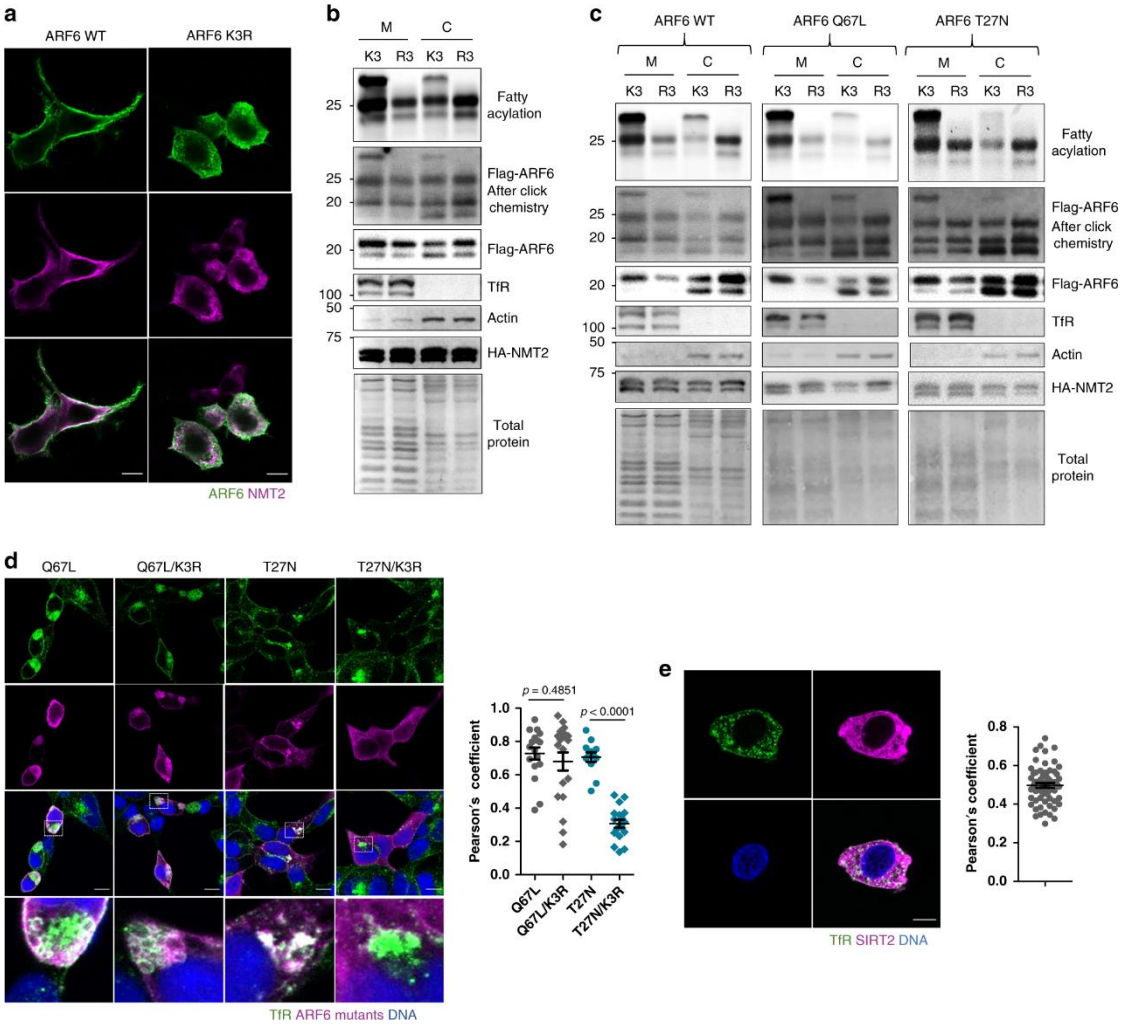

Figure 2.6 Lysine myristoylation regulates ARF6 membrane localization. **a** Confocal microscopy of overexpressed Flag-ARF6 and HA-NMT2 showing a decreased membrane localization of ARF6 K3R compared to ARF6 WT and colocalization of ARF6 with NMT2 at the plasma membrane and cytosol but not ERC in HEK293T cells. Scale bars: 10 µm. **b** Subcellular fractionation results in cells with HA-NMT2 expression and Alk12 treatment showing that K3 myristoylation promotes ARF6 membrane localization. The K3R mutant shows a decreased membrane and increased cytosolic localization compared to ARF6 WT. $n = 2$. **c** Subcellular fractionation results in cells with HA-NMT2 expression, SIRT2 KD, and Alk12 treatment demonstrating that lysine myristoylation promotes ARF6 membrane localization in different catalytic states. $n = 2$. **d** ARF6 K3R mutation does not affect ARF6 Q67L localization but inhibits ARF6 T27N localization to plasma membrane and ERC as indicated by colocalization with TfR in SIRT2 KD cells. These cells do not overexpress NMT and thus we were examining the effect of endogenous lysine myristoylation. Each point represents one cell (Q67L = 17, Q67L/K3R = 19, T27N = 12, T27N/K3R = 18). Scale bars: 10 µm. **e** SIRT2 localizes to ERC, recycling,

and early endosomes as indicated by colocalization with TfR. Each point represents one cell (63 cells). Scale bars: 10 μm. All experiments in this Figure were performed in HEK293T cells. Colocalization quantifications are presented as Pearson's correlation coefficients. For all experiments, error bars represent SEM and *n* represents biological replicates analyzed by unpaired two-tailed *t* test.

Lysine myristoylation cycle promotes ARF6 activity

Since our data suggest that lysine myristoylation increases ARF6 membrane localization, we asked whether this also promotes ARF6 GTP loading by increasing ARF6 interaction with GEFs at the membranes. To test this, we performed an ARF6-GTP pull down with GGA3, a known ARF6 effector protein, conjugated agarose and examined its levels by Western blot. NMT inhibition suppressed, but overexpression promoted ARF6 activation (Figure 2.7A). To determine the contribution of lysine myristoylation, we examined the effects of SIRT2 inhibition and K3R mutation. SIRT2 inhibition reduced GTP loading of overexpressed ARF6 WT but not K3R (Figure 2.7B), suggesting that SIRT2 demyristoylates ARF6 K3 to promote ARF6 activation.

To rule out that lysine myristoylation or K3R mutation itself affect binding to GGA3, we examined the structures of ARF1 in complex with the GGA1 binding domain as ARF6-GGA3 structures are not available. This revealed that the N-terminal helix is unlikely to participate in this interaction (Supplementary Figure 2.9A). Furthermore, it is reported that, like other effector proteins, GGA3 binds the interswitch region that extrudes upon GTP binding along with switch 1 and 2, but not N-terminal helix[44]. Finally, we observed that SIRT2 inhibition did not affect the binding of the active ARF6 Q67L mutant to GGA3 (Supplementary Figure 2.9B), which further confirms that lysine myristoylation itself does not interfere with GGA3 binding.

To find out whether the activity of endogenous ARF6 is regulated by lysine myristoylation, we examined the effect of SIRT2 KD on GTP loading of native cellular

ARF6. SIRT2 KD suppressed the abundance of GTP-bound endogenous ARF6 suggesting that this regulation is not an artifact of overexpression (Figure 2.7C).

We were initially surprised that ARF6 WT (which can be K3 myristoylated) contained more ARF6-GTP than the K3R mutant (which cannot be K3 myristoylated) in cells with active SIRT2, but the GTP loading for ARF6 WT was diminished when SIRT2 was inhibited and thus K3 myristoylation accumulated (Figure 2.7B). However, given the observed preference of NMT for ARF6-GTP and of SIRT2 for ARF6-GDP, this unexpected GTP loading result suggests that the myristoylation-demyristoylaiton cycle serves to drive the ARF6 GTPase cycle. Thus, disrupting either myristoylation or demyristoylaion inhibits ARF6 activation (Fig 2.7F).

The GGA3 – ARF6 interaction is known to promote ERK activation[45]. Since the GGA3 pull down assay demonstrated that this interaction is regulated by lysine myristoylation, we examined the effect of ARF6 K3 myristoylation on ERK phosphorylation in HEK293T cells. Serum starved cells were used to isolate the lysine myristoylation effect on ARF6 activation from other activating signals such as those from growth factors. Consistent with the GTP loading data, ARF6 WT OE promoted pERK that was further increased by NMT2 OE in control cells, while K3R had little effect (Figure 2.7D). Similarly, SIRT2 KD decreased pERK for ARF6 WT, but not K3R (Figure 2.7D). Furthermore, both NMT and SIRT2 inhibition in HEK 293T cells inhibited ERK phosphorylation suggesting that myristoylation cycle of endogenous ARF6 may regulate this pathway (Figure 2.7E).

Together these data suggest a model (Figure 2.7F) where NMT promotes ARF6 plasma membrane localization by myristoylating ARF6-GTP on K3, and after GAP-

catalyzed GTP hydrolysis the modification keeps the inactive ARF6 membrane bound. This allows its trafficking to intracellular vesicles including the ERC, where lysine demyristoylation by SIRT2 supports the efficient activation of ARF6 by GEF and subsequent trafficking back to plasma membrane. ARF6 K3R fails to retain membrane association after GTP hydrolysis and therefore cannot be efficiently trafficked and activated. This model readily explains the GTP-loading data in Figure 2.7 and the importance of active myristoylation-demyristoylation cycle for the normal GTPase cycle of ARF6 to control downstream signaling.

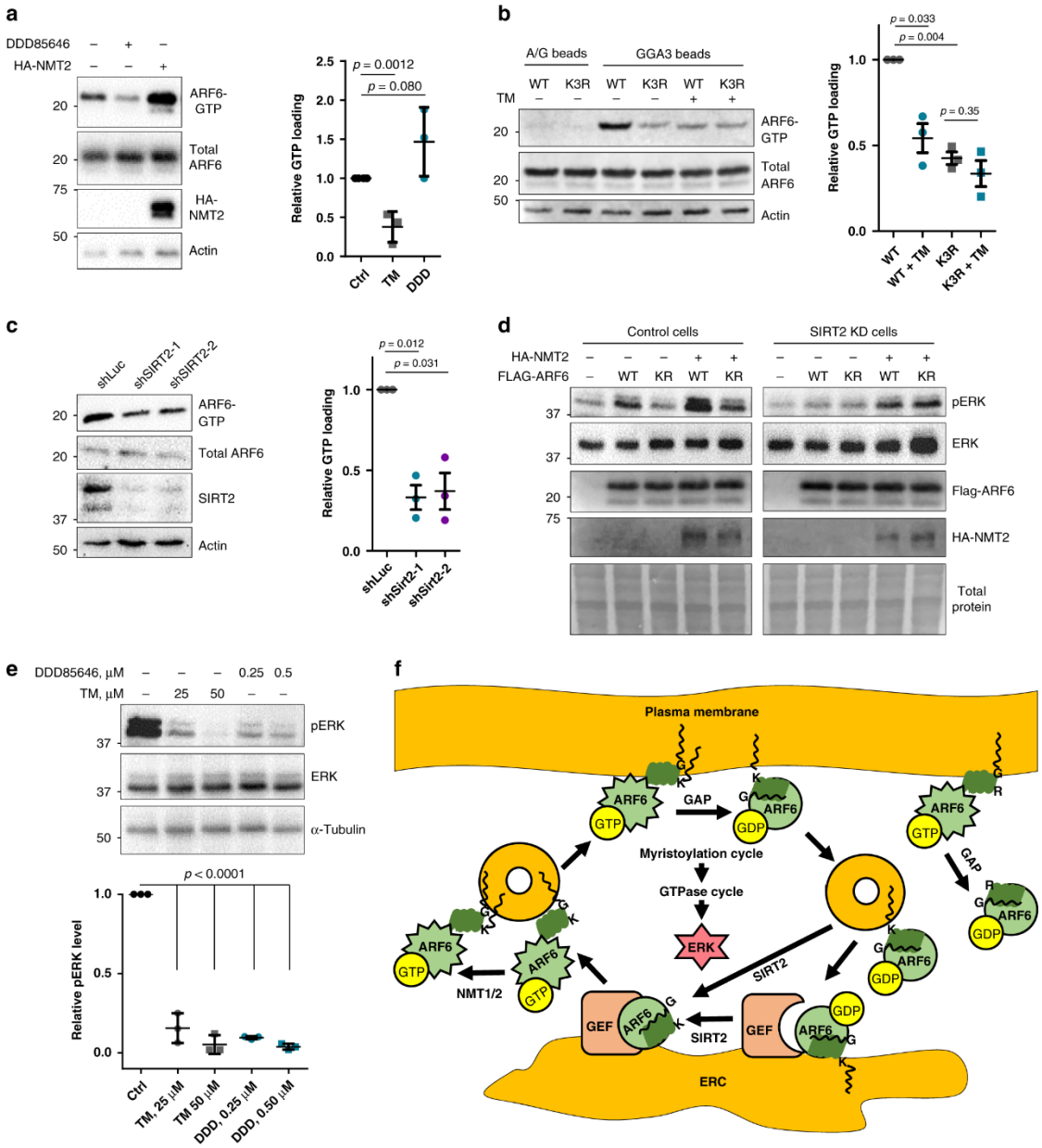

Figure 2.7 Lysine myristoylation cycle regulates ARF6 activation to control ERK phosphorylation. **a** NMT inhibition with DDD85646 suppresses, but NMT2 OE promotes, ARF6 GTP loading. GGA3 pull down in cells expressing Flag-ARF6 and subjected to NMT2 OE or NMTi. $n = 3$. **b** GGA3 pull down showing that SIRT2 inhibition by TM decreases the GTP loading of ARF6 WT, but not K3R. $n = 3$. **c** SIRT2 KD inhibits GTP loading of endogenous ARF6. GGA3 pull down was performed in HEK293T cells with transient SIRT2 KD. $n = 3$. **d** ARF6 lysine myristoylation promotes pERK in control but not in SIRT2 KD HEK293T cells. ARF6 WT or K3R mutant were overexpressed in HEK293T cells that were blotted for pERK after 15 h of serum starvation. $n = 2$ **e** SIRT2 and NMT inhibition dose-dependently inhibit pERK. HEK293T cells were treated with the indicated inhibitors for 15 h. $n = 3$. For all experiments, error bars represent SEM and n represents biological replicates analyzed by unpaired two-tailed t test. **f** Model for the coupling of ARF6 myristoylation–demyristoylation cycle and GTPase cycle. NMT myristoylates ARF6-GTP on K3, which targets ARF6 to plasma membrane and retains inactive ARF6 at the membrane after GTP hydrolysis allowing its trafficking to ERC via the endocytic pathway. SIRT2 deacylates inactive ARF6 at early endosomes or ERC to allow its efficient activation by GEFs after GDP release. ARF6-GTP on recycling endosomes gets myristoylated on K3 by NMT, which

drives its plasma membrane translocation. This cycle in turn controls ERK phosphorylation. ARF6 K3R cannot be myristoylated on K3 and therefore loses its membrane association after GTP hydrolysis, which inhibits its translocation to endomembranes and activation.

DISCUSSION

Our work uncovered an ARF6 lysine myristoylation-demyristoylation cycle, which is intimately coupled to its GTPase cycle and controlled by SIRT2, and a previously unknown activity of NMT. NMT enzymes myristoylate ARF6 on K3 to promote its membrane association and trafficking to ERC while SIRT2 removes this moiety to allow efficient ARF6 activation. This in turn regulates ARF6 activity-dependent effector binding and downstream signaling. GEFs of ARF6 are known to localize to the plasma membrane and ERC.[46, 47] The increased membrane localization of ARF6 by K3 myristoylation ensures the endocytic trafficking of ARF6 to increase its encounters with its GEFs at endomembranes, but for efficient GTP loading, K3 myristoylation needs to be removed by SIRT2. The selectivity of NMT for ARF6-GTP and SIRT2 for inactive ARF6 accelerates ARF6 activation by avoiding a futile lysine myristoylation-demyristoylation cycle (Figure 2.7F). While our study provides a mechanism for ARF6 unique plasma membrane targeting, it may not be its sole driver, since ARF6 K3R did not localize to the Golgi, like other ARFs. Membrane receptors or GAP and GEF specificities might aid this targeting. Since, unlike glycine modification, lysine myristoylation is dynamic, its lower abundance compared to glycine myristoylation is not surprising. Although we were unable to resolve dimyristoylated endogenous ARF6 with currently available methods, we observed that SIRT2 KD or inhibition increases ARF6 myristoylation and regulates its GTP loading and downstream signaling.

ARF6 – pERK axis controls an array of cellular activities such as migration[48], tubule development[49], and vesicle shedding[50]. Given our findings, these processes can be modulated by targeting the ARF6 myristoylation-demyristoylation cycle with selective inhibitors for NMT and SIRT2 offering new therapeutic strategies.

The lysine myristoyltransferase activity of NMTs tolerates small changes in the substrate sequence supporting the existence of other lysine substrates. Furthermore, conditions regulated by proteolysis such as apoptosis, immune response and viral infections might generate additional NMT lysine substrates. Our findings will facilitate the discovery of other proteins regulated by lysine fatty acylation and thus open new avenues for understanding the biological functions of this modification.

METHODS

Reagents: Anti-FLAG affinity gel (#A2220, RRID: AB_10063035) and FLAG-HRP (#A8592, RRID: AB_439702, 1:5000 dilution) were purchased from Sigma. HA-HRP (F-7, sc-7392, 1:5000 dilution), Na/K-ATPase (C464.6, sc-21712, 1:1000 dilution), β-Actin-HRP (C4, sc-47778, 1:5000 dilution), NMT1 (E-9, sc-393702, 1:1000 dilution), NMT2 (30, sc-136005, 1:1000 dilution), TfR (CD-71) (3B8 2A1, sc-32272, 1:500 dilution for WB and 1:200 dilution for IF), ARF6 (3A-1, sc-7971, 1:1000 dilution), antibodies were purchased from Santa Cruz Biotechnology, and SIRT2 (D4050, 12650S, 1:1000 dilution), SIRT6 (D8D12, 12486S, 1:1000 dilution), SIRT7 (D3K5A, 5360S, 1:1000 dilution), SIRT1 (D739, 2493S, 1:1000 dilution), SIRT3 (D22A3, 5490S, 1:1000 dilution) and Arf6 (D12G6, 5740, 1:1000 dilution), Phospho-p44/42 MAPK (Erk1/2) (Thr202/Tyr204) (D13.14.4E, 4370, 1:1000 dilution), p44/42 MAPK (Erk1/2) (L34F12, 4696, 1:2000 dilution) antibodies from Cell Signaling Technology.

^{32}P-NAD^{+} was purchased from PerkinElmer, Tris[(1-benzyl-1H-1,2,3-triazol-4-yl)methyl]amine (TBTA), Tris(2-carboxyethyl)phosphine (TCEP), hydroxylamine, NAD^{+}, and protease inhibitor cocktail were purchased from Sigma. FuGene 6 transfection reagent were purchased from Promega (Madison, WI). ECL plus Western blotting detection reagent were purchased from Thermo Scientific Pierce (Rockford, IL). 5-Tamra azide was purchased from Lumiprobe (47130) and GGA3-PBD beads from cytoskeleton (GGA05-A). PEI MAX transfection reagent (24765-1) was purchased from Polsciences. NMT1, NMT2, and SIRT2 lentiviral plasmids (pLKO.1-puro vector) were purchased from Sigma, the sequences of shRNA are:

Alk12 and Alk14 were synthesized as reported.[28] TM was synthesized as previously reported.[32] Synthetic peptides: GKVLSKIF, AKVLSKIF, AKVLSKIFWW, AK(myr)VLSKIFWW, G(myr)KVLSKIFWW and GK(myr)VLSKIFWW and the peptides listed in Figure 2.3C were purchased from Biomatik**;** acetyl-GKVLSKIF, acetyl-KVLSKIF, KVLSKIF, RKVLSKIF, AGKVLSKIF, AGGKVLSKIF, AGGGKVLSKIF were synthesized in-house using a peptide synthesizer.

Cell culture and transient transfection: Human HEK293T cells (obtained from ATCC) were cultured in DMEM with 10% heat inactivated (HI) fetal bovine serum (FBS, 10437028, Thermo Fisher) or calf serum (18439-24-2, Sigma). Transient transfection was done using FuGene 6, or polyethylenimine (PEI). Briefly, 1:3 ratio of plasmid (µg) to transfection reagent (µl) was used. Transfection reagent was added to serum free media (10% volume of culture media) followed by a 5 min incubation at room temperature for FuGene 6. Then the plasmid was added and the mix was incubated for 30 min at room temperature. Fresh complete growth media were added

to cells and the transfection mix was added dropwise. The cells were harvested 24-48 hr later depending on experimental goals.

Plasmids: C-terminal Flag-tagged mouse ARF6 and ARF1 were obtained from Addgene (Plasmids #52407 and #52402). The plasmids were then used to generate ARF6 G2A, G2A/K3R, K3R, Q67L, Q67L/K3R, T27N, T27N/K3R, ARF1 G2A, ARF1 G2A/N3K by quick change mutagenesis. To generate NMT constructs for transient mammalian expression, HA-tagged human NMT1 and NMT2 were inserted into the pCMV-Tag-4a vector. mCherry-TfR-20 was a gift from Michael Davidson (Addgene plasmid # 55144; http://n2t.net/addgene: 55144; RRID: Addgene 55144). SIRT2 and Flag-SIRT2 constructs are previously reported.[2] The primer sequences for mutagenesis and cloning are provided in Supplementary Table 2.

NP-40 lysis buffer: 25 mM Tris-HCl pH 7.4, 150 mM NaCl, 10% glycerol, and 1% Nonidet P-40, protease and phosphatase inhibitors added freshly.

IP (immunoprecipitation) wash buffer: 25 mM Tris-HCl pH 7.4, 150 mM NaCl and 0.2% Nonidet P-40.

4% SDS lysis buffer: 50 mM trimethylamine, 150 mM NaCl, 4% SDS.

ALK12 labeling to detect fatty acylation of ARF6 and ARF1 in cells: ARF6 and ARF1 WT and mutants were transfected into HEK 293T cells using PEI or FuGene 6 transfection reagent. NMT1/2 were transfected in 1:2 ratio of ARF6:NMT2. After 24 hr, the cells were treated with 50 μM – 100 μM Alk12 for 7-24 hr along with TM, DDD85646 or nicotinamide as indicated in figures. The cells were washed with cold PBS, scraped and collected at 500 g for 5 min, then were lysed in NP-40 lysis buffer with protease inhibitor cocktail for 30 min on ice with brief vortexing every 10 min.

The lysates were incubated with anti-FLAG affinity beads at 4°C for 2 hr. The affinity beads were then washed three times IP and then re-suspended in 18 µL of IP washing buffer. The click chemistry reaction was performed by adding the following reagents: TAMRA azide (1 µL of 2 mM solution in DMSO), TBTA (1 µL of 10 mM solution in DMF), $CuSO_4$ (1 µL of 40 mM solution in H_2O) and TCEP (1 µL of 40 mM solution in H_2O). The reaction was allowed to proceed at room temperature for 30-60 min. Then, SDS protein loading dye was added to 2x final concentration and the beads were heated at 95°C for 10 min. After centrifugation at 17,000 g for 2 min, the supernatant was collected and treated with 300 mM hydroxylamine at 95°C for 7 min. 1 µl of each sample was diluted into 30 µl of 1X sample loading dye and 5-10 µl were analyzed by Western blot (WB). In-gel fluorescence was detected with Typhoon FLA7000 (GE Healthcare Life Sciences). Protein loading was further analyzed by WB.

SDS-PAGE and Western Blot (WB) analysis:

Running buffer: 30.3g of Tris base, 144g of Glycine, 10g of SDS were dissolved in 1L of water to obtain 10X stock that was diluted in water to 1X before use.

Transfer buffer: 38g of Tris base, 180g of Glycine, 6.25g of SDS were dissolved in 1L of water for a 10X stock that was further diluted to 1X in 20% methanol in water before use.

Blocking buffer: 5% BSA in 0.1%Tween20-PBS.

Wash buffer: 0.1%Tween20-PBS.

6X SDS loading dye: 1.2g of SDS, 6 mg of Bromophenol Blue, 4.7 ml of glycerol, 1,2 ml of 0.5M Tris (pH 6.8) were dissolved in 4.1 ml of water and 0.93g of DTT was added and dissolved. The dye was was frozen in aliquots for further use. The samples were

denatured in the SDS loading dye and were loaded on a 12% polyacrylamide gel and were then resolved at 200V for 1 hr in running buffer. The proteins from the gel were transferred onto a PVDF membrane at 330 mAmp for 1-2 hr in transfer buffer. The membrane was then briefly rinsed with wash buffer and was blocked in a blocking buffer for 1 hr at room temperature. The primary antibody was diluted in a blocking buffer, then was added to the membrane for an overnight incubation at 4ºC. The membrane was then washed three times with the wash buffer and was incubated with the secondary antibody (diluted in the blocking buffer) for 1hr at room temperature. The membrane was then washed three times and the signals were detected with Typhoon FLA7000 (GE Healthcare Life Sciences) or ChemiDoc MP (Bio-Rad) imagers after ECL plus application. All membrane incubation steps were done on a shaker.

Co-immunoprecipitation to detect SIRT2-ARF6 interaction: Flag-SIRT2 or Flag-ARF6 were transiently overexpressed in three 10 cm plates of 50% confluent HEK293T cells. The cells were collected 24 hr later and were washed and lysed in 500 µl of NP-40 lysis buffer containing protease inhibitors for 30 min on ice with brief vortexing every 10 min. The lysates were spun down. The supernatants were combined with 500 µl of IP wash buffer (recipe above) and 20 µl of Flag beads and were subjected to 2 hr anti-FLAG-affinity immunoprecipitation at 4°C. The FLAG beads were washed three times with cold IP wash buffer and were boiled for 10 min in 15 µl of 2X SDS protein loading dye. After boiling, the beads were vortexed and spun down for 2 min at 17,000 g. The supernatants were analyzed by Western blot.

Subcellular fractionation: 4 million HEK293T cells were seeded into 10 cm plates. Flag-ARF6 and described mutants (1 µg) and HA-NMT2 (3 µg) plasmids were

transfected into the cells using the PEI reagent. After culturing for 24 hr, 100 μM ALK12 was added and the cells were cultured for additional 15 hr. They were then washed with cold PBS and were scraped into 500 μl of fractionation buffer (250 mM Sucrose, 20 mM HEPES pH 7.4, 10 mM KCl, 1.5 mM $MgCl_2$, 1 mM EDTA, 1 mM EGTA, freshly added 1 mM DTT and protease inhibitor cocktail). The samples were incubated on ice for 15 min, after which they were passed through a 27gauge needle 15 times and were left on ice for another 20 min. They were then centrifuged for 5 min at 900 g to pellet and remove the nuclei. The mitochondria was removed by another spin at 10,000 g for 5 min. Then membrane and cytosol fractions were separated by centrifugation at 17,000 g for 2.5 hr. The membrane fraction was washed twice by resuspending in 500 μl of fractionation buffer and passing through a 27 gauge needle 10 times and then centrifuging at 17,000 g for 1 hr between each wash. The membrane fractions were resuspended in 15 μl of 4% SDS lysis buffer (50 mM trimethylamine, 150 mM NaCl, 4% SDS) containing protease inhibitor cocktail followed by a dilution with 100 μl of 1% NP40 lysis buffer. Equal amounts of protein in the membrane and cytosolic fractions were subjected to FLAG IP by adding 15 μl of FLAG beads resuspended in 100 μl of IP wash buffer and rotating at 4°C for 2 hr. Click chemistry was performed as described above. 10 μl of 2X SDS protein dye was added and the samples were boiled for 7 min and were analyzed by SDS-PAGE and Western blot.

SIRT2 reaction on myristoylated ARF6 peptides: 50 μM ARF6 peptides myristoylated on glycine 2 or lysine 3, 4 μM SIRT2, and 1 mM NAD^+ were added to 20 mM Tris pH 7.5 to a 50 μl volume. The reactions were rotated at 37°C for 12 hr and were quenched with 50 μl of acetonitrile. The samples were spun down at 17,000 g for

10 min, the supernatants were mixed with 5 µl of 50% trifluoroacetic acid and were analyzed by LC-MS (LCQ Fleet from Thermo Scientific) with a binary gradient of 0.1% acetic acid in water and 0.1% acetic acid in acetonitrile using Kinetex 5 µm EVO C18 100 Å, 30 x 2.1 mm LC column from Phenomenex.

^{32}P-NAD^{+} assay to detect lysine defatty acylation by SIRT2: Flag-tagged ARF6 WT and ARF6 K3R were transiently transfected into SIRT2 KD HEK293T cells (5 plates per condition) using Fugene reagent and 5 □g of plasmid. After culturing for 24 hr, 50 □M myristic acid was added and the cells were cultured overnight. The cells were washed with cold PBS and were lysed with NP-40 lysis buffer and the expression of ARF6 and ARF6 K3R were determined by Western blot. ARF6 and ARF6 K3R were Flag-affinity purified from 10 mg of lysate using 40 µl of M2 Flag-agarose. Lysate without ARF6 or ARF6 K3R expression was also subjected to IP. The beads were split into two tubes for the ^{32}P -NAD^{+} assay. A reaction mixture containing 150 mM NaCl, 50 mM Tris, 10 mM DTT, and 2 µM SIRT2 or buffer only control was added to each reaction tube (10 µl each). Then 0.1µCi of ^{32}P-NAD^{+} (final activity) was added to each tube and the samples were briefly vortexed, spun down, transferred to 37°C heat block and incubated for 30 min with gentle tapping every 10 min. The samples were then spun down and 2 µl of supernatant was spotted onto a TLC plate. The spots were dried and the products were resolved in a TLC chamber containing 0.75 M ammonium acetate (pH 7.1) and 70% ethanol. Then, the plate was dried and exposed to the phosphor imaging screen (GE Healthcare, Piscataway, NJ) for 6 – 12 hr. The phosphorescence was detected using Typhoon FLA7000. The peptide assays were performed in the same manner using 40 µM peptides.

NMT reaction to detect the modification of ARF6 protein: HEK293T cells were transiently transfected with ARF6 WT, K3R, G2A and G2A/K3R (two 10-cm plates/construct). 24 hours later the cells were treated with 5 □M NMT inhibitor DDD85646 for 6 hr. The cells were lysed in NP-40 lysis buffer (25 mM Tris-HCl pH 7.4, 150 mM NaCl, 10% glycerol, and 1% Nonidet P-40) containing the protease inhibitor cocktail, and the proteins were isolated by Flag-affinity beads purification as described above. After three washes the beads were separated into three tubes and 100 µl of reaction mixture (50 mM Tris pH 8.0, 200 µM Alk12-CoA and 10 µM NMT1/2 or PBS) were added to the beads. The reactions proceeded for 2 hr at 30°C while rotating. The beads were washed two times and click chemistry, in-gel fluorescence, and Western blot were performed as described above.

Detection of ARF6 G2A lysine myristoylation by MS: ARF6 G2A and NMT2 were transfected into ten 10-cm plates of SIRT2 KD HEK 293T cells using FuGene 6 transfection reagent. After incubation for 24 hr the cells were treated with 50 µM myristic acid plus 7 mM nicotinamide overnight. The cells were lysed with the NP-40 lysis buffer and the protein was purified on Flag-affinity beads. Mass spectrometry was performed as previously described.[2] Briefly, the following conditions were used: LC gradient of 5-95% ACN with 0.1% formic acid (FA) from 0-160 min, 95-5% ACN with 0.1% FA from 160-161min, 5% ACN with 0.1% FA from 161-200; flow rate: 0.25 uL/min; voltage applied to the nano-LC electrospray ionization source: 2.5 kV; orbitrap resolution: 120,000; MS1 scan range: m/z 375-1575; MS2 scan range 112-867; ARF6 G2A myristoylation was identified by manual search.

NMT reaction on ARF6 N-terminal-derived synthetic peptides: Each 100 µl reaction contained 50 mM Tris (pH 8.0), 4-5 µM NMT1 or NMT2 or PBS, 200 µM myristoyl-CoA, and 100 µM peptide (added last). The mixtures were briefly vortexed and incubated at 30°C for 2 hr. The reaction were then quenched with 100 µl of acetonitrile for 30 min. The samples were centrifuged for 10 min at 17,000 g and the supernatant was transferred to a new tube and analyzed by LC-MS with a binary gradient of 0.1% acetic acid in water and 0.1% acetic acid in acetonitrile over 12 or 24 min. MS1 scan resolution was 150 – 2000 m/z and MS2 (Supplementary figure 2.2) was 200 -2000 m/z, for the precursor ion 744.5 m/z (Iso. width 1.3 m/z). The reactions in Figure 2.1D were separated on a binary gradient of 0.1% TFA in water and 0.1% TFA in acetonitrile on analytical HPLC (*Shimadzu UFLC)*.

NMT kinetics: For each reaction, 1 µM NMT1/2 and 100 µM myristoyl-CoA were added to 50 mM Tris (pH 8.0). After brief vortexing, the solution was transferred to reaction tubes in 96 µl aliquots. Then 4 µl of peptides dissolved in DMSO were added to each tube to final concentrations ranging from 200 µM to 3.13 µM. The reactions were rotated at 30°C for 1 hr (G2A peptide) or 0.5 hr (K3R peptide) followed by quenching with 100 µl of acetonitrile, vortexing and incubating for 30 min at room temperature. The samples were then spun down for 10 min at 17,000 g. The supernatants (190 µl) were transferred to new tubes and mixed with 10 µl of 50% trifluoroacetic acid. The samples were analyzed by analytical HPLC (*Shimadzu UFLC)* using a binary gradient of 0.1% trifluoroacetic acid in water and 0.1% trifluoroacetic acid in acetonitrile using an LC column Kinetex 5 µm EVO C18 100 Å, 150 X 4.6 mm from Phenomenex. Percent conversion was determined using the LabSolutions software. The

reactions were performed in duplicates. Michaelis–Menten kinetic parameters were calculated using the GraphPad Prism 5 software.

GTP loading analysis of overexpressed ARF6 WT and K3R: ARF6 WT and K3R were transfected into HEK293T cells. After culturing for 18 hr, the cells were treated with 100 μM myristic acid and 25 μM TM to promote acylation for 24 hr. The cells were washed with cold PBS and were lysed with the NP-40 lysis buffer. The GGA3-PBD or protein A/G beads were added to the lysate and were rotated for 1 hr at 4°C. The beads were washed 3 timed with the IP wash buffer, were boiled in 2x protein loading dye for 10 min, and then resolved by SDS-PAGE and analyzed by Western blot. For the analysis of the effects of NMT inhibition and NMT2 overexpression the same procedure was followed except NMT2 was co-transfected with WT ARF6 and 2 μM DDD85646 was used along with myristic acid treatment.

GTP loading analysis of endogenous ARF6 by GGA3 pull down: HEK 293T cells were seeded in a 6 well plate: 200,000 cells per well. 24 hr later 1 ml of media with lentiviral particles containing shRNA against luciferase or SIRT2 were added and after 24 hr the media were replaced with normal media. Then another 24 hr later 100 μM of myristic acid was added and the GGA3 pull down was performed as described above immediately after 24 hr.

ARF6 T27N, T27N/K3R, Q67L, Q67L/K3R colocalization with TfR: Stable SIRT2 KD, NMT1 KD, NMT2 KD or Luciferase KD HEK293T cells were plated in MatTek imaging dishes. The next day cells were transfected with Flag-tagged ARF6T27N, T27N/K3R, Q67L, Q67L/K3R. After 24 hr or 48 hr, the cells were fixed with 4% PFA-

PBS. The inhibitors (25 μM TM or 0.2 μM DDD85646) were added 24 hr post transfection and the cells were incubated for an additional 24 hr followed by fixation.

Immunofluorescence staining was performed as follows. The PFA fixed cells were permeabilized and blocked with PBS containing 5% BSA and 0.1% Triton for 30 min. The samples were than incubated with the antibodies for TfR (CD-71, 1:200 dilution) overnight at 4°C, then were washed twice with 0.1% Triton-PBS and incubated with rabbit anti-Flag antibody (1:1000) for 1 hr at room temperature. After two washes the samples were incubated with secondary antibodies (1:1000 dilution) goat anti-rabbit and anti-mouse conjugated to Cy3 or 647 or 488 fluorophores followed by three washes. All antibodies were diluted in the blocking buffer: PBS containing 5% BSA and 0.1% Triton. The samples were mounted with DAPI fluoromount-G (0100-20, Southern Biotech) and were analyzed on Zeiss 710 or Zeiss 880 confocal microscope using 63x objective.

Colocalization analysis of SIRT2 with endogenous TfR: 400,000 HEK293T cells were seeded into a well of a 6-well plate. The next day the cells were transfected with 1 μg of Flag-SIRT2 using PEI transfection reagent. 24 hr later the cells were trypsinized and 500,000 cells were seeded into Mattek 35 mm glass bottom dishes. 24 hr later the cells were washed with PBS and were fixed with 4% PFA-PBS. The staining was performed as described above using an overnight incubation at 4°C with anti-TfR (CD-71) (sc-32272) Ab at 1:200 dilution and a rabbit anti-Flag tag Ab at 1:1000 dilution.

Alk12-CoA synthesis: To a solution of Alk12 (19 mg, 0.085 mmol) in THF (0.5 ml) at room temperature was added triethylamine (11.9μl, 0.085 mmol) and then methyl chloroformate (6.6 μl). The resulting solution was stirred at room temperature for 1 hr.

This reaction solution then was added to a solution of CoA · 3Li (11 mg, 0.014 mmol) in 2.5% $KHCO_3$ aqueous (0.5 ml) slowly. The resulting solution was stirred at room temperature overnight (16 hr). The reaction was quenched with 0.05 ml of acetic acid and extracted by dicholoromethane (3 x 2 ml). The organic layer was washed by water (5 ml). The combined aqueous layer was concentrated, and the crude product was purified by silica gel column ($CHCl_3$: CH_3OH: CH_3COOH:H_2O = 15:9:1:2) to afford product (8 mg, 58.8%) as white solid. The product was further purified by HPLC using a binary gradient of 0.1% trifluoroacetic acid in water and 0.1% trifluoroacetic acid in acetonitrile. The synthesis scheme is provided in the Supplementary figure 2.17.

Full length NMT expression and purification: Human NMT1 and NMT2 were inserted into the pETHisTEV vector using the Gibson assembly strategy at NDE1 restriction site, and the plasmids were transformed into *E. coli* BL21 (DE3) cells. A single colony was grown overnight in 30 ml of LB media with 50 µg/ml kanamycin. The culture was then added to 2L of LB media with kanamycin and was grown until OD 600 reached 0.6. 0.2 mM IPTG was added to induce protein expression and the cultures were grown overnight at 18ºC. The cultures were spun down at 8000 RPM for 10 min and the pellets were resuspended in 40 mM Tris pH 8.0, 400 mM NaCl, 10 mM imidazole, 1 mM PMSF and were lysed by sonication. The lysates were spun down at 20,000g for 30 min at 4ºC. The supernatants were then applied to the equilibrated His Trap affinity column (71-5027-68 AF) and the column was washed with 50 ml of 40 mM Tris pH 8.0, 400 mM NaCl, 30 mM imidazole. The proteins were eluted with 40 mM Tris pH 8.0, 400 mM NaCl, 200 mM imidazole and were concentrated to 2 ml using 30k filters (Amicon). They were further purified by size exclusion on a Superdex 75

16/600 column FPLC into phosphate buffer saline (PBS) pH 7.4 or 20 mM Tris pH 7.5, 100 mM NaCl, 1 mM DTT.

SIRT2 Expression and purification: SIRT2 was expressed and purified from E.coli as previously described.[51]

Sample preparation for top-down mass spectrometry: Stable SIRT2 KD HEK293T cells were seeded in twenty 15 cm plates to 50 % confluency. 24 hr later each plate was transfected with 10 µg of ARF6-3XFlag (pJaff211 plasmid) and 5 µg of HA-NMT2. 24 hr later the cells were treated with 100 µM of myristic acid for 15 hr. The cells were then washed with cold PBS, lysed with NP-40 lysis buffer and Flag IP was performed for 4 hr at 4°C using 100 µL of beads. The beads were washed with the IP wash buffer 3 times followed by 5 washed with 1 ml of buffer containing 25 mM Tris pH 8.0 and 150 mM NaCl. The protein was eluted with 300 µl of 125 µM 3XFLAG peptide in 25 mM Tris and 150 mM NaCl buffer for 1 hr two times. Sample was concentrated to 100 µL and buffer exchange was performed by adding 300 µl of cold water and concentrating to 100 µl two times. Then 5 µl of acetonitrile and 0.2 µl of formic acid were added to the sample. Protein yield was estimated at 30 µg.

Top-down mass spectrometry analysis: For top-down mass spectrometry, 20 µL of the sample described above was desalted using a C4 ZipTip (Millipore) and the eluent was diluted 1:5 with Solvent A (5% acetonitrile in water + 0.2% formic acid). Sample was injected onto a trap column (150 µm ID × 3 cm) coupled with a nanobore analytical column (75 µm ID × 25 cm). The trap and analytical column were packed with polymeric reverse phase (PLRP-S, Agilent) media (5 µm, 1,000 Å pore size). Samples

were separated using a linear gradient of 10% solvent A to 45% solvent B (5% water, 95% acetonitrile, 0.1% formic acid) over 35 minutes. MS data were obtained on a Q-Exactive HF (ThermoFisher) mass spectrometer fitted with a custom nanospray ionization source. Intact mass spectrometry data were obtained at a resolving power of 120,000 (m/z 200). The top 2 m/z species were isolated and fragmented using higher energy collisional dissociation (HCD). Additional MS runs were completed targeting the specific ARF6 proteoforms of interest. Data were analyzed with both ProSightPC (ThermoFisher) and ProSight Lite (CITE https://www.ncbi.nlm.nih.gov/pubmed/25828799) against a custom ARF6 database.

Detection of endogenous ARF6 myristoylation: 10 million of HEK293 cells (control or SIRT2 KD) were seeded in 15 cm plates (1 plate per condition). 24 hr later 100 μM ALK12 and 10 mM nicotinamide were added for 15 hr. The cells were collected and washed with cold PBS. They were then lysed with 1 ml of 4% SDS lysis buffer. 1.8 mg of protein was brought to 700 μl and treated with 1 M hydroxylamine for 30 min at 37°C. The protein was then precipitated with 2 volumes of methanol, 2/3 volumes of chloroform and 4/3 volumes of water (all precipitation reagents were ice-cold). The samples were spun down at 4690 g, 4°C, for 30 min. The supernatants were discarded and the protein pellets were washed with 10 ml of ice-cold methanol twice. The pellets were air dried and were resolubilized with 400 μl of 4% SDS lysis buffer by rotating at 37°C and vortexing until dissolved. 800 μg of protein was brought up to 400 μl with 4% SDS lysis buffer and click chemistry was performed by adding 5mM azide-PEG3-biotin conjugate (Sigma-Aldrich catalog number 762024) in water to 20 μM, 10 mM TBTA in DMF to 40 μM, 40 mM TCEP in water to 2 mM, and 40 mM $CuSO_4$ in water to 2

mM final concentrations. The samples were incubated at 30°C while rotating. The proteins were precipitated as above and the pellets were resolubilized in 200 µl of 4% SDS lysis buffer. 430 µg of protein was brought up to 200 µl with 4% SDS lysis buffer and the samples were brought up to 1.4 ml with BriJ buffer (50 mM TEA pH 7.4, 150 mM NaCl, 1% BriJ v/v). 20 µl per sample of high capacity streptavidin conjugated beads were washed 3 times with 1 ml of BriJ buffer, were resuspended in the appropriate volume of BriJ buffer to add 100 µl to each sample. The samples were rotated at 4°C overnight. The beads were washed 3 times with 1 ml of BriJ buffer. After the last wash all of the buffer was removed and the beads were boiled in 15 µl of 2X SDS sample loading dye for 10 min. The samples were analyzed by SDS-PAGE and Western Blot. The signal was detected with ChemiDoc MP or Typhoon FLA7000 (when ChemiDoc was not sensitive enough to detect the input signal) scanners.

In vitro SIRT2 reaction to remove ARF6 ALK12 labeling: 1 million of HEK293T cells was seeded in 6 cm plates. 1 µg of Flag-ARF6 WT or G2A plasmids were co-transfected with 3 µg of HA-NMT2 using PEI transfection reagent. 24 hr later 100 µM ALK12 was added and the cells were treated for 15 hr. The cells were lysed with 1% NP40 lysis buffer and subjected to flag IP as described above. The washed beads were divided into three tubes for the SIRT2 reaction. The reaction was performed in 15 µl of 50 mM Tris pH 8.0, 100 mM NaCl, 2 mM $MgCl_2$, 1 mM DTT, 1 mM NAD^+, 5 µM SIRT2. The reaction components except SIRT2 were combined and added to the beads, then SIRT2 was added to start the reaction. The samples were incubated for 1 hr at 37°C with gentle agitation. The beads were washed three times with IP wash buffer and were

boiled with 10 min in 2X SDS sample loading dye. They were than analyzed by WB and in-gel fluorescence.

NMT2 co-IP with ARF6 Q67L and ARF6 T27N: One million HEK293T cells were seeded into 6 cm plates. 24 hr later the cells were transfected with the Flag-ARF6 mutant (1 μg), HA-NMT2 (2 μg) and empty vector (2μg) plasmids. 24 hr later the cells were washed with cold PBS and were lysed with 300 μl of NP40 lysis buffer. 300 μg of total protein was subjected to Flag or HA immunoprecipitation. The beads were washed three times and the proteins were eluted by boiling in 2X SDS sample loading dye. The samples were analyzed by WB.

Detection of NMT-catalyzed single lysine myristoylation: In vitro NMT reaction wit ALK12-CoA on ARF6 protein was performed as described above. The beads were then washed 3 times with the IP wash buffer and each sample was split into two tubes. Then the SIRT2 reaction was performed as described above.

Detecting the effect of ARF6 lysine myristoylation on pERK: 350,000 HEK293T (SIRT2 KD or control) were seeded in each well of 6 well plates. 24 hr later the cells were transfected with 0.5 μg of Flag-ARF6 WT or K3R and 1.5 μg of HA-NMT2 or empty vector (to achieve equal expression levels of ARF6 across conditions) using PEI transfection reagent. 24 hr later the cells were washed with serum free media once and cultured in 1 ml of serum free media for 15 hr. The cells were scraped into the media, spun down for 5 min at 500 RPM, washed with 1 ml of ice-cold PBS and spun down again. Immediately, the pellets were lysed with 4% SDS lysis buffer containing protease

and phosphatase inhibitors or were frozen at -80ºC for later lysis. 20 µg of lysates were analyzed for pERK and 10 µg for total ERK by Western Blot.

Detecting the effect of TM and DDD85646 on pERK: 400,000 HEK293T were seeded in each well of 6 well plates. 24 hr later inhibitors were added at indicated concentrations. 15 hr later the cells were harvested and analyzed as described for "Detecting the effect of ARF6 lysine myristoylation on pERK".

NMT catalytic domain cloning, expression, and purification: NMT1 (115-496) and NMT2 (115-496) were each cloned into a pETHisTEV vector with a His6 tag and a HRV 3C PreScission protease cleavage site. The proteins were purified from clarified BL21 cell lysate using Ni-NTA resin as described above for full length NMT, concentrated and buffer exchanged with a 10DG column, treated with PreScission protease overnight at 4°C, run back over Ni-NTA resin to remove tag, protease, or contaminants, and finally purified by size exclusion on a Superdex 75 16/600 column in 25 mM Tris-HCl pH 7.5, 120 mM NaCl, 1 mM DTT, 1 mM $MgCl_2$.

Crystallization, data collection, and structure solution: NMT2 was used at a final concentration of 8 mg/mL in a buffer of 25 mM Tris-HCl pH 7.5, 120 mM NaCl, 1 mM DTT, 1 mM $MgCl_2$. Before crystallization, 0.35 mM myristoyl-CoA and 3.5 mM KVLSKIF peptide were added and incubated at room temperature for 10 min. Protein solution was mixed in a 1:1 ratio with a well solution of 22% PEG 8000, 0.1 M Bis Tris pH 6.5. Rod-shaped crystals grew in 3 weeks by the hanging drop vapor diffusion method. NMT1, 7.5 mg/mL in 25 mM Tris-HCl pH 7.5, 120 mM NaCl, co-crystallized in the presence of 0.3 mM myristoyl-CoA and 0.3 mM AcKVLSKIF using a well

solution of 18% PEG 8000, 100 mM NaCl, 100 mM sodium citrate pH 5.6, 100 mM $MgCl_2$.

Crystals were cryo-protected with 25% glycerol added to well solution and flash-frozen in liquid nitrogen. Datasets were collected at the NE-CAT beamline 24-ID-E at the Advanced Photon Source (Supplementary Table 1). Images were indexed, integrated, and merged using XDS and Aimless in the RAPD pipeline at NE-CAT and further cut according to CC1/2 and I/sigmaI statistics in Phenix[52]. Structures were solved using PHASER molecular replacement.[53] Models were constructed using iterative building in COOT[54] and refinement in Phenix.[55] Omit maps were calculated by removing the CoA, peptide, and myristoyl groups followed by simulated annealing refinement.

Generation of SIRT1/2/3/6/7 and HDAC11 KD HEK293T cell lines: Packaging and shRNA plasmids for lentivirus generation were from Sigma. Luciferase targeting was used as negative control. Lentiviral particles were generated by co-transfection of shRNA plasmids with the packaging plasmids pCMV-dR8.2 and pMD2.G into HEK293T cells. The medium containing the lentivirus was collected 24 and 48 hr after transfection, was filtered with 0.45 μM filters and was later used to transduce cells. 200 thousand of HEK293T cells were seeded in 6 well plates. 1 ml of media of lentiviral particles containing the following shRNA: SIRT1-1 TRCN0000218734 and SIRT1-2 TRCN0000229630; SIRT3-1 TRCN0000038893 and SIRT3-2 TRCN0000298766; SIRT7-1 TRCN0000359663 and SIRT7-2 TRCN0000359594; SIRT6-1 TRCN0000378253 and SIRT6-2 TRCN0000232528;

HDAC11-1 CCGGGTTTCTGTTTGAGCGTGTGGACTCGAGTCCACACGCTC AAACAGAAACTTTTTG and HDAC11-2 CCGGGCGCTATCTTAATGAGCTCAAC TCGAGTTGAGCTCATTAAGATAGCGCTTTTTG;

Luciferase CCGGCGCTGAGTACTTCGAAATGTCCTCGAGGACATTTCGAAGTACTCA GCGTTTTTG;

NMT1-1: TRCN0000035713 (CCGGCCTGAGCAGAAATATGACCATCTCGAGATGGTCATATT TCTGCTCAGGTTTTTG); NMT1-2 TRCN0000289868 (CCGGCGGAAATTGG TTGGGTTCATTCTCGAGAATGAACCCAACCAATTTCCGTTTTTG); NMT2-1 TRCN0000291915 (CCGGCCAACGGTAAACTGACTGATTCTCGAGAATCAGTCAGTTTACCGT TGGTTTTTG); NMT2-2 TRCN0000303312 (CCGGGAAATTGAAGTAGTCGATAATCTCGAGATTATCGAC TACTTCAATTTCTTTTTG); SIRT2-1: TRCN0000040219 (CCGGGCCATCTTTGAGATC AGCTATCTCGAGATAGCTGATCTCAAAGATGGCTTTTTG), SIRT2-2: TRCN0000310335, (CCGGCCTGTGGCTAAGTAAACCATACTCGAGTATGGTTTACTTAGCCACA GGTTTTTG).

The cells were selected with 2 μg/mL puromycin for 1 week.

The analysis of KD efficiency by qRT-PCR: RNA was extracted from cells using the E.Z.N.A. total RNA kit I (Omega bio-tek, catalog # R6834-02). cDNA was synthesized using 0.5 – 1. 0 µg of RNA using SuperScript VILO cDNA synthesis kit (Ivitrogen, catalog # 11754050) and was diluted to 100 – 200 µl with water. qRT-PCR was performed in 20 µl reactions containing 1 µl cDNA, 500 nM primers (NMT1: GGTCAGGGACCTGCCAAAAC, CATGGGTGTTCACCACTTCG; NMT2: TCCCAGCAAACATTCGGATTT, ACCCGTTTCGA TCTCAACTTCT; HDAC11: CACGCTCGCCATCAAGTTTC, GAAGTCTCGCTCATGCCCATT; GAPDH: ACAACTTTGGTATCGTGGAAGG, GCCATCACGCCACAGTTTC) and SYBR Green (Thermo Fisher Scientific, ref 4367659). Target gene expression was normalized to the levels of GAPDH.

Colocaliztion analysis: Colocaliztion was analyzed in Fiji using the JACop plugin. Pearson's coefficients with SEM are reported.

Statistical analysis: All statistics were obtained using the unpaired two-tailed t test in GraphPad Prism 5 or 6 software.

ACKNOWLEDGEMENTS

This work was supported by NIH/NIDDK (DK107868), NIH/NIGMS (GM098621), HHMI and NSF GRFP awards. We thank the National Resource for Translational and Developmental Proteomics (supported by NIH P41 GM108569) for help with ARF6 top-down mass spectrometry, Cornell Proteomic and MS Facility for help with ARF6 G2A mass spectrometry and Jun Young Hong for help with instruments and reagents. Imaging experiments were performed at Cornell BRC-Imaging facility

(supported by NIH S10RR025502, NYSTEM C029155 grants), especially Johanna M. Dela Cruz. ARF6 (pJAF215) and ARF1 (pJAF211) plasmids were a gift from Dr. Gregory Pazour and mCherry-TFR-20 plasmid was a gift from Dr. Michael Davidson. We are grateful to Maurine Linder, Richard A. Cerione, Benjamin D. Cosgrove, Hui Jing, and Arash Latifkar for helpful discussions and suggestions. This work made use of the Northeastern Collaborative Access Team beamlines, which are funded by the National Institute of General Medical Sciences from the National Institutes of Health (P30 GM124165). The Eiger 16M detector on 24-ID-E beam line is funded by a NIH-ORIP HEI grant (S10OD021527). This research used resources of the Advanced Photon Source, a U.S. Department of Energy (DOE) Office of Science User Facility operated for the DOE Office of Science by Argonne National Laboratory under Contract No. DE-AC02-06CH11357. Preliminary X-ray crystallography experiments were also performed at the Advanced Light Source (Berkeley Center for Structural Biology, Lawrence Berkeley National Laboratory, DOE Contract No. DE-AC02-05CH11231 and NIH award P30 GM124169) and at the Cornell High Energy Synchrotron Source (CHESS, NSF award DMR-1829070), using the Macromolecular Diffraction at CHESS (MacCHESS, NIH Award GM-124166) facility.

AUTHOR CONTRIBUTIONS

TK designed and performed all the studies except those noted below. IP and SH performed crystallography and associated expression and purification of the NMT catalytic domains. IP performed structure solution and building and contributed the figures and text describing the crystallographic findings to the manuscript. SZ, IP and TK purified full length NMT1 and NMT2 and IP and XZ purified SIRT2 for in vitro

studies. XZ performed mass spectrometry for ARF6 G2A. CZ synthesized peptides that were not purchased from Biomatik. KJ and GK replicated key experiments. MY synthesized ALK12-CoA and TM. CD, PT and NK analyzed the ARF6 protein sample by top-down mass spectrometry. TK wrote and HL revised the manuscript with the input from all authors. HL directed the biochemical studies and JF directed the X-ray crystallography studies.

COMPETING INTERESTS

HL declare the following competing interests: Cornell University has patents on the SIRT2 inhibitor TM with HL as an inventor. All other authors declare no competing interests.

SUPPLEMENTARY INFORMATION

Supplementary table 2.1 Data collection and refinement statistics. Statistics for the highest-resolution shell are shown in parentheses.

	NMT2 with myristoyl-KVLSKIF and CoA (PDB: 6PAU)	**NMT1 with myristoyl-AcKVLSKIF and CoA (PDB: 6PAV)**
Wavelength (Å)	0.97918	0.97918
Resolution range (Å)	57.59 - 1.93 (2.00 - 1.93)	51.34 - 2.52 (2.61 - 2.52)
Space group	P 1 21 1	C 1 2 1
Unit cell a/b/c (Å): α/β/γ:	63.16/ 46.35/ 74.40 90°/ 114.25°/ 90°	92.36/ 58.22/ 154.04 90°/ 90.66°/ 90°
Total reflections	154166 (15911)	104948 (9898)
Unique reflections	29746 (2966)	27918 (2722)
Multiplicity	5.2 (5.3)	3.8 (3.6)
Completeness (%)	99.49 (99.56)	98.45 (97.21)
Mean I/sigma(I)	11.35 (1.54)	4.98 (0.94)
Wilson B-factor	29.29	51.51
R-merge	0.1007 (1.066)	0.3053 (1.196)
R-meas	0.1123 (1.184)	0.3558 (1.404)
R-pim	0.04867 (0.505)	0.1804 (0.7275)
CC1/2	0.998 (0.646)	0.919 (0.34)

CC*	0.999 (0.886)	0.979 (0.713)
Reflections used in refinement	29687 (2965)	27560 (2719)
Reflections used for R-free	1529 (161)	1468 (158)
R-work	0.1973 (0.3721)	0.2644 (0.4147)
R-free	0.2174 (0.4192)	0.2819 (0.4281)
CC(work)	0.963 (0.841)	0.913 (0.615)
CC(free)	0.956 (0.754)	0.900 (0.517)
Number non-hydrogen atoms	3320	6521
macromolecules	3043	6287
Ligands	101	150
Solvent	176	84
Protein residues	369	771
RMS(bonds)	0.008	0.012
RMS(angles)	1.20	1.66
Ramachandran favored (%)	96.70	96.57
Ramachandran allowed (%)	3.30	3.43
Ramachandran outliers (%)	0.00	0.00
Rotamer outliers (%)	0.29	1.58
Clashscore	5.52	13.53
Average B-factor	37.87	58.61
macromolecules	37.09	58.29
Ligands	54.37	80.85
Solvent	41.79	42.99
DPI (Å)	0.169	0.343

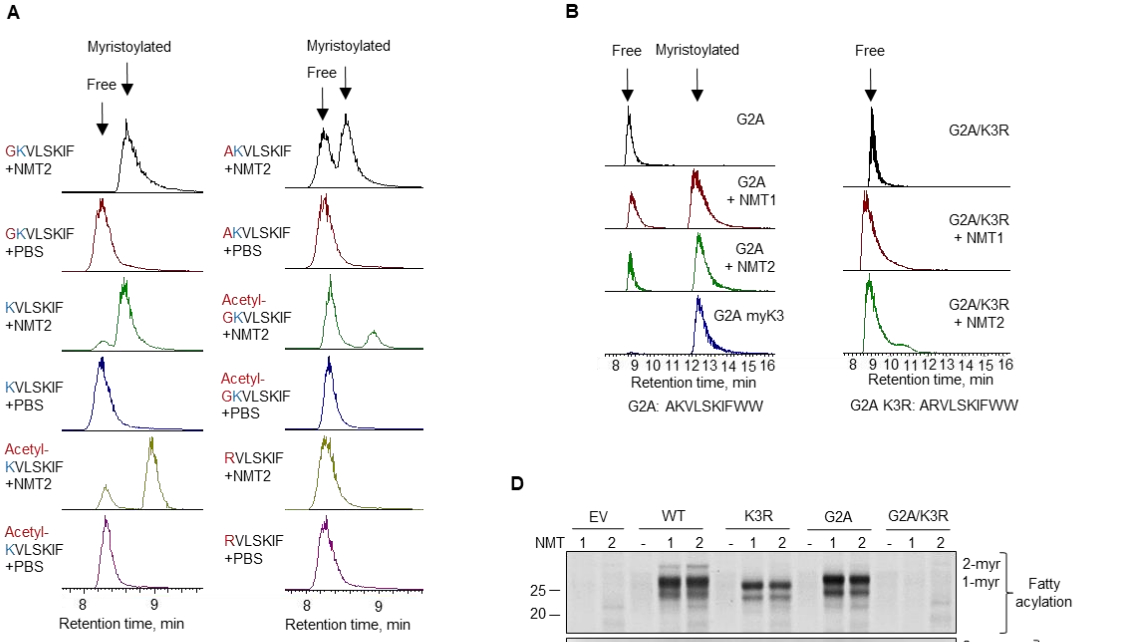

NMT1

Peptide	K_m, (μM)	k_{cat}, (s^{-1})	k_{cat}/K_m, ($s^{-1}M^{-1}$)
ARF6 K3R	7.19 ± 0.48	(30.65 ± 0.81)X10^{-4}	426 ± 167
ARF6 G2A	5.31 ± 2.84	(7.62 ± 0.17)X10^{-4}	144 ± 6

NMT2

Peptide	K_m, (μM)	k_{cat}, (s^{-1})	k_{cat}/K_m, ($s^{-1}M^{-1}$)
ARF6 K3R	14.28 ± 2.83	(36.46 ± 1.59)X10^{-4}	252 ± 56
ARF6 G2A	6.73 ± 0.14	(8.95 ± 0.07)X10^{-4}	133 ± 16

Supplementary figure 2.1 NMT myristoylates K3 of ARF6. (A) Mass traces of NMT2 reactions on ARF6 synthetic peptides are shown. (B) NMT cannot myristoylate G2A/K3R peptide. (C) NMT kinetics on indicated peptides. (D) In vitro NMT reaction with ALK12-CoA on ARF6 mutants suggests multiple acylation products. (E) Protein gel showing the purity of full-length recombinant NMT1 and NMT2.

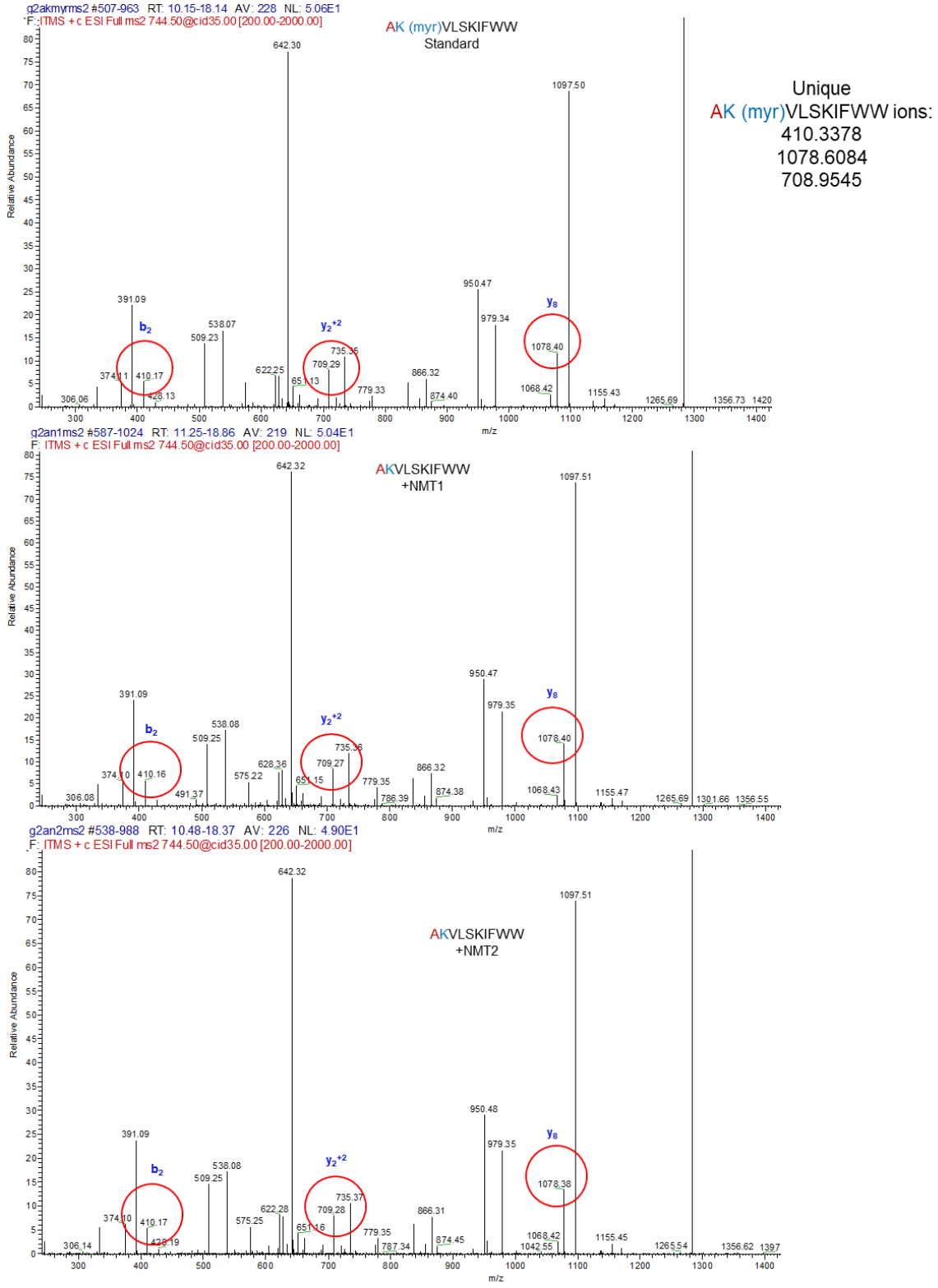

Supplementary figure 2.2 NMT1 and NMT2 modify ARF6 G2A peptide on K3. Tandem MS spectra of standard myristoyl peptide and products from NMT reactions are shown. Circled fragment ions are unique to the acylated product while others are common to both substrate and product.

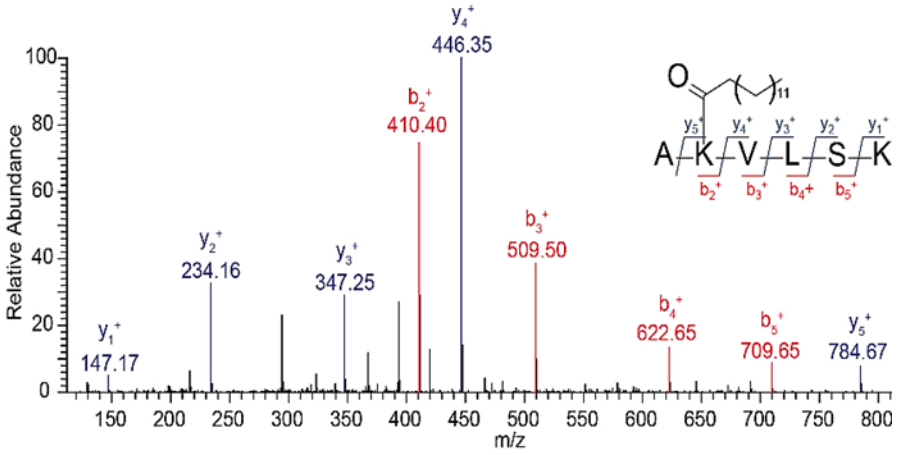

Supplementary figure 2.3 K3 myristoylation on ARF6 G2A identified by MS/MS. ARF6 G2A mutant was isolated from SIRT2 KD HEK 293T cells.

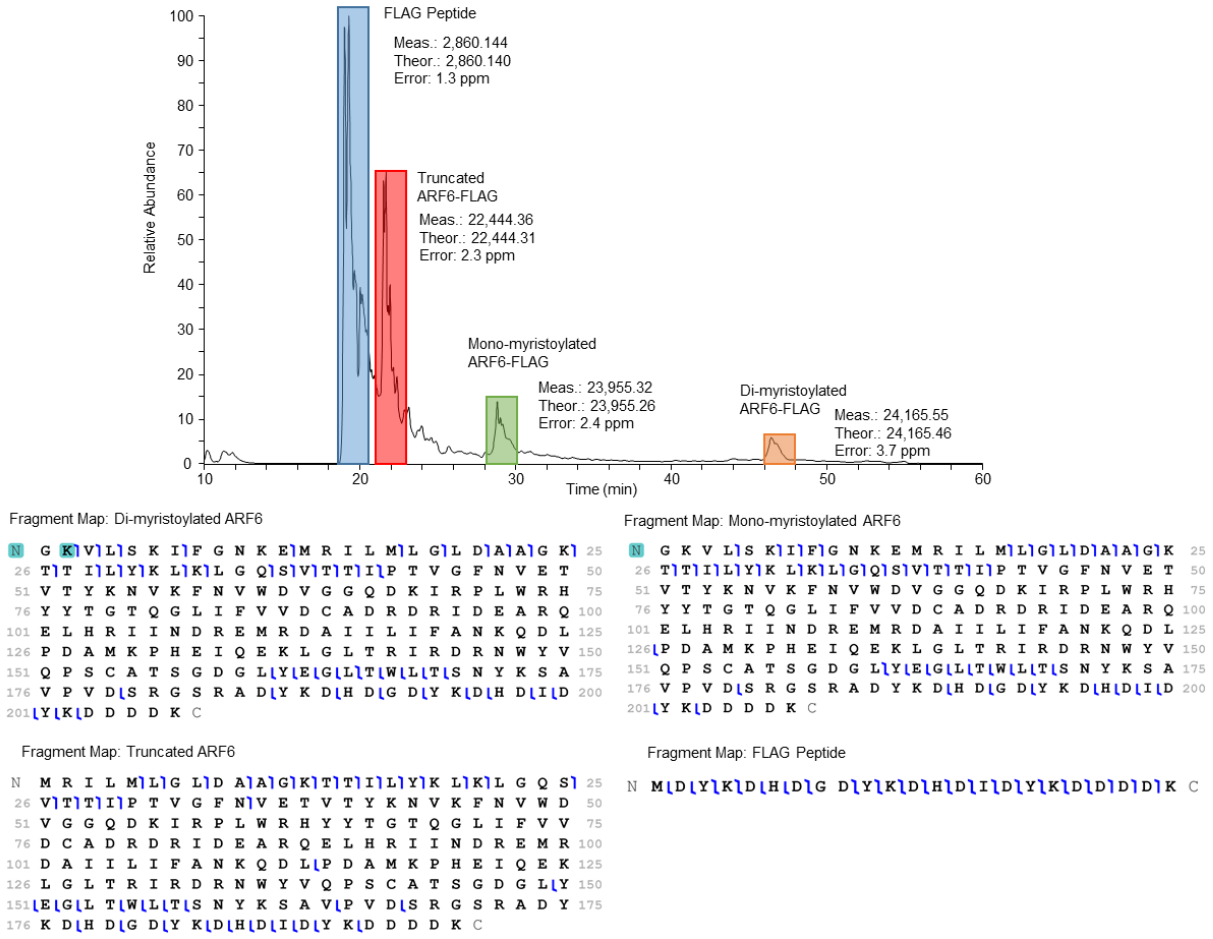

Supplementary figure 2.4 Di-myristoylated ARF6 is identified by top-down mass spectrometry. Annotated chromatogram showing identified protein species and corresponding fragment maps. Highlighted N and K indicate the modification sites at the N-terminus and lysine residue. Flag peptide was used to elute the protein during sample preparation. The truncated species is caused by the alternative start site and explains the lower band observed by western blot.

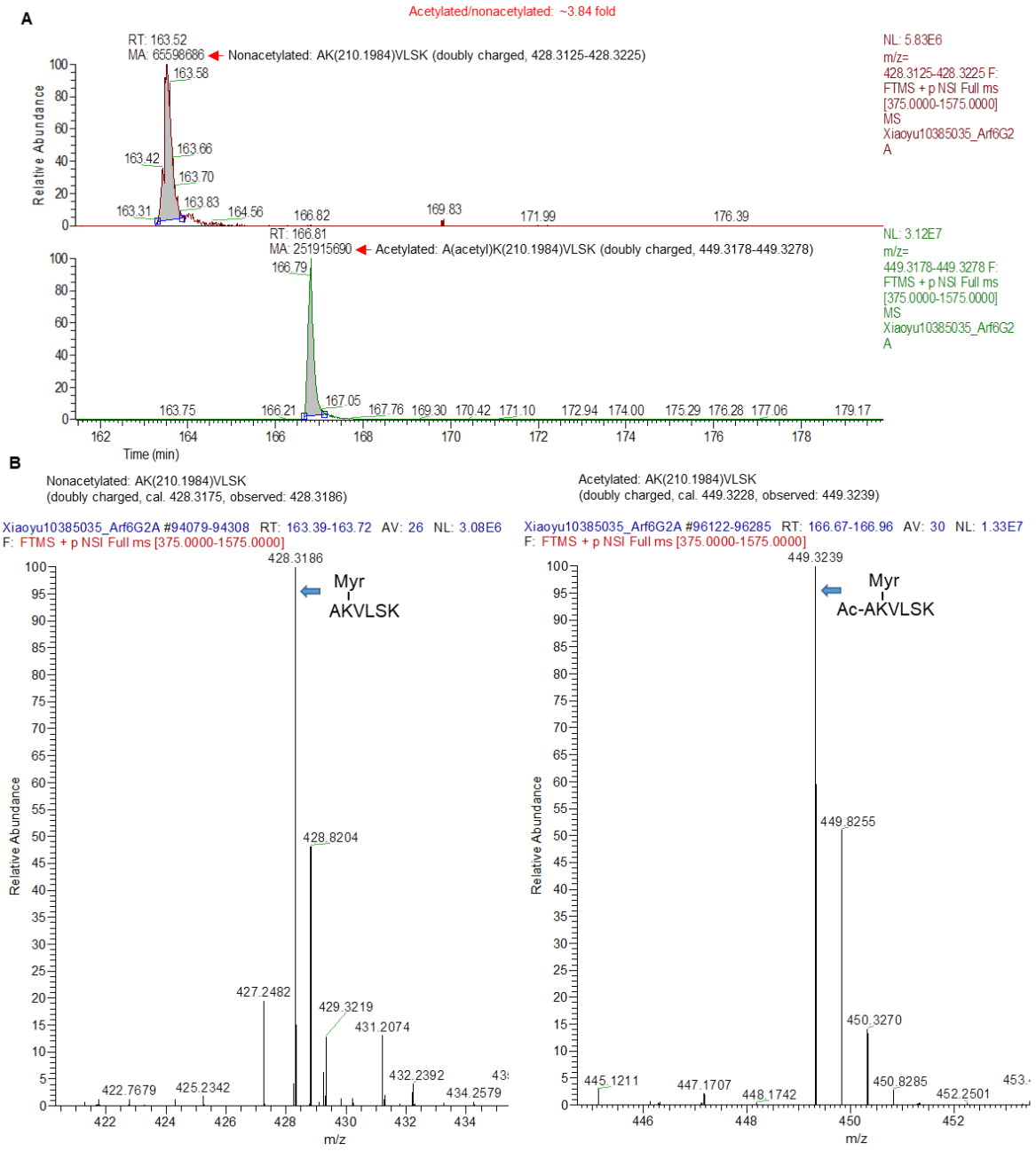

Supplementary figure 2.5 Comparison of N-terminal acetylated vs. nonacetylated ARF6 G2A K3 myristoylated sequence. A) TIC and peak quantification showing that the peptide that is both acetylated and myristoylated is more abundant than the myristoylated only peptide. B) Mass spectra for the N-terminal peptides of ARF6 G2A.

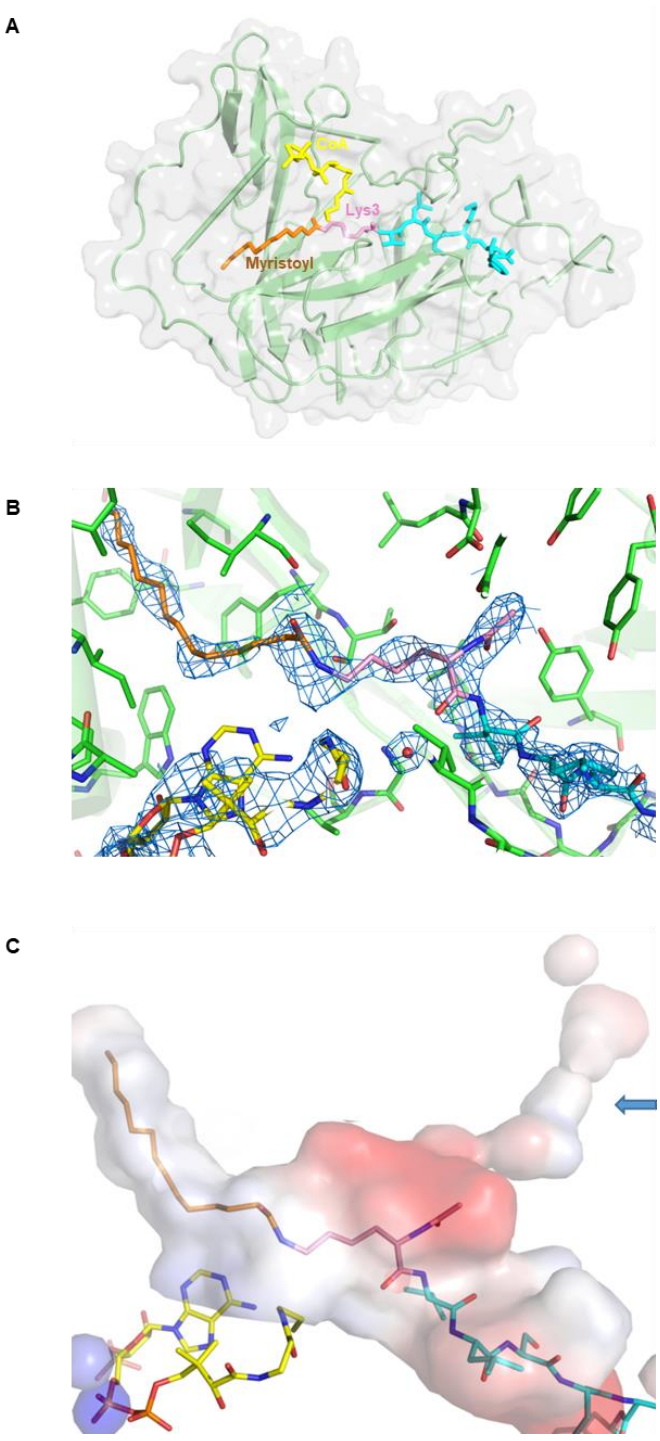

Supplementary figure 2.6 NMT bound to myristoyl-lysine peptide. (A) Overall structure of NMT2 catalytic domain with myristoyl-KVLSKIF peptide and CoA. (B) NMT1-AcKVLSKIF, $2F_O$-F_C simulated annealing omit map, 1.0 σ. (C) Interior pockets (shown as surface) around the NMT1 active site. The surface is colored by the electrostatic properties of the surrounding residues: blue (positive), red (negative), and gray (hydrophobic). Blue arrow points to the hydrophobic pocket.

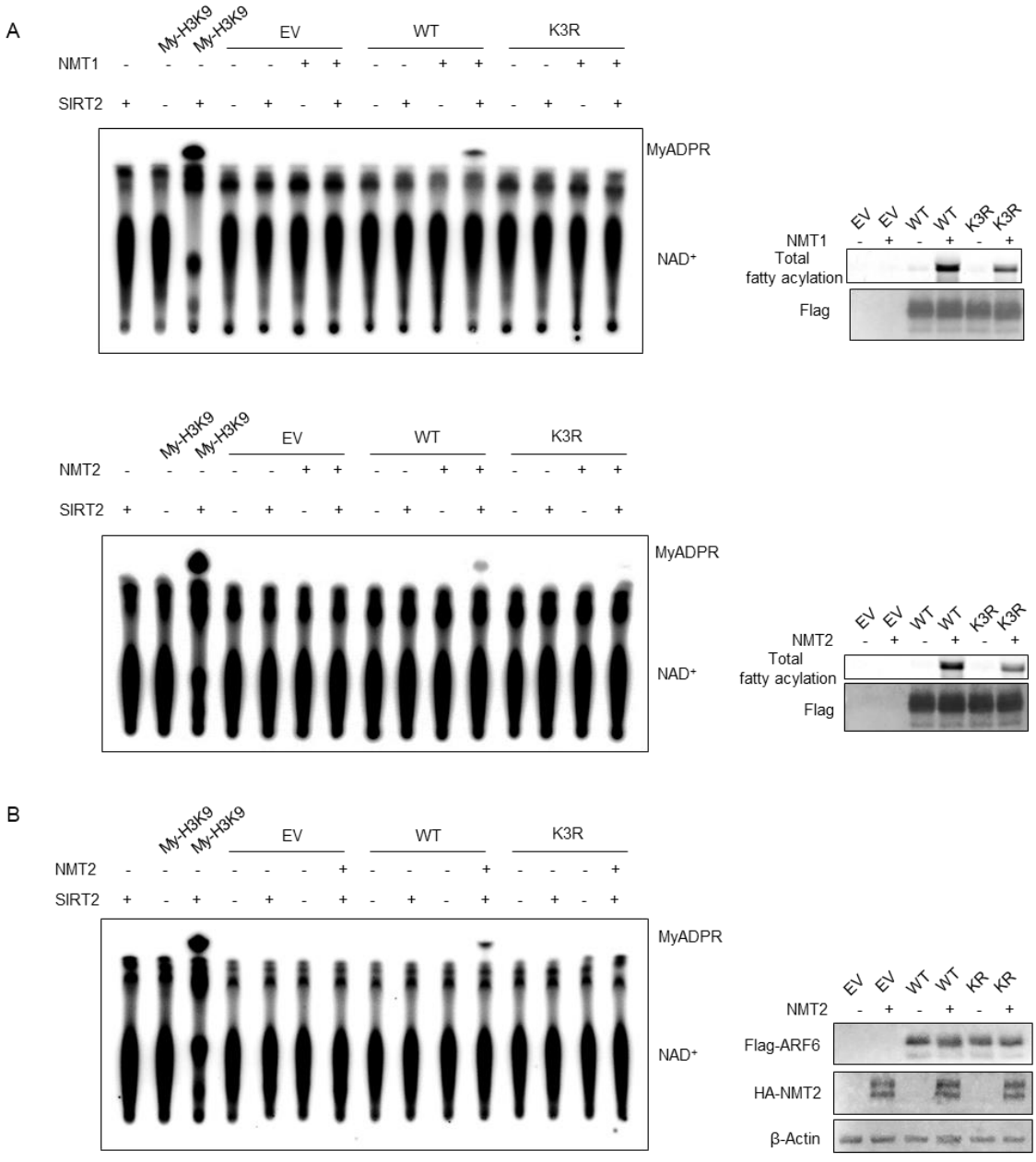

Supplementary figure 2.7 NMT myristoylated ARF6 on lysine 3. ^{32}P-NAD$^+$ assays showing that NMT1 and NMT2 modify ARF6 WT on K3. (A) ARF6 WT or K3R mutant were modified with NMT1 or NMT2 in vitro, and then subjected to ^{32}P-NAD$^+$ assay to detect lysine myristoylation. Total myristoylation levels (detected by Alk12-CoA labeling and in-gel fluorescence) and western blots showing protein levels are shown on the right. (B) NMT2 myristoylates ARF6 WT on K3 in cells. ARF6 WT and K3R were purified from HEK293T cells with or without NMT2 overexpression, and then subjected to ^{32}P-NAD$^+$ assay to detect lysine myristoylation. Western blots showing protein levels are shown on the right. One replicate for A and B.

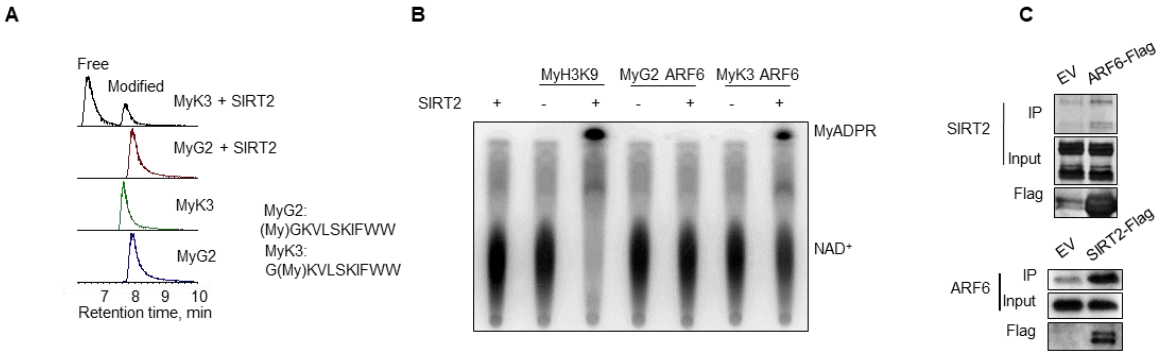

Supplementary figure 2.8 SIRT2 demyristoylates ARF6 K3. (A) LC-MS traces of SIRT2 reactions on myristoylated ARF6 N-terminal peptides showing that SIRT2 demyristoylates K3 but not G2. (B) P^{32}-NAD^{+} assay on ARF6 N-terminal peptides myristoylated on G2 or K3 showing that MyADPR is formed with the addition of SIRT2 to K3 but not G2 myristoylated peptides. (C) SIRT2 and ARF6 associate with each other as detected by co-IP.

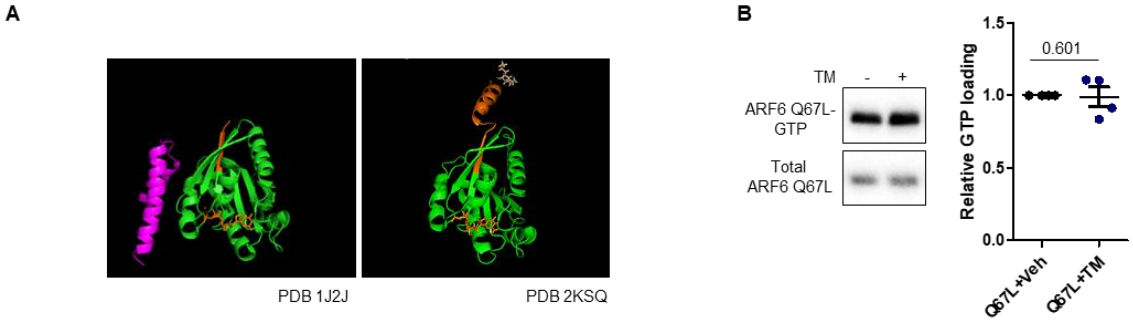

Supplementary figure 2.9 ARF6 lysine 3 myristoylation is unlikely to affect GGA3 binding. (A) Crystal structures of ARF1-GTP without N-terminal helix in complex with binding domain of GGA1 (PDB 1J2J) and ARF1-GTP with myristoylated N-terminal helix (PDB 2KSQ). ARF1 – green, GGA1 – cyan, GTP and N-terminal helix with preceding residues – orange. The myristoylated N-terminal helix is far from the binding domain of GGA1. (B) TM does not affect GGA3 binding to ARF6 Q67L, suggesting that lysine 3 myristoylation does not affect ARF6 binding to GGA3. Error bars represent SEM.

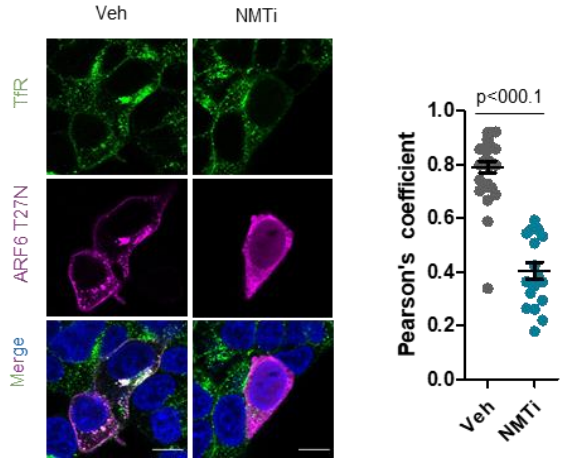

Supplementary figure 2.10 NMTi inhibits ARF6 T27N colocalization with TfR. Each point in the right quantification plot represents one cell (Veh=27, NMTi=17), quantification shows Pearson's correlation coefficient with SEM. Scale bars: 10 µM. (n=1).

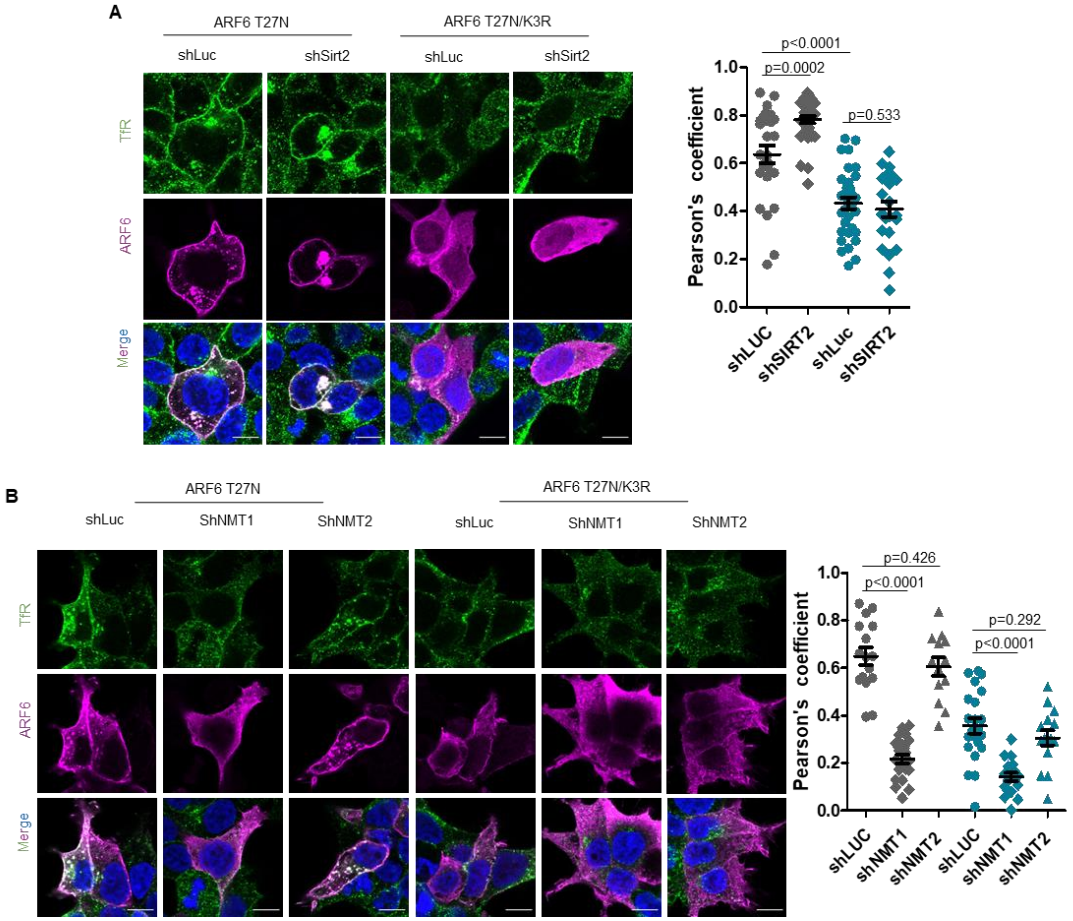

Supplementary figure 2.11 ARF6 lysine myristoylation cycle regulated membrane localization of inactive ARF6. (A) SIRT2 KD promotes ARF6 T27N (but not T27N/K3R) association with membranes as indicated by colocalization with TfR. (B) NMT1 KD inhibits ARF6 T27N colocalization with TfR. Both A and B were performed in HEK293T cells transiently overexpressing ARF6 T27N. n=3 and n=2 for SIRT2 KD and NMT KD respectively. Scale bars: 10 µM. Each point is one cell, (for (A) shLuc/T27N=27, shSIRT2/T27N=34, shLuc/T27N/K3R=33, shSIRT2/T27N/K3R=23; for (B) shLuc/T27N=16, shNMT1/T27N=22, shNMT2/T27N=13, shLuc/T27N/K3R=22, shNMT1/T27N/K3R=17, shNMT2/T27N/K3R=15) Quantifications represent Pearson's correlation coefficients with SEM. Unpaired two-tailed t-test.

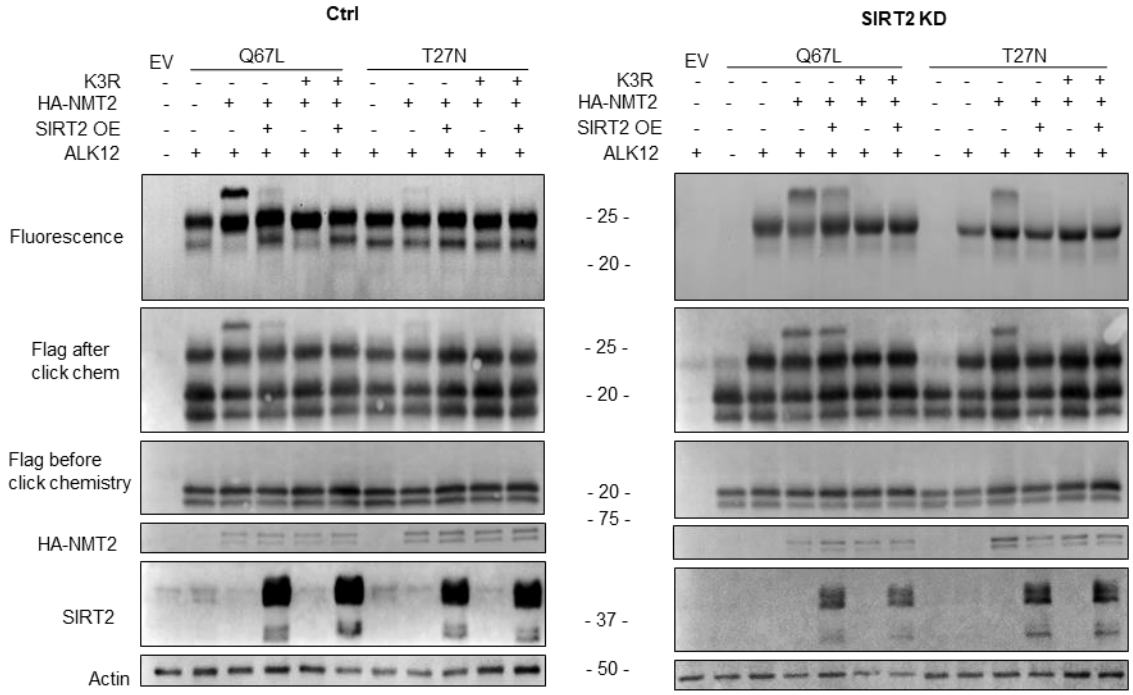

Supplementary figure 2.12 NMT and SIRT2 prefer different catalytic states of ARF6. In-cell Alk12 labeling of ARF6 Q67L and T27N mutants with NMT2 OE and/or SIRT2 OE/KD showing more lysine acylation of ARF6 Q67L.

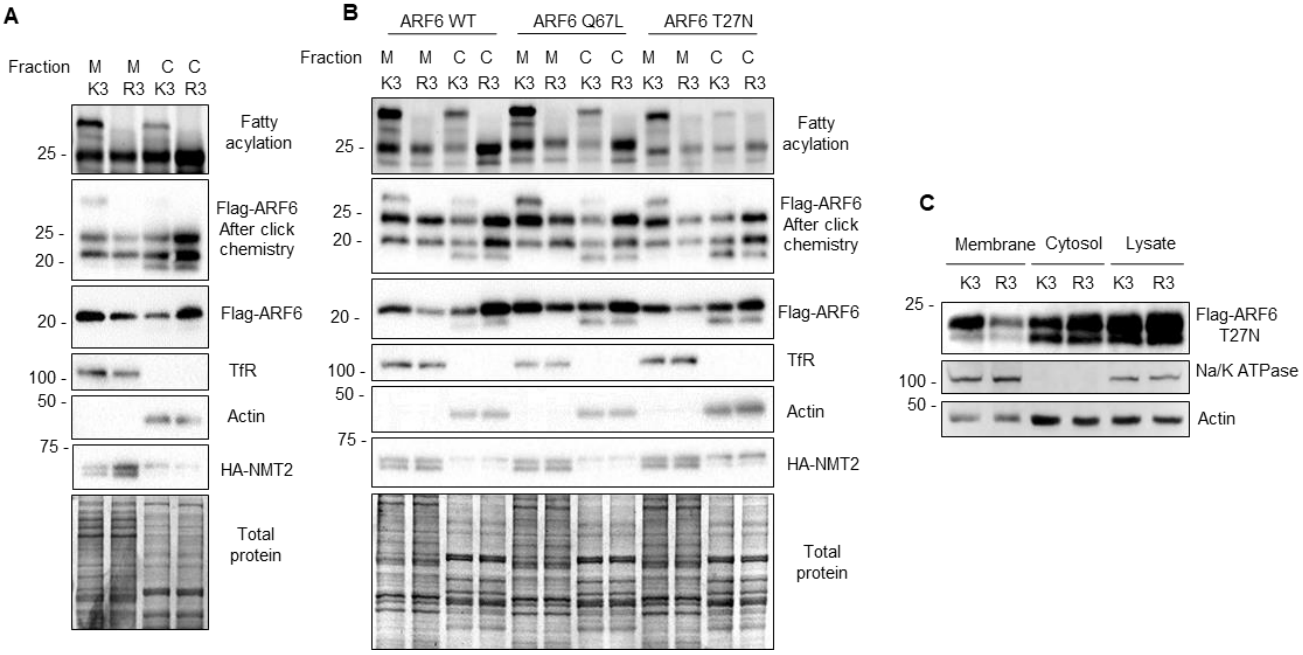

Supplementary figure 2.13 K3 myristoylation promotes ARF6 membrane localization. (A) ARF6 K3 myristoylation promotes membrane association of ARF6 WT in HEK 293T cells. (B) ARF6 K3 myristoylation promotes membrane association of active and inactive mutants of ARF6 in HEK 293T

cells. SIRT2 KD cells were used for this experiment. Cell overexpressing ARF6 WT and mutants were subjected to differential centrifugation. (C) ARF6 T27N fractionation in HEK293T cells without NMT OE showing that abrogating K3 myristoylation with K3R mutation inhibits membrane localization of inactive ARF6.

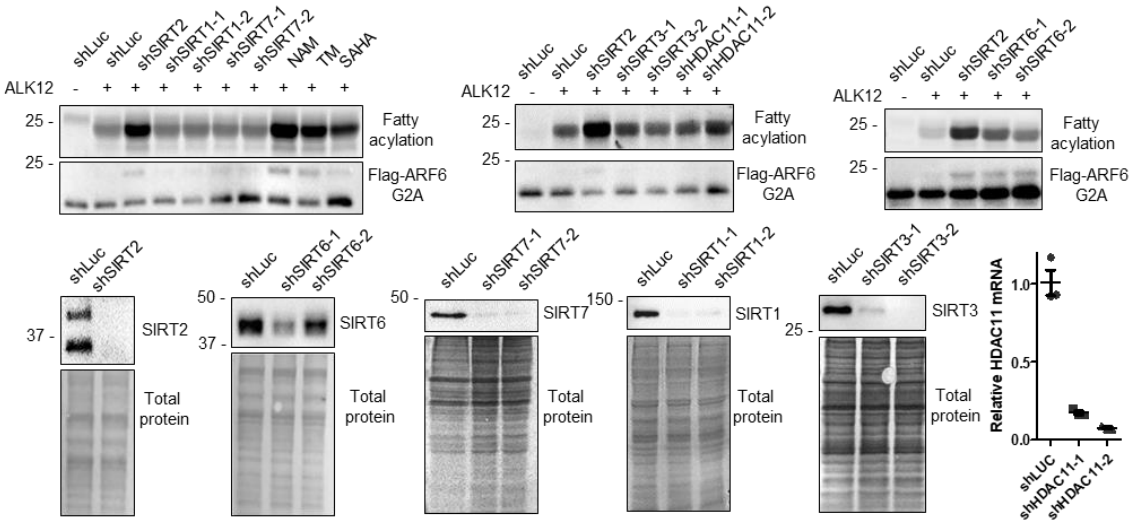

Supplementary figure 2.14 SIRT2 but not other lysine defatty acylases regulate ARF6 lysine fatty acylation. ARF6 G2A was overexpressed in HEK293T cells with stable KD of indicated proteins. HDAC11 KD efficiency was analyzed by qRT-PCR due to lack of a band of expected molecular weight by Western Blot. Error bars represent SEM from three technical replicates analyzed by unpaired two-tailed t-test.

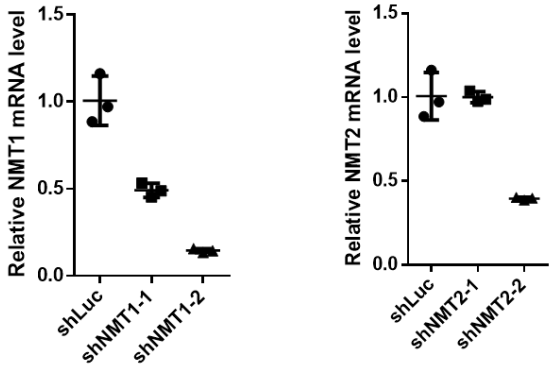

Supplementary figure 2.15 NMT KD efficiency determined by qRT-PCR. This experiment was done several months later than the Western blot results shown in Figure 2.2C and over time the knockdown efficiency of shNMT2-1 decreased. Error bars represent SEM from three technical replicates analyzed by unpaired two-tailed t-test.

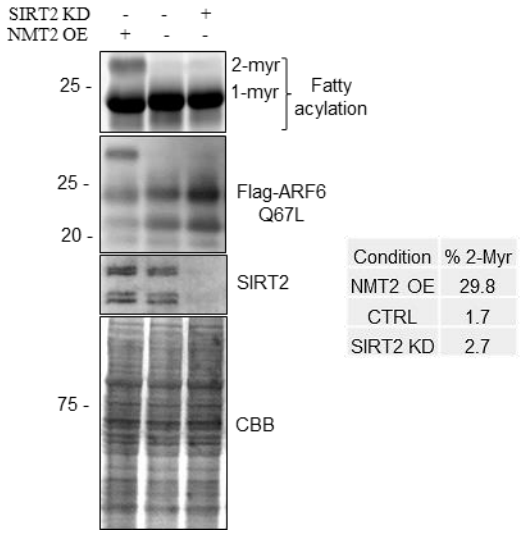

Supplementary figure 2.16 Endogenous NMT can dimyristoylate ARF6-GTP. ALK12 labeling performed in HEK293T cells transiently overexpressing ARF6 Q67L. The percentage of dimyristoylation was quantified using ImageJ.

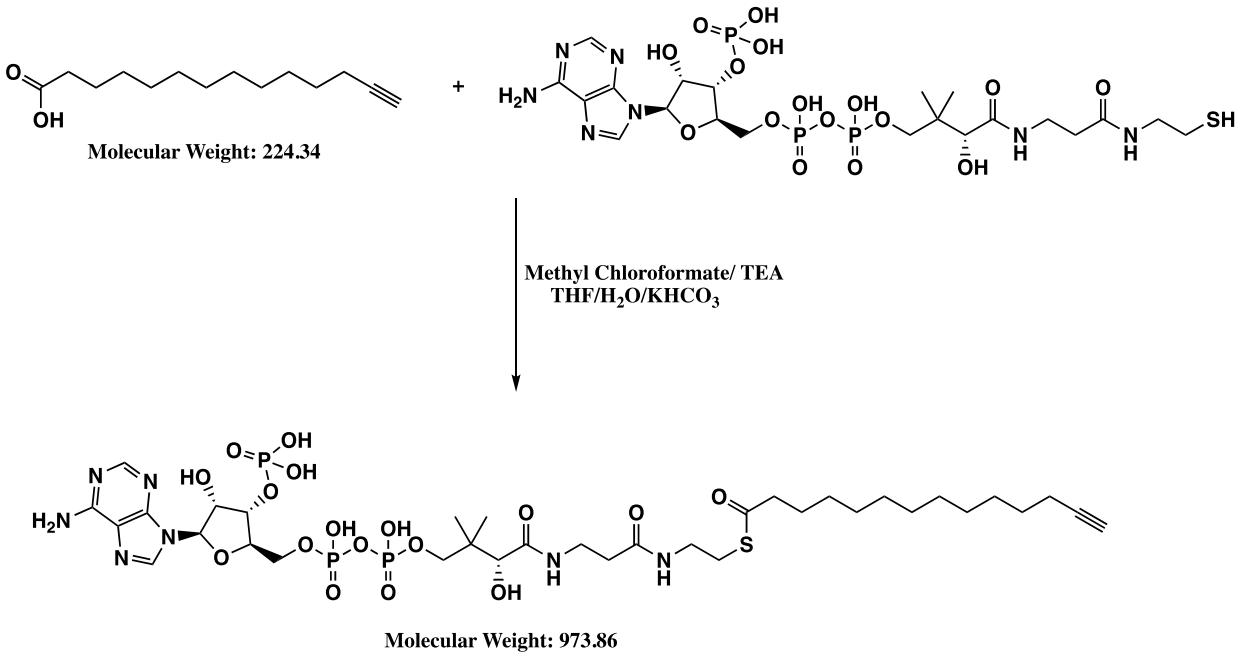

Supplementary figure 2.17 ALK12-CoA synthesis scheme.

Supplementary table 2.2 Primers used in the study.

ARF6 and ARF1 mutagenesis	
Arf6_G2A+A_F	GATATCGGTACCATGGCAGCGAAGGTGCTATCC
Arf6_G2A+A_R	GGATAGCACCTTCGCTGCCATGGTACCGATATC
Arf6_G2A+G_F	ATCGGTACCATGGCGGGGAAGGTGCTATCCAAG
Arf6_G2A+G_R	CTTGGATAGCACCTTCCCTGCCATGGTACCGAT
Arf6_G2A+2A_F	GATATCGGTACCATGGCTGCAGCGAAGGTGCTATCC
Arf6_G2A+2A_R	GGATAGCACCTTCGCTGCAGCCATGGTACCGATATC
Arf6_Q67L_F	tgggatgtgggcggcctggacaagatccggccg
Arf6_Q67L_R	gccgcccacatcccacacgttgaacttgacgtt
Arf6 T27N_F	gacgcagccggcaagaacacgatcctgtacaag
Arf6 T27N_R	cttgccggctgcgtccaggcccagcatgaggat
Arf6_G2A_F	GATATCGGTACCATGGCGAAGGTGCTATCCAAG
Arf6_G2A_R	CATGGTACCGATATCAGATCTATCGATGAATTC
Arf6_G2A_K3R_F	GATATCGGTACCATGGCGAGGGTGCTATCCAAGATC
Arf6_G2A_K3R_R	CATGGTACCGATATCAGATCTATCGATGAATTC
Arf1_G2A_F	GATATCGGTACCATGGCGAATATCTTTGCAAAC
Arf1_G2A_R	CATGGTACCGATATCAGATCTATCGATGAATTC
Arf1 g2a/n3k_F	ATCGGTACCATGGCGAAAATCTTTGCAAACCTC
Arf1 g2a/n3k_R	CGCCATGGTACCGATATCAGATCTATCGATGAA
NMT cloning into pCMV4a vector	
NMT1-5'-ecor1-ha	caattatatgaattcatgTACCCATACGATGTTCCAGATTACGCTggagcggacgagagtgagacagcagtg
NMT1-3'-xho1-stop	caattatatctcgagttattgtagcaccagtccaaccttctctg
NMT2-5'-ecor1-ha	caattatatgaattcatgTACCCATACGATGTTCCAGATTACGCTggagcggaggacagcgagtctg
NMT2-3'-xho1-stop	caattatatctcgagctattgtagtactagtccaacctttcagaatctgtacctgg
Full length NMT cloning into pETHisTEV (Gibson assembly)	
NMT1_F	GCAGCCATCATCATCATCACATGGCGGACGAGAGTGAG
NMT1_R	AAATACAGGTTTTCGCTAGCTTATTGTAGCACCAGTCCAACC
NMT2_F	GCAGCCATCATCATCATCACATGGCGGAGGACAGCGAG
NMT2_R	AAATACAGGTTTTCGCTAGCCTATTGTAGTACTAGTCCAACCTTTTCAGAATCTG
Mutagenesis to add His residue to the 5Xhis tag	
his-f	TATACCATGGGCAGCCACCATCATCATCATCAC
his-r	GCTGCCCATGGTATATCTCCTTCTTAAAGTTAA
NMT catalytic domains cloning into pETHisTEV (Gibson assembly)	
NMT1 Forward	(CCATGG) GCAGCAGCCATCATCATCATCACAGCAGCGGC CTTGAAGTCCTCTTTCAGGGACCC CATATG
NMT1 Reverse	gtcgacggagctcgaattcggatccTTATTGTAGCACCAGTCCAACC
NMT2 Forward	(CCATGG) GCAGCAGCCATCATCATCATCACAGCAGCGGC CTTGAAGTCCTCTTTCAGGGACCC CATATG
NMT2 Reverse	gtcgacggagctcgaattcggatccCTATTGTAGTACTAGTCCAACCTTTTC
qRT-PCR primers	
NMT1_F	GGTCAGGGACCTGCCAAAAC
NMT1_R	CATGGGTGTTCACCACTTCG
NMT2_F	TCCCAGCAAACATTCGGATTT
NMT2_R	ACCCGTTTCGATCTCAACTTCT
HDAC11_F	CACGCTCGCCATCAAGTTTC
HDAC11_R	GAAGTCTCGCTCATGCCCATT
GAPDH_F	ACAACTTTGGTATCGTGGAAGG
GAPDH_R	GCCATCACGCCACAGTTTC

REFERENCES

1. Zhang, X., Spiegelman, N.A., Nelson, O.D., Jing, H. & Lin, H. SIRT6 regulates Ras-related protein R-Ras2 by lysine defatty-acylation. *Elife* **6** (2017).

2. Jing, H. *et al.* SIRT2 and lysine fatty acylation regulate the transforming activity of K-Ras4a. *Elife* **6** (2017).
3. Spiegelman, N.A. *et al.* SIRT2 and Lysine Fatty Acylation Regulate the Activity of RalB and Cell Migration. *ACS Chem Biol* (2019).
4. Tong, Z. *et al.* SIRT7 Is an RNA-Activated Protein Lysine Deacylase. *ACS Chem Biol* **12**, 300-310 (2017).
5. Zhang, X. *et al.* Identifying the functional contribution of the defatty-acylase activity of SIRT6. *Nat Chem Biol* **12**, 614-620 (2016).
6. Zhou, Y. *et al.* N(epsilon)-Fatty acylation of Rho GTPases by a MARTX toxin effector. *Science* **358**, 528-531 (2017).
7. Liu, W. *et al.* N(epsilon)-fatty acylation of multiple membrane-associated proteins by Shigella IcsB effector to modulate host function. *Nat Microbiol* **3**, 996-1009 (2018).
8. Stevenson, F.T., Bursten, S.L., Locksley, R.M. & Lovett, D.H. Myristyl acylation of the tumor necrosis factor alpha precursor on specific lysine residues. *J Exp Med* **176**, 1053-1062 (1992).
9. Jiang, H. *et al.* SIRT6 regulates TNF-alpha secretion through hydrolysis of long-chain fatty acyl lysine. *Nature* **496**, 110-113 (2013).
10. Giglione, C., Fieulaine, S. & Meinnel, T. N-terminal protein modifications: Bringing back into play the ribosome. *Biochimie* **114**, 134-146 (2015).
11. Wright, M.H. *et al.* Validation of N-myristoyltransferase as an antimalarial drug target using an integrated chemical biology approach. *Nat Chem* **6**, 112-121 (2014).
12. Frearson, J.A. *et al.* N-myristoyltransferase inhibitors as new leads to treat sleeping sickness. *Nature* **464**, 728-732 (2010).
13. Spinks, D. *et al.* Development of Small-Molecule Trypanosoma brucei N-Myristoyltransferase Inhibitors: Discovery and Optimisation of a Novel Binding Mode. *ChemMedChem* **10**, 1821-1836 (2015).
14. Herrera, L.J. *et al.* Validation of N-myristoyltransferase as Potential Chemotherapeutic Target in Mammal-Dwelling Stages of Trypanosoma cruzi. *PLoS Negl Trop Dis* **10**, e0004540 (2016).
15. Mousnier, A. *et al.* Fragment-derived inhibitors of human N-myristoyltransferase block capsid assembly and replication of the common cold virus. *Nat Chem* **10**, 599-606 (2018).
16. Shrivastav, A., Varma, S., Saxena, A., DeCoteau, J. & Sharma, R.K. N-myristoyltransferase: a potential novel diagnostic marker for colon cancer. *J Transl Med* **5**, 58 (2007).
17. Rajala, R.V., Dehm, S., Bi, X., Bonham, K. & Sharma, R.K. Expression of N-myristoyltransferase inhibitor protein and its relationship to c-Src levels in human colon cancer cell lines. *Biochem Biophys Res Commun* **273**, 1116-1120 (2000).
18. Thinon, E., Morales-Sanfrutos, J., Mann, D.J. & Tate, E.W. N-Myristoyltransferase Inhibition Induces ER-Stress, Cell Cycle Arrest, and Apoptosis in Cancer Cells. *ACS Chem Biol* **11**, 2165-2176 (2016).
19. Randazzo, P.A. *et al.* The myristoylated amino terminus of ADP-ribosylation factor 1 is a phospholipid- and GTP-sensitive switch. *The Journal of biological chemistry* **270**, 14809-14815 (1995).
20. Jiang, H. *et al.* Protein Lipidation: Occurrence, Mechanisms, Biological Functions, and Enabling Technologies. *Chemical reviews* **118**, 919-988 (2018).
21. Gillingham, A.K. & Munro, S. The small G proteins of the Arf family and their regulators. *Annu Rev Cell Dev Biol* **23**, 579-611 (2007).

22. Peters, P.J. *et al.* Overexpression of wild-type and mutant ARF1 and ARF6: distinct perturbations of nonoverlapping membrane compartments. *J Cell Biol* **128**, 1003-1017 (1995).
23. Pasqualato, S., Menetrey, J., Franco, M. & Cherfils, J. The structural GDP/GTP cycle of human Arf6. *EMBO Rep* **2**, 234-238 (2001).
24. Menetrey, J., Macia, E., Pasqualato, S., Franco, M. & Cherfils, J. Structure of Arf6-GDP suggests a basis for guanine nucleotide exchange factors specificity. *Nat Struct Biol* **7**, 466-469 (2000).
25. Castrec, B. *et al.* Structural and genomic decoding of human and plant myristoylomes reveals a definitive recognition pattern. *Nat Chem Biol* **14**, 671-679 (2018).
26. Farazi, T.A., Waksman, G. & Gordon, J.I. Structures of Saccharomyces cerevisiae N-myristoyltransferase with bound myristoylCoA and peptide provide insights about substrate recognition and catalysis. *Biochemistry* **40**, 6335-6343 (2001).
27. Thinon, E. *et al.* Global profiling of co- and post-translationally N-myristoylated proteomes in human cells. *Nat Commun* **5**, 4919 (2014).
28. Charron, G., Wilson, J. & Hang, H.C. Chemical tools for understanding protein lipidation in eukaryotes. *Curr Opin Chem Biol* **13**, 382-391 (2009).
29. Hickman, A.B., Namboodiri, M.A., Klein, D.C. & Dyda, F. The structural basis of ordered substrate binding by serotonin N-acetyltransferase: enzyme complex at 1.8 A resolution with a bisubstrate analog. *Cell* **97**, 361-369 (1999).
30. Weston, S.A. *et al.* Crystal structure of the anti-fungal target N-myristoyl transferase. *Nat Struct Biol* **5**, 213-221 (1998).
31. Du, J. *et al.* Sirt5 is a NAD-dependent protein lysine demalonylase and desuccinylase. *Science* **334**, 806-809 (2011).
32. Jing, H. *et al.* A SIRT2-Selective Inhibitor Promotes c-Myc Oncoprotein Degradation and Exhibits Broad Anticancer Activity. *Cancer Cell* **29**, 297-310 (2016).
33. Wedegaertner, P.B., Wilson, P.T. & Bourne, H.R. Lipid modifications of trimeric G proteins. *J Biol Chem* **270**, 503-506 (1995).
34. Koegl, M., Zlatkine, P., Ley, S.C., Courtneidge, S.A. & Magee, A.I. Palmitoylation of multiple Src-family kinases at a homologous N-terminal motif. *Biochem J* **303 (Pt 3)**, 749-753 (1994).
35. Klein, S., Franco, M., Chardin, P. & Luton, F. Role of the Arf6 GDP/GTP cycle and Arf6 GTPase-activating proteins in actin remodeling and intracellular transport. *J Biol Chem* **281**, 12352-12361 (2006).
36. Macia, E. *et al.* The GDP-bound form of Arf6 is located at the plasma membrane. *J Cell Sci* **117**, 2389-2398 (2004).
37. D'Souza-Schorey, C. *et al.* ARF6 targets recycling vesicles to the plasma membrane: insights from an ultrastructural investigation. *J Cell Biol* **140**, 603-616 (1998).
38. Van Acker, T., Tavernier, J. & Peelman, F. The Small GTPase Arf6: An Overview of Its Mechanisms of Action and of Its Role in Host(-)Pathogen Interactions and Innate Immunity. *Int J Mol Sci* **20** (2019).
39. Mayle, K.M., Le, A.M. & Kamei, D.T. The intracellular trafficking pathway of transferrin. *Biochim Biophys Acta* **1820**, 264-281 (2012).
40. Grant, B.D. & Donaldson, J.G. Pathways and mechanisms of endocytic recycling. *Nat Rev Mol Cell Biol* **10**, 597-608 (2009).
41. D'Souza-Schorey, C., Li, G., Colombo, M.I. & Stahl, P.D. A regulatory role for ARF6 in receptor-mediated endocytosis. *Science* **267**, 1175-1178 (1995).
42. Sannerud, R. *et al.* ADP ribosylation factor 6 (ARF6) controls amyloid precursor protein (APP) processing by mediating the endosomal sorting of BACE1. *Proc Natl Acad Sci U S A* **108**, E559-568 (2011).

43. van Dam, E.M., Ten Broeke, T., Jansen, K., Spijkers, P. & Stoorvogel, W. Endocytosed transferrin receptors recycle via distinct dynamin and phosphatidylinositol 3-kinase-dependent pathways. *J Biol Chem* **277**, 48876-48883 (2002).
44. Khan, A.R. & Menetrey, J. Structural biology of Arf and Rab GTPases' effector recruitment and specificity. *Structure* **21**, 1284-1297 (2013).
45. Parachoniak, C.A., Luo, Y., Abella, J.V., Keen, J.H. & Park, M. GGA3 functions as a switch to promote Met receptor recycling, essential for sustained ERK and cell migration. *Dev Cell* **20**, 751-763 (2011).
46. Padovani, D. *et al.* EFA6 controls Arf1 and Arf6 activation through a negative feedback loop. *Proc Natl Acad Sci U S A* **111**, 12378-12383 (2014).
47. Dunphy, J.L. *et al.* The Arf6 GEF GEP100/BRAG2 regulates cell adhesion by controlling endocytosis of beta1 integrins. *Curr Biol* **16**, 315-320 (2006).
48. Davies, J.C., Tamaddon-Jahromi, S., Jannoo, R. & Kanamarlapudi, V. Cytohesin 2/ARF6 regulates preadipocyte migration through the activation of ERK1/2. *Biochem Pharmacol* **92**, 651-660 (2014).
49. Tushir, J.S. & D'Souza-Schorey, C. ARF6-dependent activation of ERK and Rac1 modulates epithelial tubule development. *EMBO J* **26**, 1806-1819 (2007).
50. Muralidharan-Chari, V. *et al.* ARF6-regulated shedding of tumor cell-derived plasma membrane microvesicles. *Curr Biol* **19**, 1875-1885 (2009).
51. Hong, J.Y., Price, I.R., Bai, J.J. & Lin, H. A Glycoconjugated SIRT2 Inhibitor with Aqueous Solubility Allows Structure-Based Design of SIRT2 Inhibitors. *ACS Chem Biol* **14**, 1802-1810 (2019).
52. Adams, P.D. *et al.* PHENIX: a comprehensive Python-based system for macromolecular structure solution. *Acta Crystallogr D Biol Crystallogr* **66**, 213-221 (2010).
53. McCoy, A.J. Solving structures of protein complexes by molecular replacement with Phaser. *Acta Crystallogr D Biol Crystallogr* **63**, 32-41 (2007).
54. Emsley, P., Lohkamp, B., Scott, W.G. & Cowtan, K. Features and development of Coot. *Acta Crystallogr D Biol Crystallogr* **66**, 486-501 (2010).
55. Afonine, P.V. *et al.* Real-space refinement in PHENIX for cryo-EM and crystallography. *Acta Crystallogr D Struct Biol* **74**, 531-544 (2018).

CHAPTER 3

SIRT2 AND NMT INHIBITION SUPPRESS COLON CANCER THROUGH ARF6 LYSINE MYRISTOYLATION

Tatsiana Kosciuk, Ji Cao, Xuan Lu, Kayla Johnson, Min Yang, Hening Lin

ABSTRACT

Oncogenic mutations of Ras genes are a common feature of colorectal cancers (CRC) causing resistance to direct targeting of EGFR in battling the disease. Thus, there is a need for identification of other molecular mechanisms for therapeutic intervention. A lot of evidence implicates SIRT2 and N-myristoyltransferase (NMT) in promoting CRC, but the underlying mechanism is not clear. SIRT2 is an NAD^+-dependent protein lysine deacylases that have been shown to regulate many proteins through either deacetylation or defatty-acylation activities. NMT is known to myristoylate N-terminal glycine of proteins, but we recently showed that it also can myrisotylate lysine residues near the N-terminal of proteins. Furthermore, NMT and SIRT2 together regulated the lysine myristoylation-demyristoylation cycle of ARF6 and this cycle promotes the activation of ARF6. Here we show that disrupting this cycle, by inhibiting SIRT2 or NMT, suppresses colon cancer cell growth in vitro and in vivo by inhibiting ERK signaling. These results provide new insights to understand the function of ARF6 in cell signaling and offers potential new targets for treating CRC.

INTRODUCTION

Colorectal cancer is one of the most common and morbid malignancies in the world. KRas oncogene mutations occur in nearly half of CRC cases conferring resistance to chemotherapy.[1, 2] Mutated KRas overactivates its downstream effectors such as those in the MAPK pathway, which causes resistance to EGFR-targeting therapies commonly used in treating CRC.[2] Thus, finding new actionable drug targets for treating CRC is needed.

SIRT2 is upregulated in CRC compared to normal colon tissue which is associated with poor patient outcome,[3] and is reported as a potential therapeutic targeting several cancers.[4, 5] We recently identified a selective SIRT2 inhibitor TM that suppresses breast cancer and inhibits growth of several colon cancer lines in an in vitro NCI-60 screen.[6] Several mechanisms are thought to account for the anticancer effects of SIRT2 inhibition. In breast cancer SIRT2 suppression destabilized c-MYC by upregulating E3 ubiquitin ligase NEDD4[6] and it promotes Slug degradation by increasing its acetylation.[7] Inhibition of SIRT2 reduces proliferation of leukemia cells by suppressing G6PD activity.[8] In CRC it is reported that SIRT2 depletion inhibits angiogenesis by suppressing VEGFA secretion and STAT3 phosphorylation and nuclear translocation.[3] Furthermore, inhibition of SIRT2 with a small molecule AK-1 caused degradation of the transcription factor Snail through suppression of the NF-κB/CSN2 pathway.[4] Therefore, it is likely that several mechanisms contribute to the tumor-supporting roles of SIRT2 in CRC, and identifying them is important to gain therapeutic advantage.

We recently identified that the small GTPase ADP-ribosylation factor 6 (ARF6) is controlled by myristoylation-demyristoylation cycle in which NMT adds the modification and SIRT2 removes it.[9] While this cycle controls the activation and downstream signaling of ARF6, further physiological effects have not been established. Because NMT is elevated in colon cancer[10] as well as SIRT2, and inhibition of either enzyme is reported to suppress the disease,[3-5, 10-12] we inquired whether this effects is through the myristoylation-demyristoylation cycle of ARF6. Here we report that selective SIRT2 and NMT inhibition in colorectal cancer cells suppresses ARF6 activation and cell growth. Moreover, ARF6 knockdown also inhibited 2D and 3D growth of colorectal cancer cells, and overexpression of ARF6 WT but not ARF6 K3R mutant lacking lysine myristoylation could promote tumor growth in mice. Together, our data point to the ARF6 lysine myristoylation cycle as a modulator of colorectal cancer growth that can be utilized in therapeutic intervention.

RESULTS

SIRT2 depletion or selective inhibition with TM suppresses colon cancer

To determine whether colorectal cancer cells rely on SIRT2, we examined the effect of previously reported selective SIRT2 inhibitor TM on proliferation of KRas mutant CRC cell models HCT116 and SW948. TM dose-dependently inhibited cell growth (Figure 3.1A) and a similar effect was produced by transient SIRT2 knockdown (KD) with two different shRNAs (Figure 3.1B). We then examined whether SIRT2 and TM can regulate anchorage-independent growth using a soft agar assay. SIRT2 KD or inhibition with TM potently suppressed colony formation of both colorectal cancer cell models (Figure 3.1C and D).

To determine whether this effect is true *in vivo* we injected HCT116 and SW948 cells into the flanks of NOD-SCID mice and once the tumors were palpable, we treated the mice with 50 mg/kg TM daily for two weeks. TM treatment caused nearly 60% reduction in tumor growth (Figure 3.1E). These data suggest that SIRT2 is a promising target against colon cancer and that TM can effectively inhibit CRC *in vitro* and *in vivo*.

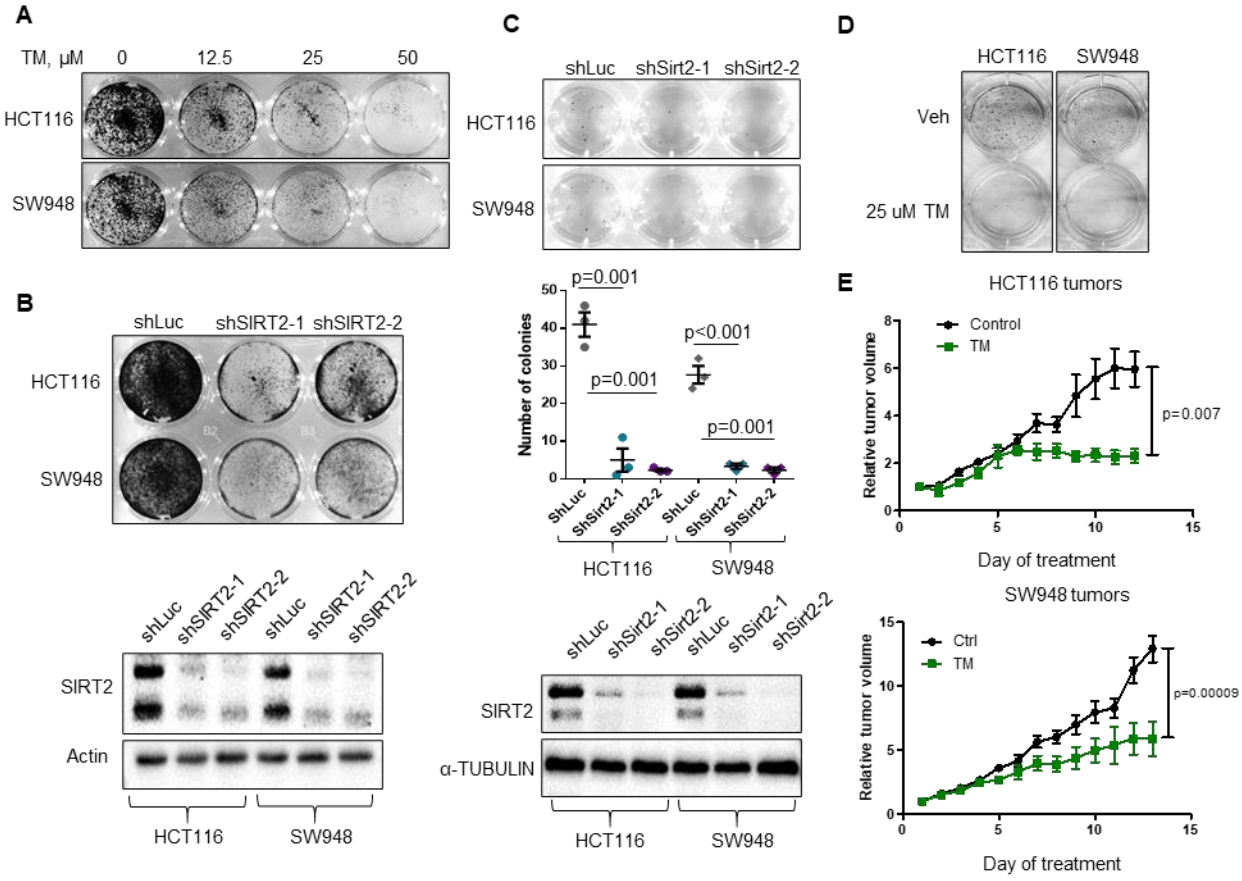

Figure 3.1 SIRT2 KD or inhibition with TM suppresses colon cancer with activating KRas mutations. (A) TM dose-dependently suppresses colon cancer cell proliferation, n=2. (B) Transient SIRT2 KD suppresses colon cancer cell growth, n=2. (C) Transient SIRT2 KD suppresses anchorage-independent growth of colon cancer cells, n=2. (D) SIRT2 inhibition with TM suppresses anchorage-independent growth of colon cancer cells, n=2; and (E) colon tumor xenograft growth in mice, n=3 for HCT116, n=1 for SW948. Shown are representative results of the indicated n trials. Unpaired nonparametric two-tailed t-test; error bars represent SEM.

ARF6 promotes colon cancer

To determine whether ARF6 supports CRC we examined the effect of ARF6 depletion on cell proliferation in 2D and on anchorage-independent growth in soft agar. Transient ARF6 KD with two shRNAs strongly suppressed both 2D proliferation and growth on soft agar suggesting that CRC relies on ARF6 (Fig 3.2 A and B). We then asked whether ARF6 lysine myristoylation contribute to CRC progression. To that end we injected 300 HCT116 cells with stable overexpression of ARF6 WT or ARF6 K3R or empty vector into the flanks of NOD-SCID mice and examined tumor weight 34 days post injection. We hypothesized that ARF6 WT will promote tumor growth better than the ARF6 K3R mutant, which abolishes lysine myristoylation. Indeed, ARF6 WT promoted tumor growth while ARF6 K3R had little effect (Figure 3.2C). Furthermore, all mice injected with ARF6 WT cells developed tumors, while only 5 out of 8 mice injected with ARF6 K3R cells had tumors (Figure 3.2C). This suggests that ARF6 and its lysine myristoylation are important for CRC.

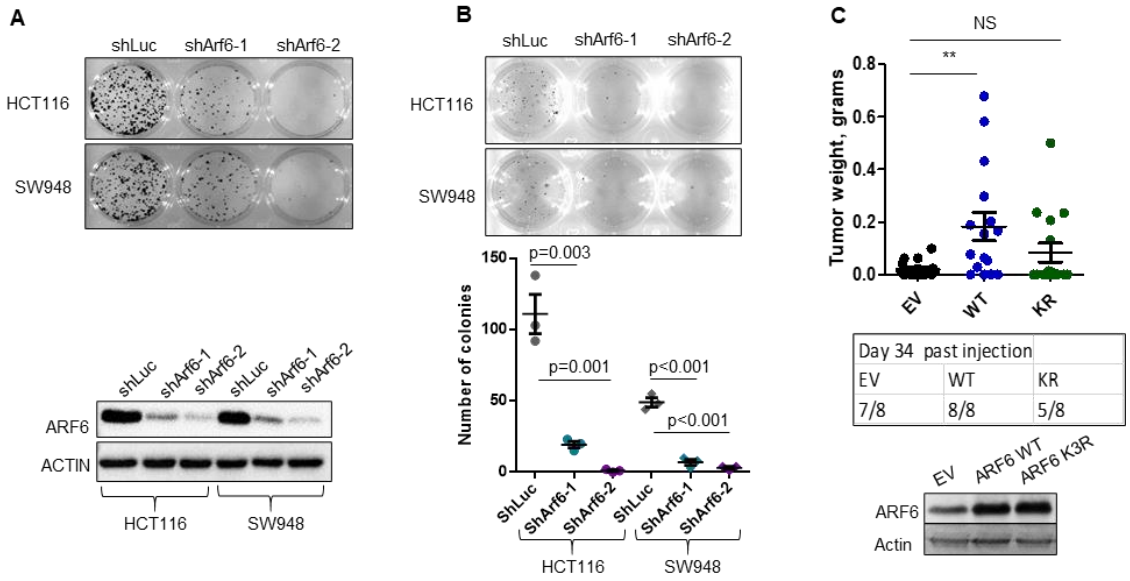

Figure 3.2 ARF6 promotes colon cancer. (A) Transient ARF6 KD suppresses colon cancer cell proliferation, n=2; and (B) anchorage-independent growth, n=2. (C) ARF6 promotes colon tumor xenograft growth in mice via lysine myristoylation cycle, n=1. Unpaired nonparametric two-tailed t-test; error bars represent SEM.

SIRT2 and NMT regulate ARF6 lysine myristoylation in colon cancer cells

We next sought to investigate whether SIRT2 regulates ARF6 lysine myristoylation, which could explain why both SIRT2 and ARF6 are important in CRC. We previously reported that SIRT2 demyristoylates ARF6 and also depalmitoylates KRas4a, which could be relevant because HCT116 and SW948 cells contain activating KRas mutations. We therefore tested whether the SIRT2 inhibitor, TM, increases lysine fatty acylation on these SIRT2 substrates in CRC. We overexpressed (OE) Flag-ARF6 G2A that has only lysine but not glycine myristylation and Flag-KRas4a in HCT116 and SW948 cells and examined the effects of TM on the labeling with alkyne analogs of myristic (ALK12) and palmitic (ALK14) acids. We isolated the proteins from the alkyne probe treated cells by Flag-affinity purification and conjugated TAMRA dye via cupper-catalyzed alkyne-azide cycloaddition. Hydroxylamine (NH_2OH) was used to remove cysteine acylation, which is known to occur on KRas4a. In-gel fluorescence revealed that TM strongly increased ARF6 G2A fatty acylation but had no effect on KRas4a palmitoylation, suggesting that TM might act through ARF6 (Figure 3.3A) but not KRas4a in colon cancer. This also illuminates a unique selectivity of TM not only for SIRT2, but also for its different substrates, offering a highly specific targeting tool for treating diseases and interrogating biological mechanisms.

To further confirm that ARF6 lysine myristoylation cycle is present in colon cancer cells, we examined the effects of NMT2 and SIRT2 overexpression and TM treatment on Flag-ARF6 wild type (WT) ALK12 labeling in HCT116 cells. As

previously reported for HEK293T cells NMT2 OE produced a distinct di-myristoylation band for ARF6 WT (but not K3R) that was removed by SIRT2 OE and enhanced by TM (Figure 3.3B). The results confirmed that the ARF6 lysine myristoylation-demyristoylation cycle regulated by NMT and SIRT2 is present in colon cancer cells.

We then investigated whether lysine myristoylation of endogenous ARF6 is regulated by SIRT2 and TM in colon cancer cells. We treated HCT116 cells stably expressing shRNA targeting luciferase (control) or SIRT2 with ALK12 for three generations and then treated the control cells with nicotinamide or TM for 15 h. Following biotin-PEG3-azide conjugation, we pulled down all conjugated proteins with streptavidin beads. The Western blot analysis revealed an increased abundance of myristoylated ARF6 with SIRT2 KD or inhibition (Figure 3.3C), suggesting that lysine myristoylation of endogenous ARF6 in CRC is regulated by SIRT2.

Because NMT also regulates the ARF6 myristoylation cycle, we speculated that, similar to TM, NMT inhibition would suppress colon cancer cell growth. Indeed, a 3-day treatment with 0.5 μM DDD85646 suppressed 2D proliferation of HCT116 and SW948 cells (Figure 3.3D). These data suggest that SIRT2 and NMT2 regulate ARF6 lysine myristoylation in colon cancer cells and that this regulation can be inhibited by TM and DDD85646.

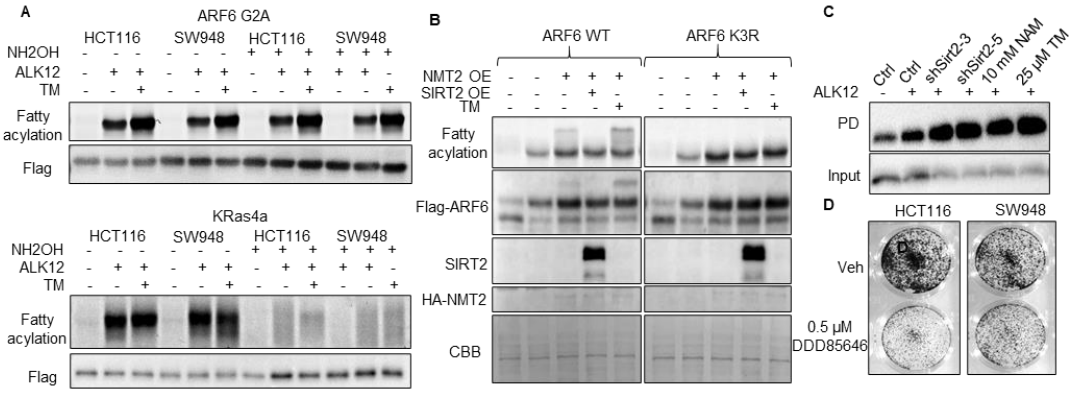

Figure 3.3 SIRT2 and TM regulate ARF6 lysine myristoylation in colon cancer cells. (A) TM increases lysine myristoylation of ARF6 G2A but not KRas4a in HCT116 and SW948 colon cancer cells, n=3. NH2OH was used to remove cysteine palmitoylation on KRas4a. (B) SIRT2 removes and NMT2 and TM increase ARF6 lysine myristoylation in HCT116 cells, n=2; (C) SIRT2 KD and inhibition increase myristoylation of endogenous ARF6, n=1. PD=pull down of myristoylated ARF6. (D) NMT1/2 inhibition suppresses colon cancer cell growth, n=2.

Inhibition of ARF6 lysine myristoylation cycle deregulates EGFR.

Thus far we have demonstrated that SIRT2 and NMT regulates ARF6 lysine myristoylation cycle in CRC and all three proteins are important for CRC. We next wanted to investigate why this cycle is important for CRC. We first examined the levels of endogenous ARF6-GTP, the activated ARF6, in cells treated with TM or DDD8565. A pull down of ARF6-GTP with GGA3, an effector that binds active ARF6, revealed that SIRT2 or NMT inhibition decreased the levels of endogenous ARF6-GTP in both colon cancer cell models (Figure 3.4A). The regulation of ARF6 by lysine myristoylation is rather interesting because the cycle of myristoylation and demyristoylation promotes its GTP loading. Thus, disrupting either lysine myristoylation or demyristoylation of ARF6 decreases its GTP loading and inhibits colon cancer cell growth.

EGFR is known to be overactivated in Ras mutated cancers due to a constitutive secretion of its ligands mediated by the mutant Ras.[13] This contributes to the

ineffectiveness of the direct targeting of EGFR with mAbs or RTKi.[14] Because ARF6 is implicated in membrane protein trafficking, we asked whether ARF6 lysine myristylation regulates EGFR function indirectly. To that end we first examined the effect of TM on EGF mediated AKT phosphorylation. TM dose-dependently suppressed AKT activation in EGF stimulated HCT116 and SW948 cells (Figure 3.4B) suggesting that endogenous ARF6 lysine myristoylation regulates signaling events downstream of EGFR.

To further confirm that TM's effect on AKT is through EGFR activation, we analyzed the effect of SIRT2 inhibition on EGFR phosphorylation. TM inhibited EGFR phosphorylation at Y1068 in a time and dose-dependent manner (Figure 3.4C, D). To confirm that the effect of TM is through SIRT2 inhibition, we tested the effect of TM analog M that contains an amide bond in place of the thioamide bond and therefore cannot effectively inhibit SIRT2 as it cannot form a stalled covalent intermediate.[6] M was unable to inhibit EGFR phosphorylation (Figure 3.4E). Finally, we observed that SIRT2 KD also inhibits EGFR phosphorylation (Figure 3.4F) supporting that the effect of TM is through SIRT2.

We now sought to learn the underlying mechanism for the effect of SIRT2 inhibition on EGFR signaling. Because disruption of the ARF6 lysine myristoylation cycle renders ARF6 inactive, we examined the effect of ARF6 T27N, the inactive ARF6 mutant on the GFP-tagged EGFR localization. Using ARF6 T27N allows a clear isolation of the effects of the inactive ARF6. For this analysis we used HEK293T cells to achieve efficient overexpression of both proteins. In cells treated with TM, ARF6

T27N promoted EGFR trapping in intracellular vesicles (Figure 3.4G), while lysine myristoylation deficient mutant ARF6 T27N/K3R had no effect. Inactive ARF6 is known to localize to the recycling compartment preventing receptor recycling back to plasma membrane.[15] We therefore hypothesized that TM-mediated accumulation of ARF6 lysine myristoylation disrupts receptor recycling. To test that, we examined the recycling of fluorescently labeled transferrin in TM treated HCT116 cells by flow cytometry. We used transferrin because unlike EGF it remains receptor-bound during recycling. Furthermore, transferrin receptor is an established model for studying the recycling pathway because, unlike EGFR that undergoes degradation, most of transferrin receptor is recycled back to plasma membrane.[16] This allows a clear measurement of unrecycled receptor via fluorescence. We found that TM treatment delayed the recycling process (Figure 3.4H). Together these data suggest that the active ARF6 lysine myristoylation cycle guarded by SIRT2 and NMT promote colon cancer cell growth by supporting EGFR recycling and downstream signaling (Figure 3.4E). Therefore, pharmacological inhibition of this axis offers a potential therapeutic strategy against Ras mutant CRC.

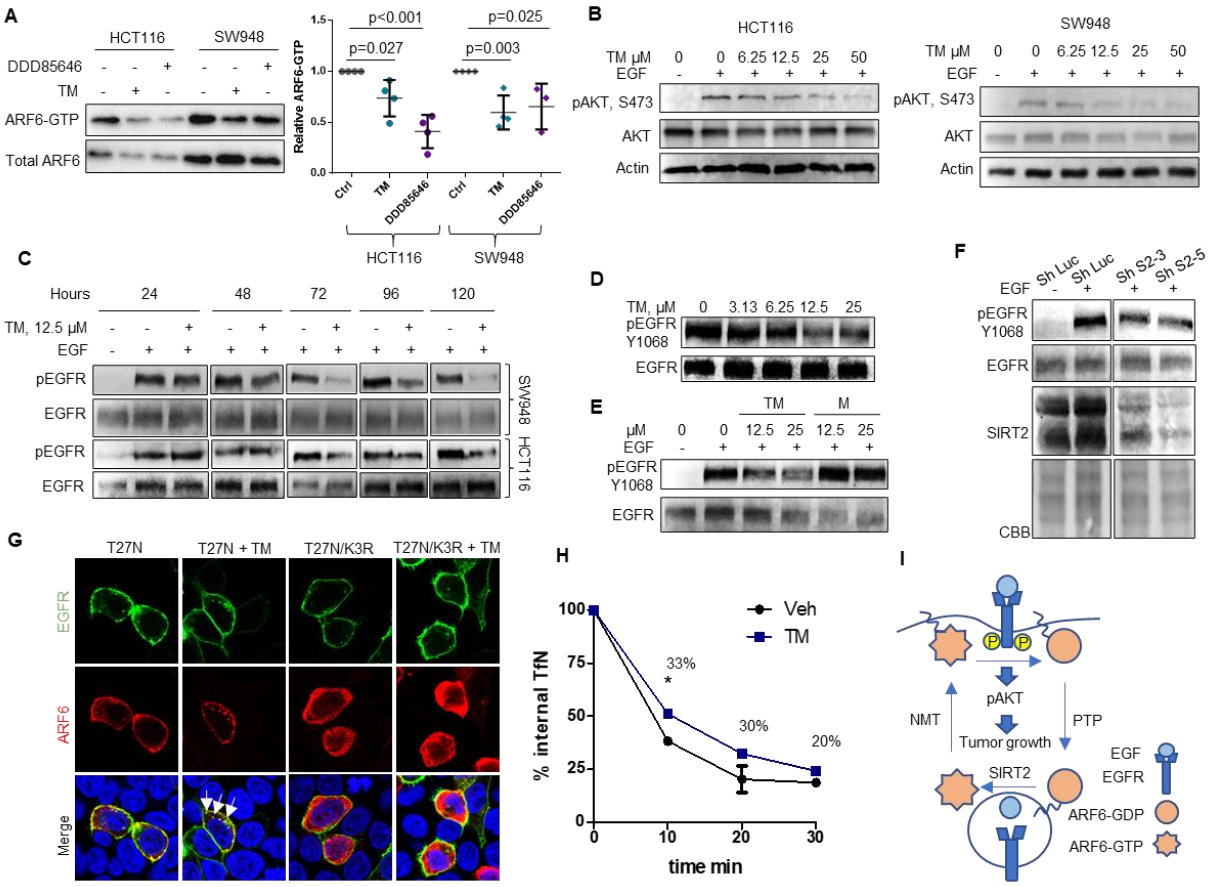

Figure 3.4 SIRT2 and TM regulate ARF6 lysine myristoylation in colon cancer cells. (A) SIRT2 and NMT inhibition suppress ARF6 GTP loading in colon cancer, n=4 (one point from DDD85646 SW948 treated cells was removed due to significant ARF6 degradation). (B) TM suppresses AKT phosphorylation upon EGF stimulation in colon cancer cells in a dose-dependent manner. Cell were treated with TM for 24 – 48 h and were serum starved for 24 hr before being stimulated with 100 ng/ml EGF for 5 min, n=2. (C) TM inhibits EGFR phosphorylation in a time dependent manner. Cell were treated with 12.5 µM TM for indicated times and were otherwise processed as indicated in B. (D) TM inhibits EGFR phosphorylation in a dose-dependent manner. HCT116 cells were treated as in B. (E) M, an analog of TM that unable to inhibit SIRT2, did not suppress EGFR phosphorylation. (F) SIRT2 KD suppresses EGF-mediated EGFR phosphorylation. (G) ARF6-GDP (inactive T27N mutant) traps EGFR in intracellular vesicles (white errors) in HEK293T cells. (H) TM suppresses receptor recycling as indicated by transferrin recycling in HCT116 cells, n=2. (H) Model showing that ARF6-GDP is anchored to plasma membrane via lysine myristoylation, and internalizes with EGFR. On the endosomes, SIRT2 removes ARF6 lysine myristoylation allowing its activation necessary for the recycling of EGFR back to plasma membrane. Lysine myristoylation by NMT allows an efficient return of ARF6 to plasma membrane to continue the cycle.

DISCUSSION

Our findings suggest that SIRT2 and ARF6 support KRas mutant colon cancer cell growth *in vitro* and *in vivo*. This is not entirely surprising given the cancer promoting

roles of these proteins in other malignancies. While the growth-suppressive effect of SIRT2 inhibition might be through several mechanisms such as c-MYC and Slug downregulation, we identify an additional axis SIRT2/ARF6/EGFR that contributes to malignant progression of CRC. Therefore, SIRT2 inhibition with a specific inhibitor TM can disrupt an array of oncogenic pathways. We found that SIRT2 inactivation inhibits EGFR phosphorylation and the phosphorylation of its downstream effector AKT. This is consistent with previous reports demonstrating that SIRT2 KD or inhibition potently suppress EGFR and AKT phosphorylation in other cells models.[17-19] In a Drosophila tumor model EGFR cooperates with oncogenic Ras through ARF6 to promote tumor growth via Hedgehog trafficking.[13] Our study establishes a missing link connecting the previously observed effects of SIRT2 and ARF6 on cancer and EGFR signaling and uncovers the physiological importance of the ARF6 myristoylation-demyristoylation cycle. Our data suggest that SIRT2 and ARF6 act in the same pathway where ARF6 demyristoylation by SIRT2 is important for ARF6 activation needed for the proper trafficking of EGFR to maintain EGF-mediated signaling events. NMT is the lysine myristoyltransferase for ARF6 and therefore its inhibition also disrupts ARF6 activation to inhibit cancer cell growth. Our study uncovered a new axis that regulates EGFR activity in KRas mutant colon cancer, which could be exploited in therapeutic strategies against this disease.

METHODS

The effect of TM and DDD85646 on ARF6 GTP loading

HCT116 or SW948 cells (500,000 each) were seeded into each well of a 6-well plate. After 24 h, the complete growth media (McCoy's 5A with 10 % FBS) containing 100

μM myristic acid (to increase myristoyl-CoA pool for ARF6 acylation) and 25 μM TM or 2 μM DDD85646 or vehicle were added to the cells. After 24 h, the cells were washed twice with ice-cold PBS and resuspended in 200 μl of 1% NP40 lysis buffer (25 mM Tris-HCl pH 7.4, 150 mM NaCl, 10% glycerol, 1% Nonidet P-40, with protease and phosphatase inhibitors added freshly). The cell suspension was put on ice for 10 min with vortexing every 5 min. After spun down at 17,000g for 10 min, the lysate was collected and protein concentration was determined using the Bradford assay. Equal amounts of total protein (~ 300 – 400 μg) were brought to 200 μl with lysis buffer and a small amount was transferred into a new tube for input analysis by WB. GGA3 beads (15-20 μl per sample) were washed with 1 ml of ice-cold IP wash buffer (25 mM Tris-HCl pH 7.4, 150 mM NaCl, and 0.2% Nonidet P-40) twice and then resuspended in IP wash buffer and transferred to each protein sample in 200 μl of IP wash buffer bringing the total volume in each sample to ~ 400 μl. After rotating for 1 h at 4ºC, the beads were washed 3 times with 1 ml of IP wash buffer. All the buffer was removed with gel loading tips. The beads were resuspended in 24 μl of 2X SDS protein loading dye and were eluted by boiling for 10 min and analyzed by Western blot (WB) for endogenous ARF6 as previously described.[9]

ALK12 labeling of overexpressed ARF6, ARF6 G2A and KRas4a in colon cancer cells

HCT116 and SW948 cells were seeded into each well of a 6-well plate (500,000 cells per well). After 14 h the cells were transfected with ARF6, ARF6 + NMT2, ARF6 G2A, KRas4a or empty vector. The transfection mix per well was prepared by adding 0.5 μg of the Flag-ARF6, Flag-ARF6 G2A, Flag-Kras4a, 1 μg of HA-NMT2 or empty vector

(pCMV-Tag-4a) and polyethylenimine (PEI) at 1:3 plasmid:PEI ratio, and adding the mixture to 150 µl of serum free media. The solution was inverted several times and was incubated for 30 min at room temperature to allow DNA incapsulation. Then 1.5 ml of fresh media was added to each well and the transfection mix was added dropwise. The next day the media were replaced with media containing 50 µM ALK12 or ALK14 (for KRas4a labeling) and 25 µM TM for 7 h. The cells were then washed with ice-cold PBS and lysed with 1%NP40 lysis buffer as above. Flag IP was performed on the supernatants with 15 µl of washed Flag beads per sample in 200 µL of IP wash buffer for 2 h with rotating at 4ºC. The beads were washed and fatty acylation was analyzed by in-gel fluorescence as previously described.[9]

The effect of transient SIRT2 or ARF6 KD on colon cancer cell 2D growth

HCT116 or SW948 cells (50,000 per well) were seeded into the wells of 12-well plates (6 wells for each cell line). After 24 h, 0.5 ml of viral particles in conditioned media with 8 µg/ml polybrene were added to each well. After 24 h, the virus media were diluted with 0.5 ml of fresh complete growth media. After another 24 h,s the media were switched to 1 ml of fresh complete growth media and the cells were cultured for 60 h. Then half the cells were collected for knockdown efficiency evaluation by WB. The rest of the cells were washed with 1 ml of ice-cold PBS in the wells twice, fixed with 1 ml of ice-cold methanol for 15 min, and stained with 1 ml of crystal violet stain (0.2% crystal violet dye, 2% ethanol in water) for 5 min. The excess dye was washed away with water until the solution was clear and the plate was air dried and imaged with the ChemiDoc MP imager.

The effect of transient SIRT2 or ARF6 KD or TM on colon cancer cell anchorage-independent growth

We seeded 200,000 of HCT116 or SW948 cells into each well of a 6-well plate and cultured the cells for15 h, before adding 1 ml of viral particles containing shRNA in conditioned media with 8 µg/ml polybrene. After culturing the cells for 24 h, the media were switched to complete growth media and cultured for another 24 h before seeding cells into soft agar in 12-well plates. The base layer of soft agar contained 1 ml of 0.6% agar in complete growth media, diluted from 3% stock in water. The cells were trypsinized, counted, and used in upper layer (a portion of the cells was seeded without agar for KD efficiency analysis by WB, which was collected the next day). The upper layer was 900 µl of 0.3% agar in complete growth media with 500 cells per well. The soft agar plates were incubated at 37ºC for 10-12 days adding 100 µl of complete growth media every 2-3 days to obtain visible colonies. The colonies were stained by adding 100 µl of nitroblue tetrazolium chloride solution per well and incubating overnight at 37ºC and imaged with ChemiDoc MP imager.

The effect of TM on EGFR signaling in HCT116 and SW948 cells

Cells (250 per well) into the wells of a 12-well plate and cultured for 24 h before adding TM at indicated concentrations. 24 h before stimulation with EGF, the cells were washed with serum free media and cultured in serum free media containing appropriate concentrations of TM for 24 h. The cells were stimulated with 100 ng/ml EGF in serum free media containing appropriate concentration of TM for 5 min at 37ºC. The media were quickly aspirated and the cells were washed with 1 ml of ice-cold PBS The cells

were immediately lysed with 50 µl of 4% SDS lysis buffer (50 mM trimethylamine, 150 mM NaCl, 4% SDS with freshly added protease and phosphatase inhibitors and Pierce Universal Nuclease) and the lysates analyzed by WB.

The effect of TM or DDD85646 on cell proliferation.

5,000 cells per well were seeded into a 12-well plate. 24 hr later DDD85646, TM or vehicle was added at the indicated concentrations. 4-5 days later the cells were washed with 1 ml of ice-cold PBS twice and fixed by incubating with ice-cold methanol for 20 min. The cells were stained with crystal violet dye (0.2% crystal violet in 2% ethanol) for 5-10 min. The excess dye was washed away with water until the solution was clear. The plate was dried and was imaged with the ChemiDoc MP imager.

The effect of SIRT2 KD on EGFR phosphorylation.

500,000 HCT116 cells stably expressing shLuc or shSIRT2 were seeded into each well of a 6-well plate. 24 h later the cells were washed with serum free media and cultured in serum free media for 24 h. 24 h later the cells were stimulated with 100 ng/ml EGF and were processed and lysed with 100 µl of 4% SDS lysis buffer as described above.

Immunofluorescence to detect the effect of ARF6 T27N vs T27N K3R and TM on EGFR localization

200,000 HEK293T cells were seeded into MatTek glass bottom dishes. 24 h later the cells were transfected with 1 µg of Flag-ARF6 T27N or T27N-K3R and 1 µg of EGFR-GFP plasmids using FuGENE 6 transfection reagent with 1:3 plasmid/reagent ratio. FuGENE 6 was mixed with 100 µl of pre-warmed serum-free media per plate and was

incubated for 5 min at room temperature. The plasmids were added, and the solution was inverted several times and was left at room temperature for 30 min. The media in the plates with cells were replaced with 1 ml of fresh complete growth media and the transfection mixture was added dropwise. 24 h later, 25 µM TM or vehicle in fresh media were added to appropriate plates and the cells were cultured for 24 h. Then the cells were washed twice with 1 ml of ice-cold PBS and fixed with 1 ml of 4% PFA in PBS for 30 min. They were then washed twice again with PBS and were blocked with blocking buffer (PBS containing 5% BSA and 0.1% Triton X-100) for 1 h followed by 1 h incubation with rabbit anti-Flag antibody diluted 1:1000 in the blocking buffer. The cells were washed 3 times with PBS-0.1% Triton X-100 and were incubated for 1 h with the anti-rabbit-Cy3 secondary antibody diluted 1:1000 in the blocking buffer. After three washes the cells were mounted with 100 µl of DAPI Fluoromount-G overnight at room temperature and were imaged on Zeiss 710 confocal microscope using the 63X objective.

ALK12 labeling of endogenous ARF6

500,000 cells were seeded into a 6 well plate. 24 h later 75 µM ALK12 was added and the cells were grown in ALK12 for three generation. Then 10 million cells were seeded into 15-cm plates in ALK12. The next day ALK12 was refreshed and 25 µM TM or 10 mM NAM were added along with it. 15 h later the cells were harvested, washed with cold ice-cold PBS, and lysed with 300 µl of 4% SDS lysis buffer. The lysates were then treated with 1 M hydroxylamine for 1 h with rotating at 30ºC. The proteins were then precipitated by adding 600 µl of methanol, 200 µl of chloroform and 400 µl of water

(all ice-cold), mixing and spinning down for 10 min at 17,000g. The protein was washed with 1 ml of methanol three times, air dried, and then resuspended in 4% SDS lysis buffer. The protein concentration was measured and click chemistry was performed on 1 mg of protein in 300 µl of SDS lysis buffer by adding 15 µl of each of the following reagents: 5 mM biotin-PEG3-azide in water, 10 mM TBTA in DMF, 40 mM CuSO4 in water, 40 mM TCEP in water, and incubating the reactions for 2 h with rotating at 30ºC. The proteins were then precipitated, washed again, and dissolved in 200 µl of the SDS buffer. 10 µl were transferred to a new tube for input analysis. The remaining samples were diluted with 1 ml of BriJ buffer (1% BriJ35, 50 mM TEA, 150 mM NaCl). 20 µl of streptavidin beads per sample were washed with 1 ml of BriJ buffer 3 times and were then added to each sample in 200 µl of BriJ buffer. The samples were rotated overnight at 4ºC and the beads were then washed 3 times with 1 ml of BriJ buffer. The buffer was completely removed, and the proteins were eluted by boiling in 24 µl of 2X protein loading buffer. The samples were spun down, and the supernatants and input samples were analyzed for ARF6 levels by WB.

The effect of TM on transferrin recycling

200,000 HCT116 cells per well were seeded in 6-well plates in duplicates. 48 h later 25 µM TM was added for 18 hr. Then the cells were incubated in serum-free media with TMfor 5 h followed by labeling with 5 ug/ml TFN-488 in serum-free media with TM for 1 h. The cells were washed with cold PBS pH 4.7 for 3 min twice (to wash away TFN that had not been internalized), then rinsed once with cold PBS pH 7.4, and 0 min time point was collected. The remaining plates were recycled in complete growth media

for 10, 20 and 30 min. At each time point, the cells were washed with cold PBS pH 4.7, rinsed with PBS pH 7.4, then scraped and fixed with 4% PFA for 30 min. The fixed cells were washed with PBS twice and resuspended in PBS for flow cytometry analysis to measure the remaining transferin-488 inside the cells.

The effect of TM on tumor growth in mice

One million of HCT116 or SW948 cells were injected into the flanks of NOD-SCID female and male mice (4 per group) and once the tumors were palpable, the mice were treated daily with 50 mg/kg TM or vehicle (5% DMSO, 5% Koliphor) in PBS for two weeks.

The effect of ARF6 or ARF6 K3R on tumor growth in mice

300 of HCT116 cells with stable overexpression of ARF6 WT or ARF6 K3R or empty vector were injected into the flanks of NOD-SCID female and male mice (4 per group). Tumor weight was measured 34 days post injection.

REFERENCES

1. Dinu, D. *et al.* Prognostic significance of KRAS gene mutations in colorectal cancer--preliminary study. *J Med Life* **7**, 581-587 (2014).
2. Beganovic, S. Clinical significance of the KRAS mutation. *Bosn J Basic Med Sci* **9 Suppl 1**, 17-20 (2009).
3. Hu, F. *et al.* Inhibition of SIRT2 limits tumour angiogenesis via inactivation of the STAT3/VEGFA signalling pathway. *Cell Death Dis* **10**, 9 (2018).
4. Cheon, M.G., Kim, W., Choi, M. & Kim, J.E. AK-1, a specific SIRT2 inhibitor, induces cell cycle arrest by downregulating Snail in HCT116 human colon carcinoma cells. *Cancer Lett* **356**, 637-645 (2015).
5. Farooqi, A.S. *et al.* Novel Lysine-Based Thioureas as Mechanism-Based Inhibitors of Sirtuin 2 (SIRT2) with Anticancer Activity in a Colorectal Cancer Murine Model. *J Med Chem* **62**, 4131-4141 (2019).
6. Jing, H. *et al.* A SIRT2-Selective Inhibitor Promotes c-Myc Oncoprotein Degradation and Exhibits Broad Anticancer Activity. *Cancer Cell* **29**, 297-310 (2016).
7. Zhou, W. *et al.* The SIRT2 Deacetylase Stabilizes Slug to Control Malignancy of Basal-like Breast Cancer. *Cell Rep* **17**, 1302-1317 (2016).

8. Xu, S.N., Wang, T.S., Li, X. & Wang, Y.P. SIRT2 activates G6PD to enhance NADPH production and promote leukaemia cell proliferation. *Sci Rep* **6**, 32734 (2016).
9. Kosciuk, T. *et al.* NMT1 and NMT2 are lysine myristoyltransferases regulating the ARF6 GTPase cycle. *Nat Commun* **11**, 1067 (2020).
10. Selvakumar, P., Smith-Windsor, E., Bonham, K. & Sharma, R.K. N-myristoyltransferase 2 expression in human colon cancer: cross-talk between the calpain and caspase system. *FEBS Lett* **580**, 2021-2026 (2006).
11. Kumar, S., Dimmock, J.R. & Sharma, R.K. The potential use of N-myristoyltransferase as a biomarker in the early diagnosis of colon cancer. *Cancers (Basel)* **3**, 1372-1382 (2011).
12. Raju, R.V., Moyana, T.N. & Sharma, R.K. N-Myristoyltransferase overexpression in human colorectal adenocarcinomas. *Exp Cell Res* **235**, 145-154 (1997).
13. Chabu, C., Li, D.M. & Xu, T. EGFR/ARF6 regulation of Hh signalling stimulates oncogenic Ras tumour overgrowth. *Nat Commun* **8**, 14688 (2017).
14. Siddiqui, A.D. & Piperdi, B. KRAS mutation in colon cancer: a marker of resistance to EGFR-I therapy. *Ann Surg Oncol* **17**, 1168-1176 (2010).
15. D'Souza-Schorey, C., Li, G., Colombo, M.I. & Stahl, P.D. A regulatory role for ARF6 in receptor-mediated endocytosis. *Science* **267**, 1175-1178 (1995).
16. Mayle, K.M., Le, A.M. & Kamei, D.T. The intracellular trafficking pathway of transferrin. *Biochim Biophys Acta* **1820**, 264-281 (2012).
17. Ponnusamy, M. *et al.* Blocking sirtuin 1 and 2 inhibits renal interstitial fibroblast activation and attenuates renal interstitial fibrosis in obstructive nephropathy. *J Pharmacol Exp Ther* **350**, 243-256 (2014).
18. Cao, W. *et al.* SIRT2 mediates NADH-induced increases in Nrf2, GCL, and glutathione by modulating Akt phosphorylation in PC12 cells. *FEBS Lett* **590**, 2241-2255 (2016).
19. Ramakrishnan, G. *et al.* Sirt2 deacetylase is a novel AKT binding partner critical for AKT activation by insulin. *J Biol Chem* **289**, 6054-6066 (2014).

CHAPTER 4

DYNAMIN2 IS AN UNCONVENTIONAL SUBSTRATE OF NMT

Tatsiana Kosciuk, Kayla Nicole Johnson, Shuai Zhang, Hening Lin

ABSTRACT

Decades of work on N-terminal myristylation have generated munch knowledge about the basic rules that govern the addition of this modification to protein substrates by the N-myristoyltransferase (NMT) enzymes. These rules were used to create bioinformatics approaches for predicting N-terminal glycine myristoylation. In recent years however the understanding of sequence requirement and mechanism of catalysis of NMT have been refined and expanded. To identify NMT substrates that may have been missed by the bioinformatics tools, here we used a quantitative proteomic approach to identify NMT substrates. Unexpectedly, we identified a new NMT substrate Dynamin2 (DNM2) that does not conform to the conventional sequence preference and is predicted as a non-myristoylated protein by bioinformatics. Our findings unravel a regulation of DNM2 by myristoylation and its potential role in colon cancer and highlights the need for further understanding of NMT catalysis and development of new tools for myristoylation prediction.

INTRODUCTION

N-terminal myristoylation is the addition of a saturated 14-carbon chain to the amino group of the N-terminal glycine on proteins. This modification is catalyzed by N-myristoyltransferases, enzymes ubiquitous in eukaryotes with two isoforms in

mammals. It is well established that NMT preferentially acts on the GXXX(S/T/C) motif and that the modification occurs on nascent peptides during translation.[1] This led to the development of bioinformatics tools that can predict proteins regulated by N-myristoylation. In recent years however it became evident that protein myristoylation is more complex. For instance, it is now known that NMT can also act in a posttranslational manner,[2, 3] that its activity is regulated by the binding protein ACBD6,[4-6] and that it can act on lysine residues.[7, 8] There is also a wider understanding now of the NMT sequence preference and how it varies among species.[9] This additional knowledge is not considered in the current bioinformatics approaches for predicting myristoylation, and thus, it is likely that some proteins could be regulated by N-myristoylation despite a negative prediction by such tools.

Protein myristylation is highly abundant in cell trafficking pathways. For instance, myristoylated ARF GTPases regulate Golgi, endoplasmic reticulum (ER), and endocytic vesicle trafficking. Dynamin (DNM) is a large GTPase in the family of dynamin-like proteins (DLPs) that plays a critical role in endocytosis by orchestrating the events in vesicle fission. Among the three DNM isoforms, DNM2 is ubiquitously expressed, while DNM1 and DNM3 are specific to nervous tissues.[10] Here we demonstrate that DNM2 is myristoylated while its N-terminal sequence does not conform to the established motif for NMT substrates. Our findings suggest that this modification regulates DNM2 protein levels, which is important for colon cancer cell survival. The work highlights the limitation of current bioinformatics tools and that additional studies are needed to fully understand the NMT regulation and its myriad of substrates.

RESULTS

DNM2 is a substrate of NMT

To identify new NMT substrates, we performed a SILAC proteomics study in HEK293T cells where we quantitatively compared two conditions with maximized versus minimized N-myristoylation. We maximized N-myristoylaiton by overexpressing (OE) NMT1 or NMT2 and inhibiting sirtuins with nicotinamide to increase lysine acylation, since NMT can also act on lysine. We minimized N-myristoylation by inhibiting NMT with DDD85646. Cells of all conditions were labeled with ALK12 (a clickable myristic acid analog) and cells with maximized myristoylation were labeled with heavy amino acids while cells with minimized myristoylation were labeled with light amino acids. Alk12 labeled proteins were affinity purified and analyzed by mass spectrometry. During the analysis, proteins with heavy/light (H/L) ratios of ≥1.30 were considered possible NMT substrates. To further increase the reliability of the proteomics result, we also carried out a reverse SILAC experiments where the heavy and light labels were switched (Figure 4.1A). In this reverse SILAC, proteins with H/L ratio of ≤ 0.75 were considered possible NMT substrates. Because we overexpressed either NMT1 or NMT2, in total we had four SILAC experiments. Proteins that appeared in at least two SILAC experiments with the desired H/L ratios were selected (Supplemental Figure 4.1). Several known NMT substrates such as those in the ARF family were identified implying the validity of the study (Supplementary Figure 4.1).

Among the selected proteins with no reported myristoylation, DNM2 appeared in one forward and two reverse SILAC conditions (Figure 4.1B). To validate that DNM2 is

myristoylated, we performed a metabolic labeling of C-terminally Flag tagged DNM2 with ALK12 in HEK293T cells with or without NMT overexpression. We used ARF6 G2A that can be myristoylated on lysine 3[7] as a positive control. After isolating DNM2 by Flag-affinity, we conjugated TAMRA-azide to the alkyne handle via copper-catalyzed click chemistry (Figure 4.1A). The in-gel fluorescence revealed that without Alk12, there was very little DNM2 fluorescent labeling, but addition of Alk12 led to significantly increase DNM2 labeling, suggesting that DNM2 was indeed myristoylated (Fig. 1B). NMT overexpression further increased the modification levels (Fig. 1B). The modification was resistant to hydroxylamine supporting that it is attached through an amide, not a thioester, linkage (Fig. 1B). To further confirm that the Alk12 labeling was due to NMT and determine which NMT enzyme is the endogenous myristoyltransferase, we analyzed DNM2 myristoylation levels by ALK12 labeling in NMT knockdown (KD) cells. NMT1 KD suppressed DNM2 myristoylation but NMT2 KD had no effect, while overexpression of either NMT could rescue the KD effect (Figure 4.1C). We then asked whether NMT and DNM2 can be found in the same cellular compartments. We overexpressed NMT1 and NMT2 along with DNM2 in HEK293T cells and analyzed colocalization by immunofluorescence. DNM2 and NMT displayed very similar localization patterns (Figure 4.1D). Together these data suggest that DNM2 contains NMT-catalyzed myristoylation.

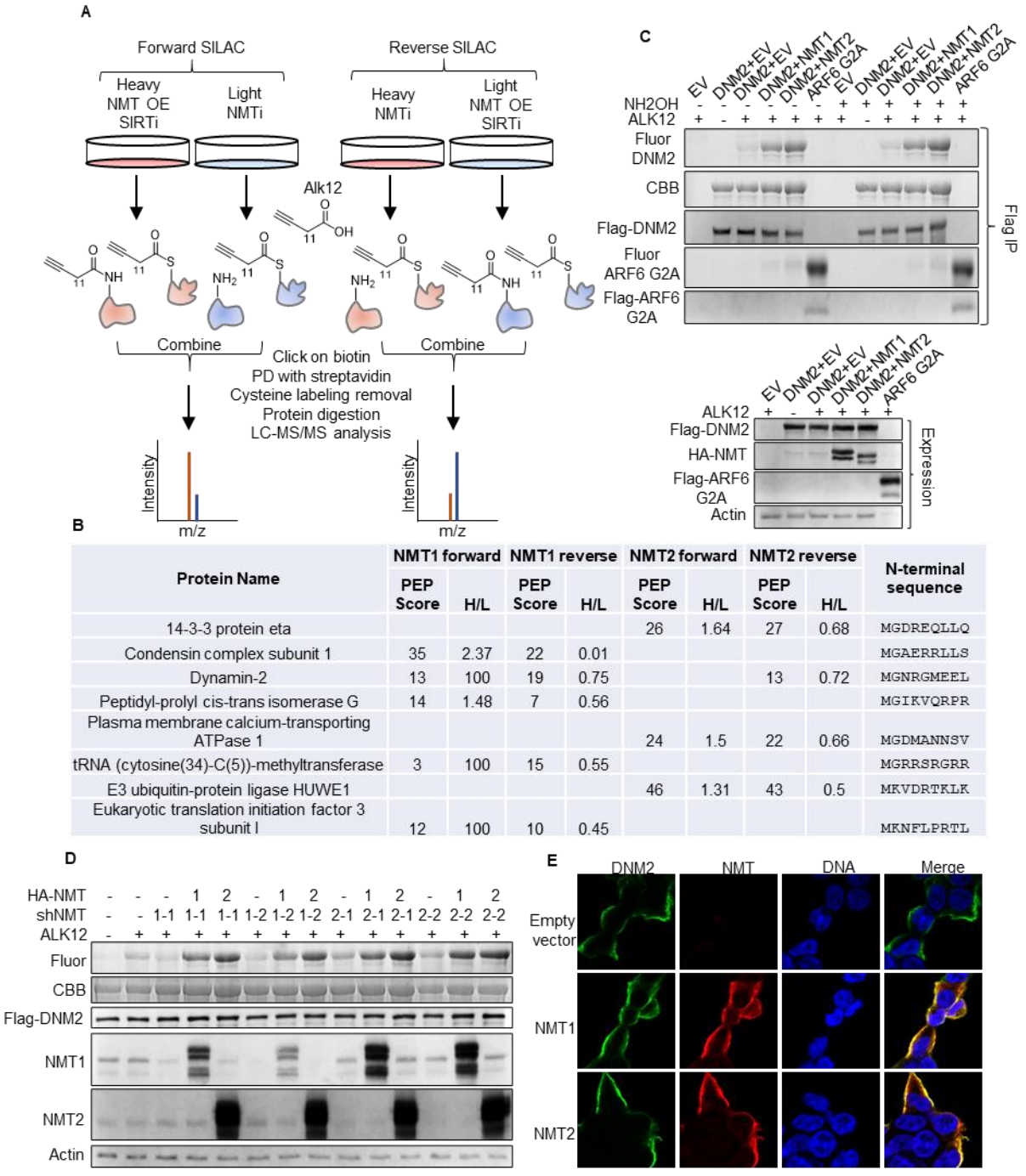

Protein Name	NMT1 forward		NMT1 reverse		NMT2 forward		NMT2 reverse		N-terminal sequence
	PEP Score	H/L	PEP Score	H/L	PEP Score	H/L	PEP Score	H/L	
14-3-3 protein eta					26	1.64	27	0.68	MGDREQLLQ
Condensin complex subunit 1	35	2.37	22	0.01					MGAERRLLS
Dynamin-2	13	100	19	0.75			13	0.72	MGNRGMEEL
Peptidyl-prolyl cis-trans isomerase G	14	1.48	7	0.56					MGIKVQRPR
Plasma membrane calcium-transporting ATPase 1					24	1.5	22	0.66	MGDMANNSV
tRNA (cytosine(34)-C(5))-methyltransferase	3	100	15	0.55					MGRRSRGRR
E3 ubiquitin-protein ligase HUWE1					46	1.31	43	0.5	MKVDRTKLK
Eukaryotic translation initiation factor 3 subunit I	12	100	10	0.45					MKNFLPRTL

Figure 4.1 DNM2 is a substrate of NMT. (A) SILAC proteomics scheme. (B) SILAC results for proteins with N-terminal glycine or lysine with no reported myristoylation suggest that DNM2 is an NMT substrate. Cut-off H/L (heavy to light ratio) values: 1.3 for forward and 0.75 for reverse. (C) ALK12 labeling confirms DNM2 myristoylation by NMT via hydroxylamine-resistant linkage. (D) NMT1 KD inhibits DNM2 myristoylation, which can be rescued by both NMT isoforms. (E) DNM2 and NMT colocalize to the same cellular compartment. All experiments were performed in HEK293T cells.

Myristoylation of DNM2 is on the N-terminal glycine

DNM2 is not reported to have N-terminal myristoylation and the N-terminal sequence does not fulfill the GXXX(S/T/C) NMT preference motif, however, it does contain an N-terminal glycine after cleavage of the initiating methionine (Figure 4.2A). We therefore speculated that DNM2 could be N-terminal glycine myristoylated. We used the ExPASY myristoylation tool to predict whether DNM2 could be myristoylated at the N-terminus. ExPASY predicted that DNM2 is non-myristoylated (Figure 4.2B). Because NMT was recently reported to catalyze lysine myristoylation that could be removed by sirtuins,[7] we next asked whether DNM2 has lysine myristoylation. We performed ALK12 labeling of DNM2 in the presence of pan-sirtuin inhibitor nicotinamide. This treatment however did not increase the myristoylation abundance, but again it was increased by NMT OE and suppressed by NMT inhibition with DDD8564 (Figure 4.2C) suggesting that this NMT-catalyzed modification was not on lysine. Examination of the N-terminal sequence conservation revealed that it was identical in several species and was nearly identical among the three human dynamins (Figure 4.2D), which suggested an indispensable role of the N-terminal glycine. Interestingly, it was recently reported that Asn3 frequently occurs in NMT substrates,[11] which is also present in DNM2 (Figure 4.2D). To test the possibility of N-terminal glycine myristoylation of DNM2, we generated a G2A mutant of DNM2 and tested its ability to be ALK12-labeled in HEK293T cells. The mutation abolished the ALK12 incorporation and this effect could not be rescued with NMT OE (Figure 4.2E). We wondered whether there are known myristoylated proteins that also would not be predicted as myristoylated by bioinformatics. The tyrosine kinase c-Abl isoform 1b has

the N-terminal sequence of MGQQPGKVLG that does not contain the preferred NMT motif but is myristoylated on the N-terminal glycine.[12] We therefore tested whether c-Abl would be predicted as myristoylated by ExPASY. Similar to DNM2, c-Abl was predicted as non-myristoylated (Supplementary Figure 4.1). These data suggest that DNM2 is myristoylated on the N-terminal glycine by NMT and that the ExPASY myristoylation prediction tool results should be interpreted with caution to avoid missing important biology.

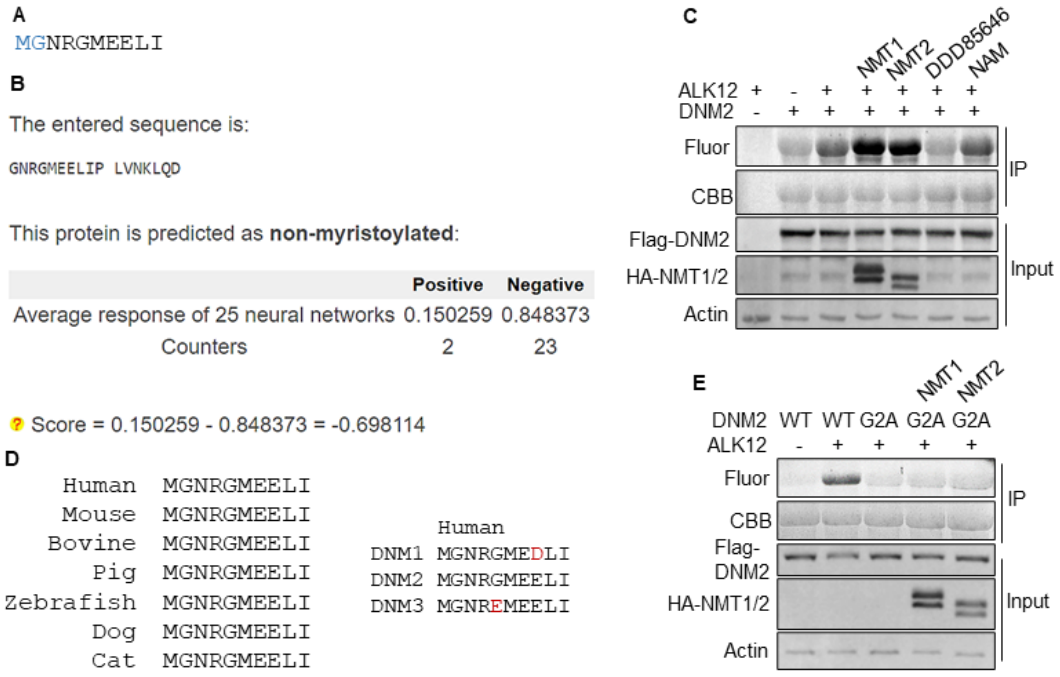

Figure 4.2 DNM2 is myristoylated at the N-terminal glycine. (A) The N-terminal amino acid sequence of DNM2. (B) ExPASY myristoylation tool predicts that DNM2 is not myristoylated at the N-terminal glycine. (C) DNM2 myristoylation is inhibited by NMT inhibition with DDD85646, but not increased by sirtuin inhibition with nicotinamide. (D) The DNM2 N-terminal amino acid sequence is conserved among several species and strongly conserved among three human dynamins. (E) DNM2 WT but not DNM2 G2A is labeled with ALK12. All experiments were performed in HEK293T cells.

Myristoylation of DNM2 may be co-translational and require additional regulators

Since the N-terminal sequence of DNM2 does not satisfy the NMT preference for N-terminal glycine myristoylation, we asked whether NMT alone is sufficient to catalyze the modification or whether additional regulators might be involved. We first tested whether human NMT1 and NMT2 expressed and purified from *E. coli* could modify the N-terminal of DNM2 in vitro. To obtain non-myristoylated DNM2, we overexpressed Flag-DNM2 in HEK293T cells and inhibited NMT with DDD85646. We then isolated DNM2 via Flag affinity beads and performed an on-beads NMT reaction. DNM2 did not get modified, suggesting that its myristoylation is co-translational or requires additional regulators (Figure 4.3A). We reasoned that if the modification occurs co-translationally, then NMT and DNM2 proteins should not interact. We therefore tested the interaction of HA-tagged NMT with Flag-tagged DNM2 overexpressed in HEK293T cells. The proteins did not co-IP suggesting that the modification occurs on a nascent peptide and likely requires a translation machinery or other factors (Figure 4.3B).

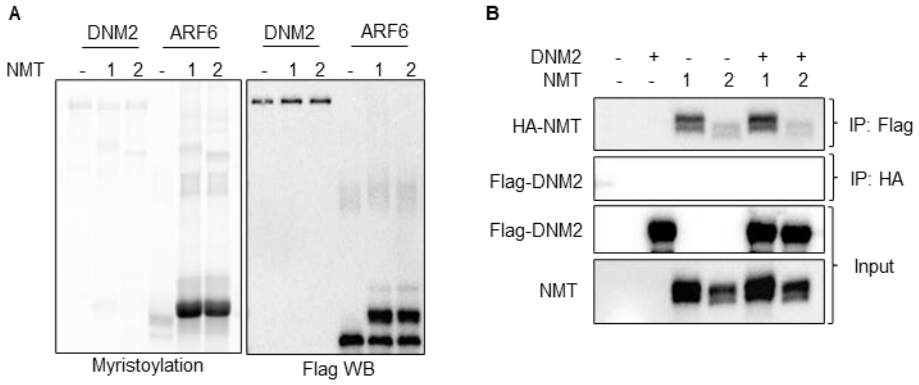

Figure 4.3 DNM2 myristoylation is likely cotranslational and requires additional factors. (A) DNM2 protein cannot be myristoylated by NMT in vitro. ARF6 serves as a positive control. (C) DNM2 protein does not interact with NMT.

N-terminal myristoylation regulates DNM2 stability but not localization

We next asked whether N-terminal myristoylation has a functional effect on DNM2. Because one of the most common functions of the N-terminal myristoylation is to serve as a membrane anchor, we asked whether the DNM2 modification serves this function. We therefore analyzed the effect of the G2A mutation on DNM2 localization by confocal microscopy and subcellular fractionation. Both analyses revealed that the mutation did not alter DNM2 localization (Figure 4.4A, B). Myristoylation of c-Abl also does not confer membrane binding. Instead, its myristoyl group is sequestered into a hydrophobic pocket rendering the kinase soluble.[12] Given the localization of DNM2, we asked whether DNM2 contains an analogous hydrophobic pocket. The myristoylated N-terminus is in the bundle signaling element (BSE) of DNM2. There is no crystal structure available of this region, however it does exist for DNM1. We therefore examined the DNM1-GDP crystal structure of the G domain with the BSE region and found that BSE forms a hydrophobic pocket reminiscent of the myristoyl binding pocket of c-Abl (Figure 4.4C).

Another role of N-terminal myristoylation is in protein stability where free N-terminal glycine serves as the signal for ubiquitination and subsequent degradation. To determine whether DNM2 is stabilized by myristoylation, we examined the effect of NMT inhibition on the protein levels of DNM2 in HEK293T cells. A 7-hour treatment with DDD85646 resulted in a dose-dependent depletion of DNM2 (Figure 4.4D). We then examined the ubiquitination levels of the wild type DNM2 and the G2A mutant in HEK293T cells treated with MG132 proteasome inhibitor to accumulate ubiquitinated

proteins. Blocking the N-terminal glycine with the G2A mutation strongly suppressed the ubiquitination levels (Figure 4.4E).

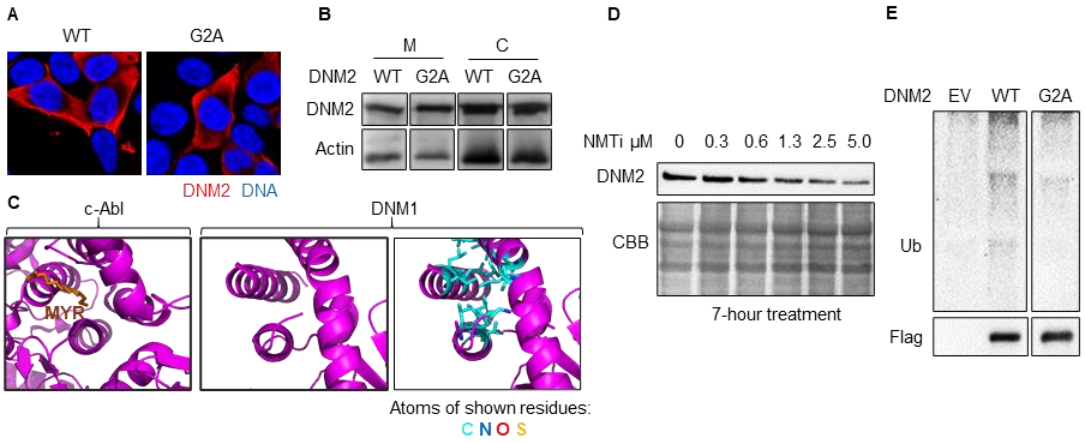

Figure 4.4 Myristoylation affects DNM2 levels but not localization. (A) Confocal microscopy showing that G2A mutation does not affects DNM2 localization. (B) Subcellular fractionation showing that DNM2 G2A distribution between membranes (M) and cytosol (C) is similar to that of DNM2 WT. (C) The hydrophobic pocket of DNM1-GDP BSE PDB 5D3Q) is reminiscent of the myristoyl binding pocket of c-Abl (PDB 1OPK). Myristoyl group is orange. (D) NMT inhibition dose-dependently reduces DNM2 protein levels. (E) DNM2 WT contains more ubiquitination than DNM2 G2A.

NMT and DNM2 support colon cancer cell growth.

Colon cancer cells are reported to have high levels of DNM2 in The Human Protein Atlas database, which indicates that DNM2 might be important for colon cancer progression. We therefore investigated whether targeting DNM2 myristoylation could inhibit colon cancer cell growth. We first tested whether endogenous DNM2 is myristoylated in HCT116 colon cancer cells. To that end we treated HCT116 cells with ALK12 or DMSO for three generations and then conjugated azido-PEG3-biotin to labeled proteins via click chemistry in lysates. We then isolated all ALK12-labeled proteins via streptavidin affinity purification and examined the presence of DNM2 among them by Western blot. This analysis revealed that DNM2 can be labeled with

ALK12, suggesting that endogenous DNM2 is myristoylated in colon cancer cells (Fig 4.5A). We then tested whether DNM2 protein levels are important to colon cancer cell survival. Transient DNM2 KD with shRNA led to a severe cell growth impairment four days after shRNA delivery via lentiviral particles (Figure 4.5B and C). Finally, we tested whether NMT inhibition could suppress colon cancer cell growth. Treatment with DDD85646 caused a dose-dependent growth inhibition of HCT116 colon cancer cells within 4 days (Figure 4.5D) and a reduction in DNM2 protein levels after 24 hours (Figure 4.6E). While NMT has many substrates in cells, it is possible that DNM2 degradation contributes to the cell growth suppression caused by NMT inhibition. Together, these data suggest that endogenous DNM2 is myristoylated, which supports colon cancer cell survival.

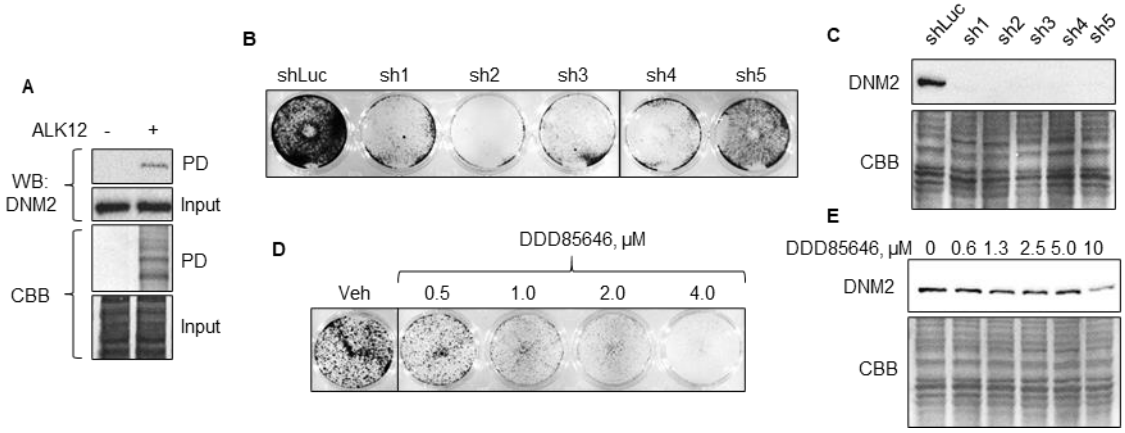

Figure 4.5 Endogenous DNM2 myristoylation might regulate colon cancer cell survival. (A) Endogenous DNM2 is labeled with ALK12. PD: pull down. (B) DNM2 KD strongly suppresses colon cancer cell proliferation. (C) DNM2 KD efficiency for (B). (D) NMT2 inhibition suppresses HCT116 colon cancer cell growth. (E) NMT inhibition dose-dependently reduces DNM2 protein levels.

DISCUSSION

Much effort has been put into identifying the "rules" for protein N-terminal myristoylation, and decades of work established that NMT prefers the GXXX(S/T/C) motif and acts in a co-translational manner. It is however becoming increasingly

apparent that these rules are fluid and there is still much to learn about the NMT catalysis. For example, c-Abl is a well-established substrate of NMT with the N-terminal sequence MGQQPGKVLG not conforming to the NMT substrate sequence preference. Furthermore, there is growing evidence for posttranslational N-terminal myristoylation[2] and the ability of NMT to act on lysine residues.[7, 8] We found that the large GTPase DNM2, that does not appear to satisfy the NMT sequence selectivity and is predicted as non-myristoylated protein by the ExPASY tool, is myristoylated at the N-terminal glycine by the human NMT enzymes. The established myristoylated tyrosine kinase c-Abl is also predicted as non-myristoylated. This implies that there might be additional levels of regulation of N-terminal myristoylation that are yet to be discovered. Therefore, the information gathered from predictive tools such as ExPASY, while very useful, should be interpreted with an open mind. It is possible that the only absolute requirement of NMT for the N-terminal glycine myristoylation is the actual presence of Gly at the N-terminus, while the rest is dictated by the overall favorability of the combination of the residues following Gly2 and other regulatory factors. Human NMT appears to have a strong bias toward Asn following the N-terminal Gly,[11] which is present in DNM2. This potentially could compensate for the lack of preferred residues at other positions. In c-Abl this compensation could come from Lys7. We further find that DNM2 cannot be myristoylated by NMT in vitro and does not appear to interact with NMT, while in cells, they seem to localize to the same compartments. This is not surprising given that a number of NMT substrates are modified co-translationally on a nascent polypeptide and thought to require the NMT-ribosome interaction.[13] It is possible that DNM2 modification is also co-translational. Alternatively, a

conformational change induced by other NMT regulators such as ACBD6 could be needed to facilitate the activity on DNM2. Ankyrin (ANK) repeat domain of ACBD6 is reported to activate NMT.[6] Interestingly MxA, a dynamin like protein, interacts with the ankyrin-like repeat domain of TRPC.[14] Therefore, it is tempting to speculate that the ANK domain of ACBD6 brings NMT and DNM2 together to facilitate the modification.

Overall plasma membrane levels of DNM2 were not affected by myristoylation. While the Pleckstrin Homology (PH) domain of DNM2 is known to bind membrane lipids, it is thought to acquire strong phosphoinositide binding once DNM2 is already oligomerized.[15] What causes the nucleation of DNM2 to initiate oligomerization at the vesicle neck is not well understood. Since fatty acylation is known to target proteins to membranes, we speculate that myristoylation serves as a second signal in addition to the PH domain that strengthens the initial membrane binding followed by oligomer formation. Such mechanisms have been observed. For example, like dynamin, the viral Gag protein can form oligomers in vitro without myristoylation, but in the cells myristoylation is important to initiate Gag oligomerization at the membrane.[16] It would be interesting to examine via high-resolution imaging such as cryo-EM whether DNM2 myristoylation confers a similar effect at the vesicle neck. Alternatively, like in c-Abl, myristoylation may not regulate DNM2 membrane binding but instead affects it activity. We observed a hydrophobic pocket in BSE of DNM1-GDP analogous to the myristoyl binding pocket of c-Abl, and therefore it would be of interest to determine whether this pocket can indeed bind the myristoyl group and promote or inhibit oligamerization.

Our data suggests that a small molecule NMT inhibitor decreases DNM2 protein levels, which is in agreement with reports establishing the free N-terminal glycine as the degradation signal.[17] Therefore, N-terminal myristoylation blocks the degradation signal and increases DNM2 protein stability. We found that DNM2 knockdown is detrimental to colon cancer cell growth. Because NMT inhibition also suppressed colon cancer cell growth, it is likely that the effects of NMT inhibition is at least partially through DNM2 degradation. Our findings thus imply that there might be more NMT substrates with important biological roles than previously thought, and that controlling colon cancer through DNM2 myristoylation might be a viable therapeutic strategy.

METHODS

Detecting DNM2 myristoylation by in-gel fluorescence

Three to four million HEK293T cells (for NMT KD experiment, stable NMT KD or shLuciferase control cells were used) were seeded into 10 cm plates, one plate for each condition. The next day the cells were transfected with 5 µg of DNM2 plasmids and 3 µg of NMT plasmids or empty vector. A day later 50 µM of ALK12 was added and incubated for 6 h (5 µM DDD85646 or 10 mM nicotinamide where added along with ALK12 for NMT and sirtuin inhibition experiment). The cells were then washed with ice-cold PBS, collected and spun down at 500 g for 5 min at 4ºC. All the PBS was removed, and the cells were lysed with 300-500 µl of ice-cold 1% NP-40 lysis buffer (25 mM Tris-HCl pH 7.4, 150 mM NaCl, 10% glycerol, 1% Nonidet P-40, with protease and phosphatase inhibitors added freshly) for 30 min with vortexing every 10 min. The lysates were spun down at 17,000 g for 15 min at 4ºC and protein concentration was determined. Flag beads (15 µl per sample) were washed with 1 ml of IP wash buffer

(25 mM Tris-HCl pH 7.4, 150 mM NaCl, and 0.2% Nonidet P-40) three times, resuspended in the IP wash buffer, and added to equal amounts of total protein (around 500-1000 µg). The final mixture contained 1:1 volumes of lysate to IP wash buffer and 15 µl of Flag beads in a final volume of 500 – 1000 µl. The samples were rotated at 4ºC for 2 h and then washed with ice-cold IP wash buffer three times. All the buffer was carefully removed with gel loading tips, the beads were resuspended in 20 µl of click chemistry mix prepared by adding TAMRA azide (1 µl of 2 mM solution in dimethyl sulfoxide (DMSO)), TBTA (1 µl of 10 mM solution in dimethylformamide (DMF)), CuSO4 (1 µl of 40 mM solution in H_2O), and TCEP (1 µl of 40 mM solution in H_2O) per 20 µl of IP wash buffer. The reaction proceeded for 40 - 60 min in the dark. Then 9 µL of 6X protein loading dye was added and the samples were boiled for 10 min. They were then spun down for 2 min, the supernatant was removed, divided into two equal parts that were then boiled with 300 µM hydroxylamine or water for 7 min. The samples were briefly spun down and subjected to SDS-PAGE. The gel was destained in destaining buffer (10% acetic acid and 40 % methanol in water) for 2 hr at room temperature or overnight at 4ºC and then scanned with Typhoon FLA7000. The gel was then stained with Coomassie brilliant blue to detect the DNM2 loading. 5 µg of lysate was analyzed for the expression of DNM2, NMT1/2, and actin by Western blot. SDS-PAGE and Western blot (WB) were performed as previously reported.[7]

ALK12 labeling of endogenous DNM2 in HCT116 cells

Cells were treated with 75 µM of ALK12 or DMSO for three generations. One confluent 10-cm plate of cells per condition was used. The cells were washed with ice-cold PBS,

harvested, and lysed with 300 µl of 4% SDS lysis buffer. 2 mg of total protein was diluted to 1 ml with 4% SDS lysis buffer and click chemistry was performed by adding 50 µl of the following: 5 mM biotin-PEG3-azide in water, 10 mM TBTA in DMF, 40 mM $CuSO_4$ in water, 40 mM TCEP in water. The reaction proceeded for 2 h at 30ºC followed by protein precipitation with 4:1:3 volumes of ice-cold methanol:chloroform:water. The precipitation mix was spun down at 5000 RPM for 20 min (or until a protein pellet is formed between layers). The pellet was washed 3 times with 1 ml of ice-cold methanol, were air dried and re-dissolved in 200 µl of 4% SDS lysis buffer. The samples were diluted with 1 ml of BriJ35 buffer (1% BriJ35, 50 mM TEA, 150 mM NaCl). 50 µl of each sample were taken for WB analysis of input. 20 µl per sample of streptavidin beads were washed 3 times with 1 ml of BriJ buffer and were then added to each sample in 200 µl of BriJ buffer. The samples were rotated for 2.5 h at room temperature and the beads were then washed with 1 ml of BriJ buffer 3 times. All the buffer was removed, and the proteins were eluted by boiling in 24 µl of 2X protein loading dye. The samples were spun down, and the supernatants were analyzed for DNM2 by Western blot.

Immunofluorescence to analyze DNM2 colocalization with NMT1/2

200,000 HEK293T cells were seeded into MatTek glass bottom dishes. 24 h later the cells were transfected with 1 µg of Flag-DNM2 and 1 µg of HA-NMT1, HA-NMT2 or empty vector (pCMV-tag-4a) using FuGENE 6 transfection reagent (1:3 plasmid/reagent ration). For each plate, room temperature FuGENE 6 was mixed with 100 µl of pre-warmed serum-free media and incubated for 5 min at room temperature.

Then the plasmids were added, the solution was mixed by inversion and was left at room temperature for 30 min. The media in the plates were replaced with 1 ml of fresh complete growth media and the transfection mix was added dropwise. After culturing the cells for 24 h, the cells were washed twice with ice-cold PBS and fixed with 1 ml of 4% PFA for 30 min. They were then washed twice with PBS and blocked with blocking buffer (PBS containing 5% BSA and 0.1% Triton X-100) for 1 h followed by 1 h incubation with mouse anti-Flag and rabbit anti-HA antibodies diluted 1:1000 in the blocking buffer. The cells were washed 3 times with PBS-0.1% Triton X-100 and incubated for 1 h with the secondary antibodies (anti-mouse-488 and anti-rabbit-Cy3) diluted 1:1000 in the blocking buffer. The cells were washed 3 times and were mounted with 100 µl of DAPI Fluoromount-G. The images were taken on Zeiss 710 confocal microscope using the 63X objective.

DNM2 KD in HCT116 cells

150,000 cells were seeded into each well of a 6-well plate and cultured for 24 h. Then 1 ml of viral particles were added with 8 µg/ml polybrene and the cells were cultured for another 24 h Before 1 ml of fresh complete growth media was added. After incubating for 24 h, the media were replaced with 2 ml of fresh complete growth media. 48 h later the plates were imaged using colored bright field function of Cytation 5. The cells were collected, washed with ice-cold PBS and lysed with 100 µl of 4% SDS lysis buffer (50 mM trimethylamine, 150 mM NaCl, 4% SDS with freshly added protease and phosphatase inhibitors and Pierce Universal Nuclease). 15 µg of protein were analyzed for KD efficiency by WB.

Time and dose-dependent effect of NMT inhibition with DDD85646 on pERK and DNM2 levels.

500,000 of HEK293T cells were seeded into 6-well plates and cultured for 24 h before 2.5 µM DDD85646 or DMSO were added to the cells. The cells were cultured with the inhibitor for the indicated time. Cells were scraped into the media and were spun down for 3 min at 1000g at 4ºC. They were then resuspended in 1 ml of ice-cold PBS and were spun down again. All the PBS was removed, and the pellets were frozen at -80ºC. They were then rapidly resuspended in 50 µl of 4% SDS lysis buffer with PIC and nuclease, and 25 µg of protein were used for DNM2 and pERK and 10 µg for total ERK analyses by WB. The dose-dependence experiment was performed in the same manner, except one time point, 7 h, was used.

In vitro NMT reaction with DNM2 N-terminal peptides

The reaction consisted of 100 µM myristoyl-CoA, 50 µM peptide and 2 µM NMT in 50 mM Tris pH 8.0. NMT and myristoyl-CoA were first combined in the buffer, then 99 µl were transferred into appropriate tubes and 1 µl of 5 mM peptides dissolved in DMSO were added. After a brief vortexing the reactions were rotated at 30ºC for 1 hr. They were then quenched by incubating with 100 µl of acetonitrile for 10 min. To pellet the protein, the samples were spun down at 17,000g for 10 min. The supernatants were transferred to a new tube, mixed with 10 µl of 50% TFA and analyzed by LC-MS with a binary gradient of 0.1% acetic acid in water and 0.1% acetic acid in acetonitrile over 12 min.

The effect of NMT inhibition on HCT116 cells growth

5,000 cells were seeded into each well of a 12-well plate and cultured for 24 hr before DDD85646 or DMSO was added at the indicated concentrations. Four days later the cells were washed twice with 1 ml of ice-cold PBS and fixed with ice-cold methanol for 20 min. The cells were stained with a crystal violet (0.2% crystal violet in 2% ethanol) for 10 min. The dye was removed, and the cells were washed with water until the solution became clear. The plate was dried and imaged on ChemiDoc MP imager.

In vitro NMT reaction on DNM2 protein

Three million HEK293T cells were seeded into two 10-cm plates per condition (DNM2 or the positive control ARF6) and cultured for 24 h. The cells in each plate were transfected with 5 µg of plasmids using the PEI (polyethylenimine) transfection reagent. Briefly, DNA and PEI were added to 500 µl of serum-free media, mixed by inversion and incubated at room temperature for 30 min. To each plate, 6 ml of complete growth media were added, and then the transfection mix was added dropwise. After incubating for 24 h, 5 µM DDD85646 was added and incubated for 8 h. The cells were then washed with ice-cold PBS, collected and lysed with 1% NP-40 lysis buffer. DNM2 protein was immune-precipitated from the lysates with 45 µl of Flag beads. After washing the beads, they were divided into three equal parts and all the wash buffer was removed. 100 µl of 50 mM Tris pH 8.0 containing 8 µM NMT1/2 or buffer and 200 µM ALK12-CoA[7] was added to appropriate tubes and the samples were incubated at 30ºC for 1 h. The samples were then put on ice and washed with 1 ml of ice-cold IP wash buffer three times. The buffer was removed and click chemistry was performed in 15 µl reactions for 1 h as described above. 8 µl of protein loading dye was added after the reaction, the samples

were boiled for 10 min, spun down and analyzed by in-gel fluorescence as described above.

Co-IP to detect DNM2-NMT2 interaction

Flag-DNM2, HA-NMT1, HA-NMT2 or empty vector were overexpressed in HEK293T cells alone or together (one 10 cm plate per condition) by transfecting 3 µg of each plasmid. 24 hr later the cells were washed with ice-cold PBS, collected, and lysed with 400 µl of 1% NP-40 lysis buffer. The lysates were spun down at 17,000 g for 15 min at 4ºC and the supernatants were divided into two equal parts and subjected to Flag or HA IP for 2 h. The beads were washed three times with IP wash buffer and were boiled in 2X protein loading dye for 10 min. The supernatants were analyzed for HA and Flag signals by WB.

SILAC to detect NMT substrates

HEK293T cells were cultured in DMEM containing dialyzed FBS and heavy ([13C6, 15N2]-L-lysine and [13C6, 15N4]-L-arginine) or light amino acids for five generations. Six 10 cm plates per condition were transfected with 5 µg of HA-NMT1, HA-NMT2, or empty vector and every plate was transfected with 0.5 µg of ARF6 G2A (an internal lysine myristylation control). After culturing for 24 h, the cells were treated with 5 µM DDD85646 (empty vector) or 10 mM NAM (NMT OE) for 30 min and then 50 µM Alk12 (along with inhibitors) was added and the cells were cultured for 6 h. The cells were washed with ice-cold PBS, harvested, and lysed with 4% SDS lysis buffer. Equal amounts of total protein (5 mg) from NMT OE + NAM and EV + NMTi (heavy and light, or light and heavy) were combined and click chemistry was performed by adding

150 µM azide-PEG3-biotin, 0.5 mM TBTA, 1.7 mM CuSO4 and 1.7 mM TCEP (final concentrations are indicated). The reaction proceeded for 1 h at room temperature and the proteins were precipitated with 4:1:3 methanol:chloroform:water (all ice-cold), spun down at 5000 RPM for 30 min, and washed with ice-cold methanol. The pellets were air dried and were re-solubilized in 4 % SDS lysis buffer, whichwas then diluted to 0.4 % with 1% Brij97, 100 mM NaCl, and 50 mM triethanolamine. Streptavidin agarose beads were added and incubated with the lysates at room temperature for 2 hr. The beads were then washed three times with 0.2% SDS-PBS and treated with 0.5 M hydroxylamine at room temperature for 1 h followed by three washes with 0.2% SDS-PBS. The beads were then treated with 6 M urea and 10 mM TCEP in PBS for 30 min at 37°C, followed by adding 400 mM iodoacetamide and treating for 30 min at 37°C. The beads were washed with 1 M urea-PBS and the proteins were digested with 2 µg trypsin in 1 M urea-PBS at 37°C overnight. The reaction was quenched with 0.1% trifluoroacetic acid and the supernatant was desalted using a Sep-Pak C18 cartridge. The lyophilized peptides were analyzed by nano LC-MS/MS using LTQ-Orbitrap Elite mass spectrometer as previously described.[18]

DNM2 vs DNM2 G2A localization

Subcellular fractionation was performed as previously described.[7] Immunofluorescence was performed as described above.

Ubiquitination of DNM2 WT and DNM2 G2A

Two million HEK293T cells were seeded into five 10-cm plates and cultured for 15 h. The cells were then transfected with 3 µg of Flag-DNM2, Flag-DNM2 G2A or empty

vector as described above. 24 h later the cells were pretreated with 20 µM MG132 for 2 h in 5 ml of media followed by 3 h treatment with 5 µM DDD85646 or DMSO (2.5 µl of 10 mM stock was added directly to cell media already containing MG132). The cells were then washed twice with ice-cold PBS, collected, and lysed with 400 µl of NP-40 lysis buffer containing protease and phosphatase inhibitors. The lysates were then incubated for 2 h with Flag beads. The beads were washed three times with IP wash buffer and the proteins were eluted and analyzed by WB as described above.

SUPPLEMENTARY INFORMATION

Supplementary table 4.1 SILAC results for NMT substrates

Protein Name	NMT1 F		NMT1 R		NMT2 F		NMT2 R		N-terminal sequence	Reported myr.?
	PEP Score	H/L	PEP Score	H/L	PEP Score	H/L	PEP Score	H/L		
14-3-3 protein eta	-	-	-	-	26	1.64	27	0.68	MGDREQLLQ	-
Condensin complex subunit 1	35	2.37	22	0.01	-	-	-	-	MGAERRLLS	-
Dynamin-2	13	100	19	0.75	-	-	13	0.72	MGNRGMEEL	-
Peptidyl-prolyl cis-trans isomerase G	14	1.48	7	0.56	-	-	-	-	MGIKVQRPR	-
Plasma membrane calcium-transporting ATPase 1	-	-	-	-	24	1.5	22	0.66	MGDMANNSV	-
tRNA (cytosine(34)-C(5))-methyltransferase	3	100	15	0.55	-	-	-	-	MGRRSRGRR	-
E3 ubiquitin-protein ligase HUWE1	-	-	-	-	46	1.31	43	0.5	MKVDRTKLK	-
Eukaryotic translation initiation factor 3 subunit I	12	100	10	0.45	-	-	-	-	MKNFLPRTL	-
ADP-ribosylation factor 3	77	2.5	41	0.17	46	1.83	53	0.19	MGLLSILRK	✓
ADP-ribosylation factor 4	47	2.11	27	0.01	28	2.68	43	0.14	MGLTISSLF	✓
ADP-ribosylation factor 6	42	2.72	26	0.12	25	5.52	36	0.05	MGKVLSKIF	✓
A-kinase anchor protein 12	22	100	63	0.02	-	-	-	-	MGAGSSTEQ	✓
Brain acid soluble protein 1	5	100	19	0.01	-	-	-	-	MGGKLSKKK	✓
Calcineurin B homologous protein 1	6	100	11	0.01	-	-	-	-	MGSRASTLL	✓
Cytochrome c-type heme lyase	12	2	9	0.01	-	-	-	-	MGLSPSAPA	✓
Golgi reassembly-stacking protein 2	22	100	20	0.01	-	-	-	-	MGSSQSVEI	✓
Guanine nucleotide-binding protein G(i) subunit alpha-1	24	100	13	0.01	-	-	-	-	MGAGASAEE	✓
Guanine nucleotide-binding protein G(i) subunit alpha-2	62	2.42	56	0.2	42	1.68	77	0.22	MGCTVSAED	✓
Guanine nucleotide-binding protein G(k) subunit alpha	62	2.18	38	0.2	49	1.98	64	0.19	MGCTLSAED	✓
MARCKS-related protein	66	12.12	88	0.01	47	19.1	86	0.01	MGSQSSKAP	✓
Myristoylated alanine-rich C-kinase substrate	60	5.08	80.00	0.02	42	4.87	72	0.02	MGAQFSKTA	✓
Protein FAM49B	28	1.3	16.00	0.01	-	-	-	-	MGNLLKVLT	✓
Protein phosphatase 1G	60	2.73	70.00	0.16	28	3.59	78	0.13	MGAYLSQPN	✓
Ragulator complex protein LAMTOR1	24	1.32	21.00	0.39	-	-	-	-	MGCCYSSEN	✓

The entered sequence is:

MGQQPGKVLG DQRRPSLPAL

This protein is predicted as **non-myristoylated**:

	Positive	Negative
Average response of 25 neural networks	0.373894	0.624597
Counters	11	14

Score = 0.373894 - 0.624597 = -0.250703

Supplementary figure 4.1 c-Abl is predicted as non-myristoylated by ExPASY.

REFERENCES

1. Jiang, H. *et al.* Protein Lipidation: Occurrence, Mechanisms, Biological Functions, and Enabling Technologies. *Chemical reviews* **118**, 919-988 (2018).
2. Thinon, E. *et al.* Global profiling of co- and post-translationally N-myristoylated proteomes in human cells. *Nat Commun* **5**, 4919 (2014).
3. Zha, J., Weiler, S., Oh, K.J., Wei, M.C. & Korsmeyer, S.J. Posttranslational N-myristoylation of BID as a molecular switch for targeting mitochondria and apoptosis. *Science* **290**, 1761-1765 (2000).
4. Soupene, E. *et al.* Association of NMT2 with the acyl-CoA carrier ACBD6 protects the N-myristoyltransferase reaction from palmitoyl-CoA. *J Lipid Res* **57**, 288-298 (2016).
5. Soupene, E. & Kuypers, F.A. ACBD6 protein controls acyl chain availability and specificity of the N-myristoylation modification of proteins. *J Lipid Res* **60**, 624-635 (2019).
6. Soupene, E., Schatz, U.A., Rudnik-Schoneborn, S. & Kuypers, F.A. Requirement of the acyl-CoA carrier ACBD6 in myristoylation of proteins: Activation by ligand binding and protein interaction. *PLoS One* **15**, e0229718 (2020).
7. Kosciuk, T. *et al.* NMT1 and NMT2 are lysine myristoyltransferases regulating the ARF6 GTPase cycle. *Nat Commun* **11**, 1067 (2020).
8. Dian, C. *et al.* High-resolution snapshots of human N-myristoyltransferase in action illuminate a mechanism promoting N-terminal Lys and Gly myristoylation. *Nat Commun* **11**, 1132 (2020).
9. Castrec, B. *et al.* Structural and genomic decoding of human and plant myristoylomes reveals a definitive recognition pattern. *Nature Chemical Biology* **14**, 671-679 (2018).
10. Ferguson, S.M. & De Camilli, P. Dynamin, a membrane-remodelling GTPase. *Nat Rev Mol Cell Biol* **13**, 75-88 (2012).
11. Castrec, B. *et al.* Structural and genomic decoding of human and plant myristoylomes reveals a definitive recognition pattern. *Nat Chem Biol* **14**, 671-679 (2018).
12. Hantschel, O. *et al.* A myristoyl/phosphotyrosine switch regulates c-Abl. *Cell* **112**, 845-857 (2003).
13. Giglione, C., Fieulaine, S. & Meinnel, T. N-terminal protein modifications: Bringing back into play the ribosome. *Biochimie* **114**, 134-146 (2015).
14. Lussier, M.P. *et al.* MxA, a member of the dynamin superfamily, interacts with the ankyrin-like repeat domain of TRPC. *J Biol Chem* **280**, 19393-19400 (2005).

15. Klein, D.E., Lee, A., Frank, D.W., Marks, M.S. & Lemmon, M.A. The pleckstrin homology domains of dynamin isoforms require oligomerization for high affinity phosphoinositide binding. *J Biol Chem* **273**, 27725-27733 (1998).
16. Li, H., Dou, J., Ding, L. & Spearman, P. Myristoylation is required for human immunodeficiency virus type 1 Gag-Gag multimerization in mammalian cells. *J Virol* **81**, 12899-12910 (2007).
17. Timms, R.T. *et al.* A glycine-specific N-degron pathway mediates the quality control of protein N-myristoylation. *Science* **365**, eaaw4912 (2019).
18. Zhang, X., Spiegelman, N.A., Nelson, O.D., Jing, H. & Lin, H. SIRT6 regulates Ras-related protein R-Ras2 by lysine defatty-acylation. *Elife* **6** (2017).

CONCLUSIONS AND FUTURE DIRECTIONS

During my graduate work I first identified lysine myristoylation on ARF6 which led to the discovery of NMT and SIRT2 as the enzymes catalyzing the addition and removal of this modification. ARF6 is unique in the ARF family, because unlike ARF1-5, it does not regulate vesicular transport between ER and Golgi but instead orchestrates the endocytic trafficking at the plasma membrane. Moreover, it tends to stay membrane bound even in its inactive, GDP-bound or nucleotide-free states.[1] Lysine myristoylation, in addition to the glycine myristoylation that is common to all ARFs, offers an explanation for these unique features. A number of N-terminal myristoylated proteins, require a second signal for efficient plasma membrane binding such as palmitoylation on cysteine residues near the N-terminus in some Src and G proteins.[2, 3] I found that for ARF6 this second signal is lysine myristoylation.[4] Abolishing this modification by mutating lysine to arginine does not relocalize ARF6 to the Golgi, which suggests that additional factors such as GEF specificities might also help guiding it to plasma membrane. The K3R mutation however prevents the inactive ARF6 from associating with endomembranes, which are most likely recycling and early endosomes as they colocalize with transferrin receptor, a known marker for those compartments.

I then found that NMT catalyzes lysine myristoylation on ARF6 which is a new activity for NMT and the first report of a mammalian lysine fatty acyl transferase. This activity can be readily explained: both lysine and N-terminal glycine modifications happen on a sterically unrestricted primary amines that are near the N-terminus. Interestingly, NMT can di-myristoylate ARF6. This remained puzzling until we

identified a long hydrophobic channel in the second GNAT domain of the enzyme that is a similar length to the canonical myristoyl pocket. Based on the modeling studies, this pocket can accommodate myristoylated glycine reorienting the lysine into the catalytic site for the second reaction. To confirm this possibility and fully understand its structural basis, one could co-crystallize the ARF6 peptide acylated on the N-terminal glycine with NMT and myristoyl-CoA. If the hypothesis is true, the acylated glycine will occupy the newly identified hydrophobic channel and the lysine will react with myristoyl-CoA in the active site. It appears that NMT activity on lysine decreases as the lysine moves further away from the N-terminus, suggesting that NMT may not modify internal lysines, but that modifications on other positions near the N-terminus are possible. NMT is proteolytically cleaved during apoptosis and thus it would be of interest to explore the activity of the cleaved species on lysine residues in various positions. Perhaps once the confining regions are cleaved, it might accommodate internal lysine residues. ARF6 so far is the sole physiological lysine substrate of NMT, which warrants identification of additional substrates to understand the extent of this new function of NMT in cells.

Unlike N-terminal glycine myristoylation, lysine myristoylation is known to be reversible, and therefore I sought to identify the eraser of this modification on ARF6. I focused on sirtuins and HDACs as some of them recently emerged as lysine fatty acylation erasers. Knockdown and small molecule inhibition studies revealed that SIRT2, but not other sirtuins or HDAC11 is the eraser of ARF6 lysine myristoylation in HEK293T cells, which is consistent with the primarily cytosolic localization of SIRT2. Finding the modification eraser completes the cycle of lysine myristoylation-demyristoylation of ARF6, and further demonstration that NMT prefers the active

ARF6 and SIRT2 prefers the inactive ARF6 suggests that the cycle isn't futile, but productive. I further found that this cycle is intimately connected to the GTPase cycle of ARF6 where both myristoylation and demyristoylation are important for efficient ARF6 activation and downstream signaling. This concluded the characterization of ARF6 lysine myristoylation, and opened avenues for further understanding. We now know how ARF6 is regulated by this modification, it allows proper trafficking and activation of the small GTPase. But what impact does it have on proteins that depend on the function of ARF6? ARF6 orchestrates the endocytosis and recycling events of proteins important for cell migration, signaling and nutrient transport. It is therefore tempting to speculate that these molecules and their downstream events would depend on ARF6 lysine myristoylation cycle and could be an important broad topic for future work.

Given the role of ARF6 in cancer[5-8] and the implication of NMT[9, 10] and SIRT2[11-13] in colon cancer, I next explored whether the ARF6 lysine myristoylation cycle is important for this disease. In mouse tumor xenograft models of colon cancer SIRT2 inhibition with TM strongly suppressed tumor growth raising a question whether ARF6 lysine myristoylation could contribute to this effect. We then overexpressed wild type ARF6 or the K3R mutant in mouse tumor xenografts of colon cancer and observed that only wild type ARF6 could promote tumor growth. This suggested that the modification is important for the disease. I further confirmed that ARF6 has lysine myristoylation in colon cancer cells via biochemical studies. The analysis of signaling events showed that ARF6 lysine myristoylaiton cycle regulate EGFR phosphorylation and its downstream effector AKT and my preliminary results suggest that this happens by delaying EGFR

recycling. Because direct inhibition of EGFR, a standard colon cancer therapy, provides no therapeutic advantage for KRas mutant colon cancer, disrupting EGFR trafficking and signaling via SIRT2 inhibition could be a viable treatment strategy.

In chapter 4 I described the search for other unconventional substrate proteins of NMT via a SILAC study where I hoped to identify other lysine substrates. A number of proteins with known N-terminal glycine myristoylation were identified as well as a handful of proteins with an N-terminal glycine or lysine 2 with no reported myristoylation. Dynamin 2 was identified with high confidence heavy-to-light ratios. While it has glycine at the N-terminus, it does not contain the preferred NMT substrate sequence and is predicted as non-myristoylated via the ExPASy tool, which raised a speculation that it might be myristoylated on lysine. Bioorthagonal fatty acid labeling confirmed that DNM2 is indeed myristoylated by NMT, however the levels of modification did not change with sirtuin inhibition. I therefore challenged the ExPASy results by testing the effect of G2A mutation on the levels of fatty acylation. This unambiguously confirmed that the modification is on the N-terminal glycine, warranting caution in interpreting bioinformatics predictions of myristoylation. Interestingly, while DNM2 strongly colocalized with NMT, it could not be myristoylated in vitro and did not interact with NMT, which suggests that the modification might occur cotranslationally. To verify this, one could monitor DNM2 ALK12 labeling during translation inhibition with cycloheximide. A suppression of myristoylation by translation inhibition would imply a cotranslational mode of DNM2 modification. The myristoylation appeared important for DNM2 stability and cell growth. Future validation of the remaining SILAC hits might help identify other nonconventional

substrates of NMT and aid better understanding of the principles underlying its activity. While our data suggests that DNM2 modification is important for its stability and cell survival, the steps in between are unknown. Given the well-established function of DNM2 in endocytosis, it would be natural to examine the role of myristoylation in this process. The G2A mutation does not confer obvious localization differences in confocal imaging and fractionation studies, which is not surprising given that other proteins such as c-Abl also do not utilize myristoylation to bind membranes.[14] It is also possible that lysine myristylation serves as a nucleation signal promoting oligomerization at the vesicle neck. High resolutions imaging examining the efficiency of the oligomerization at the vesicle neck could address this possibility. Alternatively, the function of myristoylation could be analogous to that of c-Abl – it could regulate the enzymatic activity of DNM2.

Altogether, my graduate work resulted in the discovery of the previously unknown regulation of ARF6 by lysine myristoylation which led to the finding of the lysine myristoylatransferase activity of NMT and the modification eraser SIRT2. This has broad implications for understanding the physiological events regulated by these enzymes. One such event is colon cancer progression, which was the focus of my follow up work described in chapter 3. Finally, in a search for other unconventional substrates of NMT via proteomics, I discovered that a crucial regulator of membrane fission DNM2, is myristoyated at the N-terminal Gly, which could not be predicted via bioinformatics. This points to the existence of yet to be unveiled levels of regulation of the NMT enzymes, which should be investigated in the future.

REFERENCES

1. Peters, P.J. *et al.* Overexpression of wild-type and mutant ARF1 and ARF6: distinct perturbations of nonoverlapping membrane compartments. *J Cell Biol* **128**, 1003-1017 (1995).
2. Koegl, M., Zlatkine, P., Ley, S.C., Courtneidge, S.A. & Magee, A.I. Palmitoylation of multiple Src-family kinases at a homologous N-terminal motif. *Biochem J* **303 (Pt 3)**, 749-753 (1994).
3. Wedegaertner, P.B., Wilson, P.T. & Bourne, H.R. Lipid modifications of trimeric G proteins. *J Biol Chem* **270**, 503-506 (1995).
4. Kosciuk, T. *et al.* NMT1 and NMT2 are lysine myristoyltransferases regulating the ARF6 GTPase cycle. *Nat Commun* **11**, 1067 (2020).
5. Chabu, C., Li, D.M. & Xu, T. EGFR/ARF6 regulation of Hh signalling stimulates oncogenic Ras tumour overgrowth. *Nat Commun* **8**, 14688 (2017).
6. Haines, E., Saucier, C. & Claing, A. The adaptor proteins p66Shc and Grb2 regulate the activation of the GTPases ARF1 and ARF6 in invasive breast cancer cells. *J Biol Chem* **289**, 5687-5703 (2014).
7. Ye, Z. *et al.* Abrogation of ARF6 promotes RSL3-induced ferroptosis and mitigates gemcitabine resistance in pancreatic cancer cells. *Am J Cancer Res* **10**, 1182-1193 (2020).
8. Qi, S. *et al.* Arf6-driven endocytic recycling of CD147 determines HCC malignant phenotypes. *J Exp Clin Cancer Res* **38**, 471 (2019).
9. Selvakumar, P., Smith-Windsor, E., Bonham, K. & Sharma, R.K. N-myristoyltransferase 2 expression in human colon cancer: cross-talk between the calpain and caspase system. *FEBS Lett* **580**, 2021-2026 (2006).
10. Kumar, S., Dimmock, J.R. & Sharma, R.K. The potential use of N-myristoyltransferase as a biomarker in the early diagnosis of colon cancer. *Cancers (Basel)* **3**, 1372-1382 (2011).
11. Cheon, M.G., Kim, W., Choi, M. & Kim, J.E. AK-1, a specific SIRT2 inhibitor, induces cell cycle arrest by downregulating Snail in HCT116 human colon carcinoma cells. *Cancer Lett* **356**, 637-645 (2015).
12. Hu, F. *et al.* Inhibition of SIRT2 limits tumour angiogenesis via inactivation of the STAT3/VEGFA signalling pathway. *Cell Death Dis* **10**, 9 (2018).
13. Farooqi, A.S. *et al.* Novel Lysine-Based Thioureas as Mechanism-Based Inhibitors of Sirtuin 2 (SIRT2) with Anticancer Activity in a Colorectal Cancer Murine Model. *J Med Chem* **62**, 4131-4141 (2019).
14. Hantschel, O. *et al.* A myristoyl/phosphotyrosine switch regulates c-Abl. *Cell* **112**, 845-857 (2003).